CO measurements from MTG IRS and UVS missions

P.-F. Coheur[1], B. Barret[1], C. Clerbaux[1,2], J. Hadji-Lazaro[2]
M. Kruglanski[3], A.C. Vandaele[3] and D. O'Brien[4]

1. Spectroscopie de l'Atmosphère, Service de Chimie Quantique et Photophysique, Université Libre de Bruxelles, Bruxelles, Belgium

2. Service d'Aéronomie/CNRS, Université Paris 6, Paris, France

3. Belgian Institute for Space Aeronomy, BIRA-IASB, Bruxelles, Belgium

4. Department of Atmospheric Science, Colorado State University, Fort Collins, U.S.A.

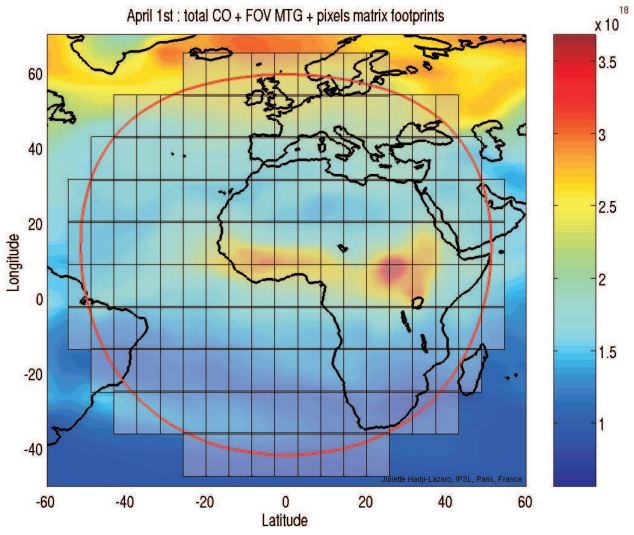

EUMETSAT contract EUM/CO/04/1296/SAT

Final report

April 2005

pfcoheur@ulb.ac.be, bbarret@ulb.ac.be (new e-mail: brice.barret@aero.obs-mip.fr), ccl@aero.jussieu.fr, jha@aero.jussieu.fr, annc@bira-iasb.oma.be, michelk@bira-iasb.oma.be obrien@atmos.colostate.edu

Contents

1 Summary

In the atmosphere carbon monoxide (CO) is an important precursor of tropospheric ozone and poses serious health risks. It is also responsible for about 75% of the OH sink and therefore prevents the atmosphere from removing other pollutants. Approximately two third of CO comes from human activity (mainly industry and transportation in the northern hemisphere and the burning of vegetation in the southern hemisphere). Once in the atmosphere, CO follows the course of atmospheric circulation and, given its relatively long lifetime, impacts on air quality over distant regions. Tracking CO plumes is essential to identify emission sources, to characterize atmospheric motion of pollution plumes, and to study the global consequences of air pollution.

In the last decade, satellites on low-Earth orbit (LEO) have demonstrated the benefit of the space-based observations for monitoring CO on the global scale. Instruments operating either in the thermal infrared (MOPITT, IMG) or the short-wave infrared (SCHIAMACHY), have provided CO distributions, and have thereby given a better insight on tropospheric chemistry and dynamics. Due to a limited revisit time, regional aspects of air quality, can, however, not be accessed from the satellites on LEO.

This study examines the capabilities of spectroscopic instruments on geostationary orbit (GEO) to monitor tropospheric carbon monoxide with 10 % accuracy, 10 km horizontal resolution and a temporal sampling of one hour, as specified by Golding *et al.* [1] and Lelieveld [2]. The study relies on instrument performances defined in preparation of the Meteosat Third Generation (MTG) satellite program [3]. The possible achievements for measuring CO from MTG are examined both for the UV sounder (UVS) and for the IR sounder (IRS) alone and in synergy. The analyses make use of a series of assessment methods to characterize the impact of the instrument performances (radiometric noise and spectral resolution) and the atmospheric state (temperature, humidity and other gases profiles, aerosols and clouds) to the target measurements.

Spectral windows

CO absorbs thermal infrared radiation in the 1–0 fundamental band, which is entirely covered by the IRS band 7, extending from 2000 to 2250 cm^{-1}. In that spectral range, other significant absorptions are due to H_2O, CO_2, O_3 and N_2O. In this study, a narrow micro-window between 2142 to 2185 cm^{-1} is selected, to avoid interferences due to O_3 and CO_2, while keeping the relevant information from the spectra.

CO can also be measured by the UVS using reflected/scattered solar radiation in the short-wave infrared channel, between 4180 and 4320 cm^{-1}. This channel contains the entire 2–0 vibration–rotation band of CO. In the SWIR region, other absorbing species are H_2O and CH_4, which have optical thickness much larger than that of CO. A narrow window of the SWIR band is selected, spanning 4220–4240 cm^{-1}, where absorption by CO is stronger and the structure of H_2O and CH_4 lines is less complicated.

Assessment methods

In most parts of the study, the feasibility to measure CO is assessed by means of the Optimal Estimation theory [4], which requires statistics of the errors in the measurements and the model parameters, as well as prior information about the atmospheric state, the latter consisting of estimates of the mean and covariance of a realistic ensemble of states. Detailed characterizations of the retrievals, in terms of information content and error budget, are performed, as well as

retrieval experiments for several reference scenarios, corresponding to clear–sky or to aerosol or cloud–containing atmospheres. The prior data used for these assessments were obtained from the MOZART chemical transport model.

In other parts of the study, dealing only with the measurement of CO from the SWIR, a series of case studies with increasing complexity are used to illustrate the biases and errors that can arise. Finally, Monte Carlo simulations, in which noisy spectra are submitted to an inversion algorithm, similar in principle to the DOAS algorithm, are performed. This approach allows the bias and random errors in the estimated parameters to be assessed without the ambiguity introduced by the statistical assumptions of the Optimal Estimation method.

Results

Globally, the results support the conclusion that the spectroscopic instruments onboard MTG enable measuring CO with an accuracy similar to that of the demonstrated instruments on LEO, the latter being close to the 10% accuracy in the tropospheric column. In principle, the combination of the thermal infrared radiances from the IRS with the shortwave infrared radiances from the UVS would be most suitable, as it would allow retrieving vertically resolved CO profiles (2 independent pieces of information), with good sensitivity in the boundary layer and in the middle troposphere. The IRS measurements alone is expected to deliver CO products with an accuracy matching the requirements, provided, however, that the spectral resolution and radiometric performances are not relaxed significantly beyond the target values given in the Mission Requirement Document, issue 1.1 [3]. The high resolution of the IRS is a further requisite for measuring a vertically resolved CO profile, if not combined to the UVS. Finally, while the UVS measurements should theoretically provide CO columns with the required accuracy, achieving the accuracy in practice appears to be challenging.

Retrieval of CO vertical profiles from the IRS

CO total column measurements can be achieved with 10 % accuracy by the IRS, for radiometric noise values smaller than 5 10^{-9} W / (cm^2 sr cm^{-1}) and a spectral resolution of either 0.625 cm^{-1} or 1.250 cm^{-1}. At the coarser spectral resolution (2.5 cm^{-1}) the error on the CO column is unacceptably large. Retrieving the tropospheric (0-12 km) CO content with a similar 10% accuracy, which corresponds to the user-defined breakthrough level for chemistry applications [1, 2], requires somewhat lower noise and preferably the highest spectral resolution, to minimize the impact due to uncertainties on the temperature and humidity profiles. Furthermore, the combination of low noise and high spectral resolution is absolutely needed for separating the lower (0-6 km) and upper (6-12 km) tropospheric columns.

The main sources of errors in the retrieval of CO from the IRS–7 channel are the smoothing and the measurement errors, which are both tightly related to the instrument specifications. Other sources of errors include uncertainties on the surface properties and the atmospheric state. While the uncertainties on the surface properties (emissivity and temperature) contribute little to the total error, those on the temperature and humidity profiles have an important impact on the CO tropospheric column retrieval, the extent of which depends strongly on the atmospheric conditions and instrumental performances. For instance, the uncertainty on the temperature profile (a 1.5 K uncertainty was considered), generates a radiance error of about 1 10^{-9} W / (cm^2 sr cm^{-1}), which is of the same order of magnitude as the radiometric noise at the center of the CO lines. The error introduced on the CO retrieval varies from a few percent at the highest spectral resolution to about 5% at the coarser spectral resolution. The uncertainty on the humidity profile (10% was considered) generates also considerable errors, which could partly be avoided at the best spectral resolution by selecting narrow micro-windows where H_2O

lines are absent. At the coarser spectral resolution, however, the impact of water vapor can hardly be avoided, and errors from 5–10% are likely to result, especially in the case of a very humid atmosphere. The impact of interfering trace gases on the retrieval of CO is negligible, provided that an optimal micro-window in IRS–7 is selected. Finally, the impact of tropospheric aerosols (urban, biomass-burning and maritime aerosols) is weak whereas high-altitude aerosols (stratospheric aerosols or thin cirrus clouds) can lead to errors as large as 20%, if not properly considered in the radiative tranfer.

The conclusions for the IRS are confirmed by performing retrieval experiments corresponding to selected scenes, associated to 'clean', 'urban', 'biomass-burning' and 'transport' CO emission scenarios. The results point to the limits of the IRS, even in the best configuration of spectral resolution and noise, to catch extreme CO vertical distributions, such as those characterizing high pollution and biomass-burning (high level of CO in the boundary layer) or pollution transport events.

Retrieval of CO vertical profiles from the UVS

Spectra at the top of the atmosphere in the SWIR band show very little sensitivity to the vertical distribution of CO. At best one can hope to resolve the stratospheric and tropospheric components of the CO mass density. Even with an appropriate micro-window selection, which enables to minimize the impact of H_2O and CH_4 the errors in the retrieved CO are unacceptably large unless the spectral resolution lies in a narrow range, within which the random errors (smoothing, cloud, aerosol and temperature) are minimized, while the biases introduced by cloud and aerosol pass through zero. There is only qualitative agreement on the location of this range between the different methods of assessment; the statistical analysis suggests 0.4–0.6 cm^{-1}, whereas the Monte Carlo simulations indicate 0.2–0.3 cm^{-1}. The sensitivity of the error to the spectral resolution is so great that this difference is significant.

Even with the spectral resolution so chosen, achievement of the required accuracy for tropospheric CO is marginal for SNR within the range specified in the Statement of Work. In the best case studied, the random error is about 4%, while the biases due to high cloud and aerosol are 2.5% and 3%, respectively. Temperature errors contribute an additional bias, estimated at 2.9%. However, other cases (such as the bio-mass scenario with clean prior) have biases and random errors outside the acceptable range.

Monte Carlo simulations broadly support the conclusions of the statistical analysis, though there is some disagreement over the optimal spectral resolution. Furthermore, the magnitude of the biases appears to be sensitive to the scenario assumed for CO. This instability reinforces the conclusion that the proposed measurement strategy is marginal.

Retrieval of CO vertical profiles from IRS and UVS

The retrieval of the CO profile from a synertic use of the IRS and UVS takes full advantage of the different sensitivity of the thermal infrared and short-wave channels to the CO vertical distribution. While the measurements taken individually do not contain much more than a single piece of information on the vertical CO profile, their combined use increases the DOFS to about 2. The sensitivity becomes important in both the boundary layer, where the SWIR measurements are mostly sensitive, and in the middle troposphere, where the thermal IR measurements show high sensitivity. The combination allows significant reduction of the retrieval error (smoothing and measurement errors), which is of the order of 3% on the tropospheric column. The results suggest, however, that the total error remains important for CO tropospheric column retrieval, unless water vapor and methane contents are known very accurately.

2 Introduction

The MTG system, to be placed on geostationary orbit, is planned to be available around 2015. It will provide observations over Europe and Africa. MTG priorities are on meteorological applications, with some relevance to atmospheric chemistry and air quality. The needs of the user community in the 2015-2025 timeframe, with respect to these fields, have been assessed by a post-MSG user consultation process, which was used for the MTG definitions studies (pre-phase A) and for producing the so-called MTG Mission Requirement Document (MRD).

This work aims to consolidate the MRD by studying the possible achievements of MTG IRS and UVS instruments for monitoring carbon monoxide (CO), with the spatial and temporal accuracy required for atmospheric chemistry and air quality applications. It relies on instrumental specifications, as documented in the MRD version 1.1 [3] and on the user-defined chemistry requirements for CO, as given in Golding *et al.* and Lelieveld [1, 2]. These two aspects are briefly summarized in sections 2.1 and 2.2.

Section 3 provides an overview of earlier scientific studies, on which the present work naturally draws on. They include:

- Previous expert studies undertaken in the preparation of MTG program, which have surveyed the possibilities of the UVS [5, 6, 7] and IRS [8] instruments to contribute to the understanding of those aspects relevant of atmospheric chemistry, in general, and to CO in particular.
- Results obtained from the analysis of actual tropospheric remote sounders on LEO. Three concepts of passive remote sensors have in particular demonstrated their ability to provide CO measurements: correlation radiometers (MOPITT), UV-visible-SWIR radiometers using the reflected/scattered solar radiation (SCIAMACHY), and infrared spectrometers using the Earth's thermal emission as a source (e.g. IMG and follow-on AIRS, IASI and TES).

After the description of theory and methodology in section 4, the principal results gathered in the context of this study are presented in section 5. The questions which are addressed have for objective to:

- Characterize the sensitivity of carbon monoxide (CO) retrievals to different atmospheric variables (surface and upper-air temperatures, other atmospheric gases, aerosols and thin clouds) using either the IRS or the UVS observations alone or in synergy. The results are critically reviewed in light of the chemistry requirements [1, 2].
- Investigate possible improvement or relaxation of the radiometric noise and the spectral resolution, while ensuring that the chemistry requirements remain fulfilled.

The issues dealing with the retrieval and characterization of CO from the IRS and the UVS instruments are described in section 5.1 and 5.2 respectively. More detailed results regarding the feasibility to measure CO using the UVS instrument are given in an annex report by O'Brien [9]. The results obtained from a synergetic use of the IRS and UVS instruments are finally presented in section 5.3, for a typical combination of instrumental specifications.

The conclusions of the study are provided in section 6, while section 7 briefly points to some intrinsic limitations of the theoretical approaches.

2.1 Chemistry requirements

Carbon monoxide (CO) is produced by the burning of fossil fuels, such as gasoline, and by the burning of forests and grasslands. As an important precursor of tropospheric ozone, CO is a major species that impacts on air quality. It is generally considered as one of the primary air pollutants. In the atmosphere CO is converted to carbon dioxide by reaction with the hydroxyl radical (OH). Globally, CO is responsible for about 75% of the OH sink, and is thereby a key species to monitor modifications to the oxidizing capacity of the atmosphere and to climate changes.

The increase of human population in cities and the associated increases in industrial and agricultural activity are causing increasing amounts of carbon monoxide to be released into the air. Once in the atmosphere, CO, which has a lifetime of several weeks to a few months in the troposphere, can be transported over long distances. It can therefore be used as a tracer of pollution. If the spatial and temporal resolution permits, its observation from space allows the characterization of both emission sources and atmospheric motion of pollution plumes, especially well suited to track Long-Range Transboundary Air Pollution (LRTAP).

Instruments such as MOPITT and SCIAMACHY, which operate from LEO but provide global coverage, have already demonstrated the potential of remote-sensing from space to determine the main CO emission sources. However, in order to make further substantial contributions to atmospheric chemistry and air quality studies, in particular on the regional scale, the requirements for monitoring CO from space have to be more stringent. They have been set to the following [1, 2]:

- Measurement of a tropospheric column with 10% accuracy (threshold). Higher vertical resolution (2 km) and accuracy (5%) would be desirable.
- Day and night measurements, with 0.5 (target) to 2 (threshold) hours sampling.
- 2 km (target) to 10 km (threshold) horizontal resolution.

In the above requirements, the threshold and target requirements refer to values above which an observation would have no benefit at all and below which an observation would not provide additional benefit. For CO, the breakthrough level to be achieved, which is defined as the performance that will provide delta improvement in the targeted service, corresponds to the threshold values, except for the temporal sampling, which is 1 hour.

2.2 Instrument specifications

The instrument specifications are documented in the MTG Mission Requirements Document (MRD). The document is elaborated and evolves following the analysis and interpretation of high level user needs and of the identification and assessment of relevant observing techniques by remote sensing and satellite experts. The MRD issue 1.1 specifications [3], which are related to the IRS and UVS instruments, are briefly described hereafter.

2.2.1 IRS

In its current design, the IRS covers the thermal infrared spectral range from 667 to 2500 cm^{-1} in 10 adjacent bands. It is dedicated in priority to meet the needs for NWP at the global and regional scales, which is expected to be achieved through the provision of Atmospheric Motion

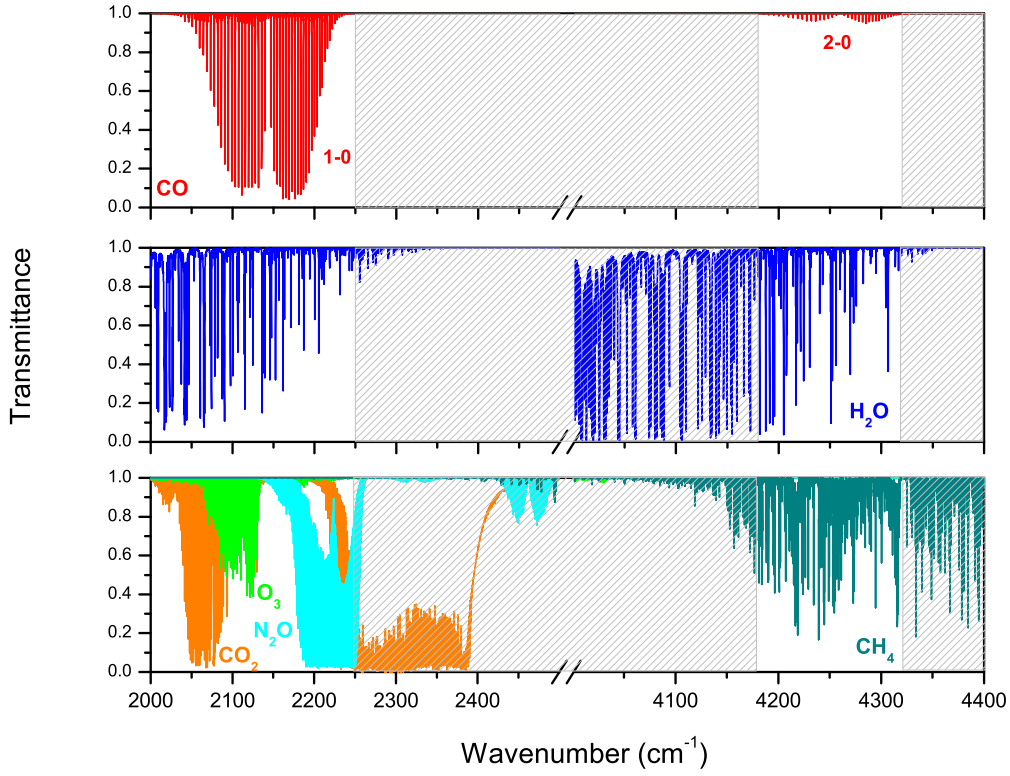

Figure 1: CO 1–0 and 2–0 absorption bands in the thermal infrared and the short-wave infrared, in transmittance unit (top panel). The bottom panels give the individual contribution of water vapor and of the strongly absorbing trace gases in these spectral regions. The two white areas correspond to the spectral intervals of the IRS band 7 (2000–2250 cm^{-1}) and of the UVS SWIR band (4180–4320 cm^{-1}).

Vectors (AMV) with high vertical resolution in clear air and of frequent information on temperature and water vapor profiles. Accordingly, the emphasis for the IRS mission is on high horizontal resolution (better than 10 km), high vertical resolution (better than 1 km) and frequent observations (better than 1 hour) of the full Earth disk. As a secondary objective, the IRS will support chemical weather and air quality applications.

Spectral coverage

CO absorbs the thermal infrared radiation in the fundamental 1–0 rotation-vibration band, centered at about 4.7 μm (Figure 1). The CO 1–0 band is entirely covered by the IRS–7 spectral band, which extends from 2000 to 2250 cm $^{-1}$. Only those instrumental specifications applicable to IRS–7 are considered below.

Spectral resolution:

The spectral resolution, $\Delta\tilde{\nu}$ (or $\Delta\lambda$), is defined as the Full Width at Half Maximum (FWHM) of the Instrumental Response Function (ISRF) — after apodisation if applied — given through the resolving power ($R = \tilde{\nu}/\Delta\tilde{\nu}$ or $\lambda/\Delta\lambda$). The goal and threshold resolution for IRS–7 correspond respectively to a resolving power of 3400 and 1800 at the center of the band.

The results presented in this work have been obtained relying on a FTS instrumental concept, without apodization. The FWHM, taken as the spectral resolution, is then defined as a

function of the Maximum Optical Path Difference (l) of the FTS according to

$$\text{FWHM} = \Delta\tilde{\nu} = 0.6033/l \quad (1)$$

Three different values of spectral resolution have been considered for the purpose of this study. They correspond to FWHM of 0.625, 1.250 and 2.500 cm^{-1}, which span a range between goal and threshold resolutions, and above. It is worth stressing that the results presented hereafter could in principle be extended to a dispersive instrument concept with ISRF of similar FWHM.

Radiometric resolution:

The radiometric resolution is specified in terms of noise equivalent temperature difference (NeDT) associated with a reference temperature of 280 K, at which the NeDT is computed.

Different radiometric resolutions, corresponding to NeDT values between 0.125 K and 2.5 K (respectively 1 10^{-9} and 2 10^{-8} W/(cm^2 sr cm^{-1}) at the center of the IRS–7 band) have been considered to compute the sensitivity of the CO retrieval to this parameter. The noise levels specified in the MRD are 0.1 K (goal) and 0.2 K (threshold).

2.2.2 UVS

Many of the species having an impact on air quality display significant absorption in the UV-visible spectral range. The spectroscopic instruments using this energy range to probe the troposphere are therefore obvious sounders to be part of an atmospheric chemistry satellite mission. The UVS mission on MTG would benefit from the geostationary orbit and from the specific capabilities of the other instruments. It is justified for the tropospheric gases that vary rapidly in space and time and that affect human health and security. The UVS is expected to observe the diurnal cycle of these atmospheric trace gases, including their spatial variability, horizontal transport, and potentially vertical exchange associated with weather and climate processes. Accordingly, the emphasis and priority of the UVS is on frequent (less than 1 hour) observations of mainly O_3, CO, NO_2, SO_2 and H_2CO.

Spectral coverage:

CO does not absorb radiation in the UV or the visible spectral range. Therefore, in order to measure CO and other key constituents such as CH_4 or CO_2, the UVS has to include channels in short-wave infrared (SWIR). According to the MRD [3], the SWIR band of the UVS extends from 4180 to 4320 cm^{-1} (2315–2392 nm). It includes the entire CO 2–0 overtone rotation-vibration band (Figure 1).

Spectral resolution:

The spectral resolution for the UVS instrument is defined in a similar way as for the IRS, that is as the FWHM of the ISRF. Here the concept of a dispersive instrument is considered, in agreement with the possible heritage of MTG-UVS from GOME/(ERS and EPS) and SCIAMACHY/ENVISAT.

A wide range of values from 0.08 to 2.0 cm^{-1} (corresponding to spectral resolving power of 52875 and 2115 respectively) have been considered for the spectral resolution in this study. This range of values includes the threshold (R = 5000) and goal (R = 20000) resolving power defined in [3].

Radiometric resolution:

The radiometric resolution includes all noise contributions which are independent of the scene and which have a time constant less than or equal to the radiometric period. The radiometric resolution is specified in terms of a signal-to-noise ratio (SNR) associated with a reference radiance. The threshold and goal radiometric resolutions for a reference scene of 1 10^{-7} W/(cm^2 sr nm) are 120 and 700, respectively. Results are illustrated for SNR values of 100, 250, 400, 550 and 700.

3 Scientific background

3.1 Overview of results from previous studies

3.1.1 IRS

Many key atmospheric species have absorption signatures in the thermal infrared. The IRS has therefore the potential to provide, in addition to meteorological data, measurements useful for atmospheric chemistry applications. This was examined in the study by Clerbaux *et al.* [8].

The study shows that CO, a medium absorber in the thermal IR, can easily be detected and measured in both polluted and unpolluted atmospheric conditions, with the different instrumental characteristics considered for the IRS ($\Delta\tilde{\nu}$ between 0.2 and 0.75 cm^{-1} and NESR up to 5 10^{-8} W/(cm^2 sr cm^{-1})). The analysis concludes that the horizontal target and threshold resolution requirements match the goal and threshold instrument specifications. Taken globally, the results show that, under idealized scenarios, corresponding to a perfect knowledge of the atmospheric state, the radiometric noise is a more limiting factor than the spectral resolution towards the chemistry requirements of [2]. For CO in particular, it was concluded that the total column could be retrieved with accuracy between target and threshold, and that a vertically resolved profile could be retrieved with 1.3 to 2.2 independent pieces of information depending on the spectral resolution and noise. It is suggested that improvements for measuring CO could be gained by combining the radiances from IRS, which covers the CO fundamental band, and from additional measurents in the SWIR (CO overtone absorption band).

3.1.2 UVS

Three independent studies have been performed in preparation of the MTG mission, in order to determine the capabilities of an intrument measuring the reflected/scattered solar radiation in the UV-visible and SWIR from a GEO, for monitoring air quality [5, 6, 7]. The main findings are the following:

Despite the fact that the spectrum is dominated by the spectral signatures of CH_4 and H_2O, both the O'Brien and Pickett Heaps [5] and Bovensmann *et al.* [6] studies concluded that CO tropospheric columns could be retrieved from the SWIR radiances, with the required accuracy, under most scenarios and with the specified instrumental performances. For a standard case, it was found that the number of independent pieces of information on the CO vertical profile lies between 1 and 2 [6]. The stratospheric errors were shown not to produce large errors on the CO tropospheric column. As for the IRS study, the analyses were conducted assuming idealized atmospheric conditions.

The benefit gained by coupling the radiances from the SWIR and IRS was briefly addressed in the study by Siddans and Kerridge [7]. Relying on earlier work, the authors argue that measurements of CO at 2.3 microns would probably not add information to the retrievals from

IRS, although the SWIR channels tend to increase the sensitivity near the surface. Siddans and Kerridge recommend, however, that a detailed study be conducted to verify this specific question.

3.2 Measurements of tropospheric CO from space

Several satellite borne instruments, all on LEO, have recently demonstrated their ability to optimally probe the troposphere, and thereby to help in accessing the impact of human activities on the chemical composition of the atmosphere and on climate change. Among these tropospheric sounders, which use the nadir geometry, several have successfully measured CO, using the thermal infrared or the reflected/backscattered short-wave infrared radiances. The results obtained from the analyses of these satellite spectra provide an essential scientific background for this study.

3.2.1 Retrieval of CO from thermal infrared radiances

Tropospheric CO columns have been retrieved in the thermal infrared from MAPS on the Space Shuttle, IMG/ADEOS and MOPITT/TERRA. AIRS/AQUA and TES/AURA, presently on orbit, should both deliver CO global distributions. The 15 years of operation of the suites of IASI/MetOp instruments is expected to provide an interesting continuous series of CO measurements.

MAPS:

Historically, the first global measurements of CO were retrieved from measurements provided by MAPS, which flew onboard the Space Shuttle for short missions in 1981, 1984 and 1994 [10]. MAPS was a correlation radiometer, measuring the CO fingerprint between 2080 and 2220 cm^{-1}. It enabled the identification of the main CO sources, e.g. over the industrialized northern hemisphere and from biomass burning over the tropics and southern hemisphere (Figure 2). Only CO total columns were measured by MAPS.

MOPITT:

The Measurement Of Pollution In The Troposphere (MOPITT) instrument has operated on the NASA EOS Terra satellite since 1999. As MAPS, it uses the technique of correlation spectroscopy to measure CO [11]. The initial objective of MOPITT was to probe the atmospheric CO in both short-wave (52 cm^{-1} wide channel centered at 4285 cm^{-1}) and thermal infrared (40 cm^{-1} wide channel centered at 2166 cm^{-1}) regions, such as to allow measuring CO profiles with good accuracy (10–20%) from the boundary layer to the upper troposphere. CO profiles with 3 independent pieces of information were expected from the measurements, depending on the measurement noise and surface properties.

However, in flight, the MOPITT SWIR channels did not produce the expected results. As a matter of consequence, only the thermal infrared channel measurements were fed to the operational retrieval algorithm to retrieve the CO profiles [12]. Detailed characterization showed that, in this less favorable situation, the MOPITT measurements contain a maximum of 1.5 independent pieces of information on the CO vertical profile [13].

Given its ability to sound the atmosphere off the nadir, MOPITT has provided an unprecedented vision of the global carbon monoxide distributions. The analysis of the CO fields has enabled the identification of the main emission sources, related to industry or the burning of vegetation, as well as the characterization of the transport of pollution over long distances. The

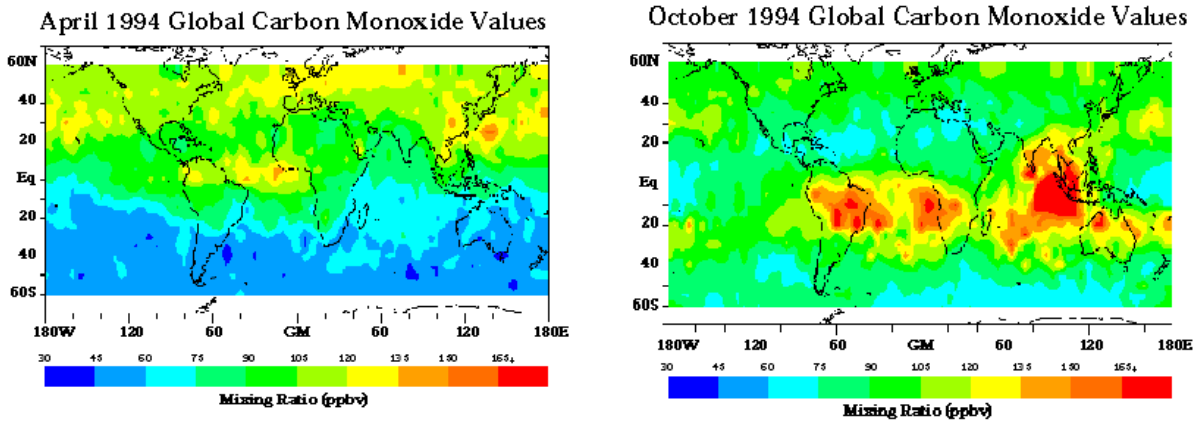

Figure 2: CO contents obtained by MAPS for the April 9-19, 1994 (left panel) and September 30 - October 11, 1994 (right panel) periods. High concentrations are found in April over the industrialized northern hemisphere and in the October period over the grasslands and savannas in central South America, southern Africa, and over the Indonesian Islands, as a result of burning events. From *http://oea.larc.nasa.gov/PAIS/MAPS.html*

relatively long lifetime of the mission (2000-present) is also key for characterizing the seasonal and yearly variability of CO [14].

MOPITT also gives the opportunity to study regional pollution aspects. A clear correlation between the CO content, the NO_2 content as measured by the SCIAMACHY instrument, and the population density has been established (Figure 3). The measurements also make it possible to observe, in some situations, CO pollution originating from cities (Figure 4).

IMG:

The IMG [15] instrument was developed under the initiative of the Japanese Ministry of International Trade and Industry (MITI), to be part of the ADEOS sun-synchronous, ground-track repeat, polar-orbiting satellite. The instrument, which was designed to measure the distributions of the main atmospheric greenhouse gases, was a high spectral resolution FTS (10 cm Maximum Optical Path Difference — MOPD), operating in three separate bands, extending from 2387 to 3030 cm^{-1} (band 1), 2000 to 2500 cm^{-1} (band 2) and 600 to 2000 cm^{-1} (band 3).

Detailed analysis of the IMG spectra [16, 17] showed that the instrument response function in flight was broadened in each band, a result of FOV effects (the FOV was 8 km$\times$8 km footprint on the ground) and also the impact of off-axis light entering the instrument. The spectral resolution exceeded therefore the nominal value in all bands. For instance, the total ILS in band 2, which covers the 1–0 fundamental band of CO, was approximately 0.12 cm^{-1}.

Total column amounts of CO have been obtained from the IMG spectra, convolved with a Gaussian function such as to match an instrument of 0.5 cm^{-1} FWHM, using SA-NN retrieval algorithm developed for the IASI mission [18, 19, 20]. The averaged accuracy in the retrieved column amount was estimated to 10%, including all sources of errors.

More recently, the global distribution of CO vertical profiles were inferred from the IMG spectra [17]. The study, which includes a thorough characterization of the retrievals, shows that the IMG measurements, combining a high resolution and a low noise, contain between 1.5 to 2.2 pieces of information on the CO vertical profiles. In the best cases, this enables separating the CO concentrations in lower-middle troposphere and the UTLS (Figure 5). The error on the vertical profile, dominated by the smoothing error with additional contribution from the mea-

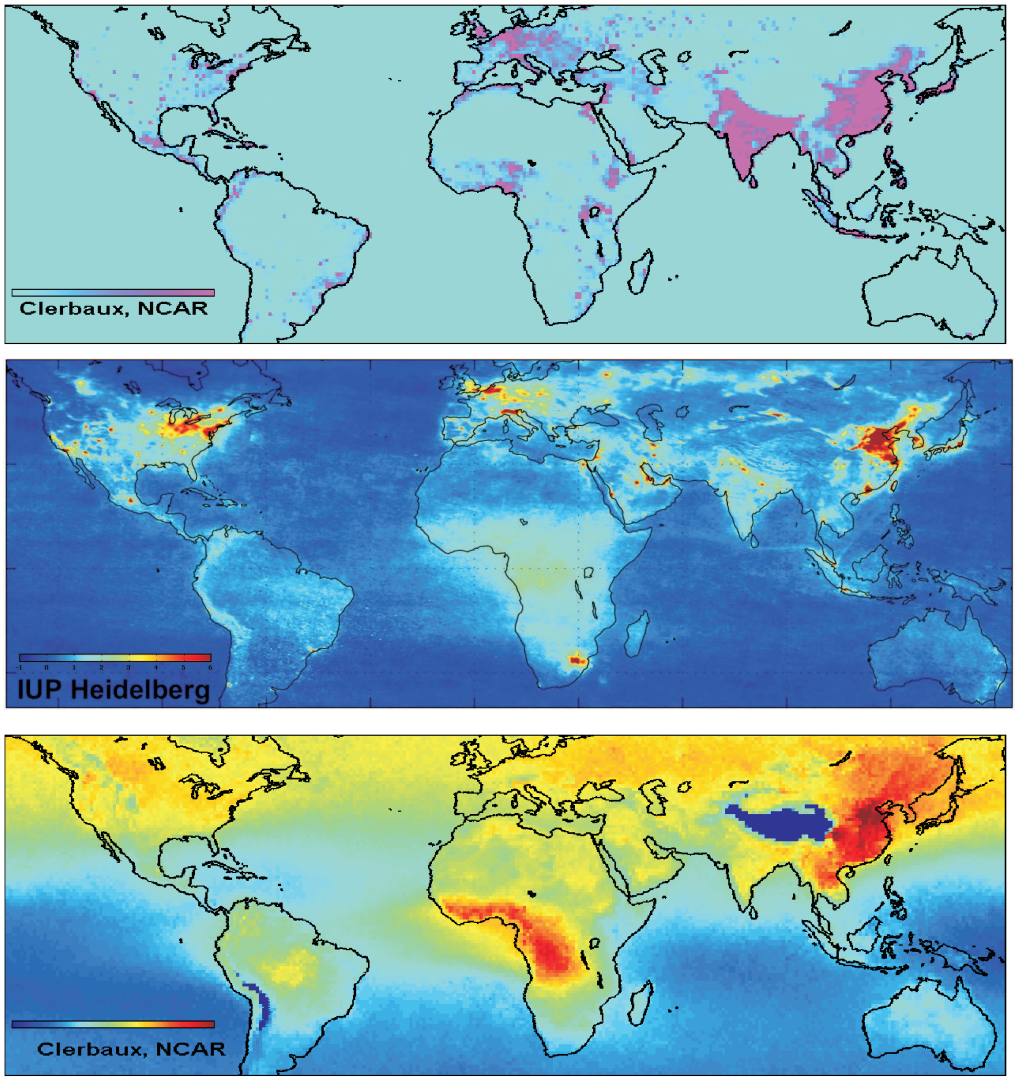

Figure 3: Comparison between the world's population density (1 $\times$1 degrees grid, top panel), the global distribution of NO_2 measured by SCIAMACHY and averaged over 18 months (centre panel) and the global CO distributions from MOPITT, averaged over 50 months (bottom panel). High NO_2 values are found in eastern Asia, the East coast of the U.S.A., northern Europe and some other more localized sites, in good correlation with the density of population. The CO content is very high in eastern Asia and high over most of the northern hemisphere. This is explained by the longer lifetime of CO compared to NO_2 and the resulting long-range transport of CO from the emission sources to remote locations. Emission of CO from biomass burning events in Africa and South America are also obvious.

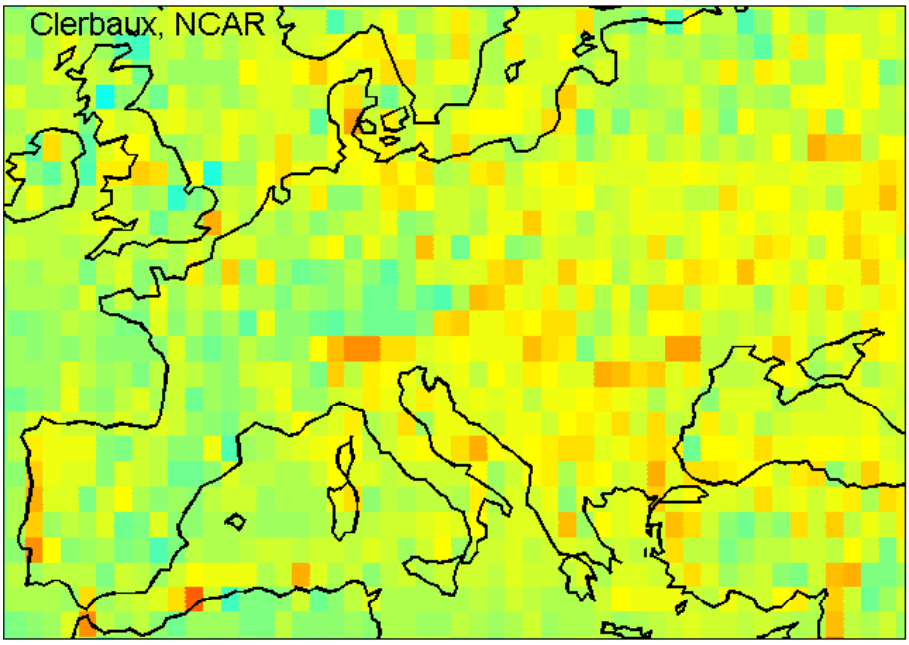

Figure 4: MOPITT CO measurements over Europe, for the summer of 2000, which was characterized by a relatively low CO background. The CO emissions from several cities can be seen.

surement noise and from the errors due to the uncertainties on the temperature profile and on the ILS, is estimated to 10-20% in the boundary layer and to better than 10% higher up. The results are validated with independent measurements, and excellent agreement is obtained between the retrieved CO content in the boundary layer and the surface measurements performed at different NOAA/CMDL stations (Figure 6). This result, which is explained by the strong correlation that bounds CO in the lower-middle troposphere — to which IMG is mostly sensitive — and the surface CO measured at the CMDL stations, is essential to evaluate the potential of satellite observations for air quality studies.

TES:

The Tropospheric Emission Spectrometer (TES) was successfully launched on the AURA satellite in June 2004. The instrument, designed to study ozone, air quality and climate, is a high-resolution (0.1 cm^{-1} apodized) infrared-imaging FTS, covering the 650 to 3050 cm^{-1} spectral range in a limb-viewing and nadir mode [21]. The footprint on the ground is 5.3 km $\times$ 8.4 km. As a result of significant radiometric noise in the CO retrieval window, the measurements are expected to contain not more than 0.5 to 0.9 independent pieces of information, depending on the scene [22]. The predicted error on the CO vertical profile varies between 10 and 30%, the sensitivity being maximal between 5 and 13 km.

Preliminary retrievals of CO have shown that the TES measurements reproduce qualitatively the large-scale features on the globe, as calculated by the GEOS-CHEM CTM. Further analysis should provide quasi-global CO distributions, with high horizontal resolution.

AIRS:

The Atmospheric InfraRed Sounder (AIRS) operates from the EOS AQUA platform, along with two operational microwave sounders, AMSU and HSB. AIRS is a high-spectral resolution grating spectrograph (resolving power of 1200), which measures radiation in the thermal

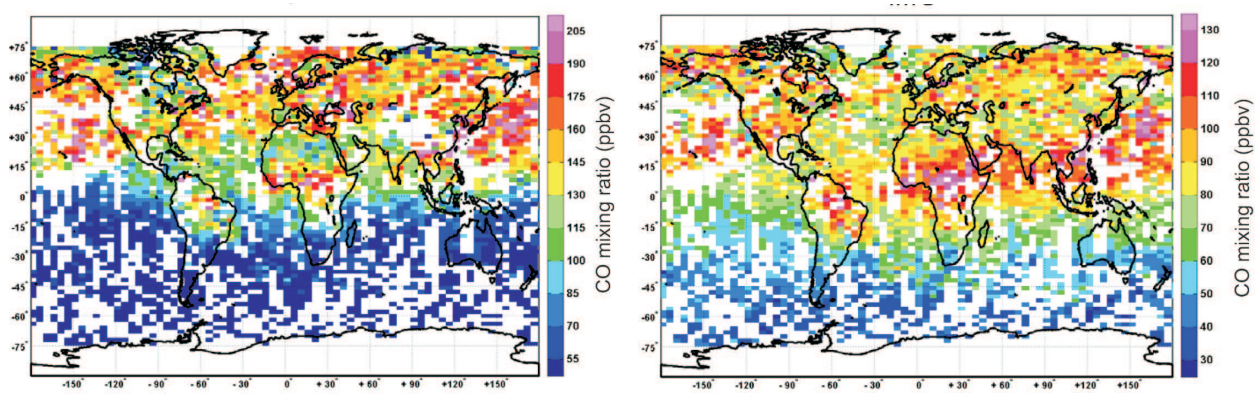

Figure 5: CO volume mixing ratios (ppbv) for April 1-10 1997, retrieved from the cloud filtered IMG spectra (averages on a $2^o \times 5^o$ grid), in the lower troposphere at 1.2 km (left panel) and in the UTLS at 10.2 km (right panel). Only measurements for which the ratio of the inversion error (sum of the smoothing and measurement errors) to the *a priori* variability does not exceed 0.5 are plotted.

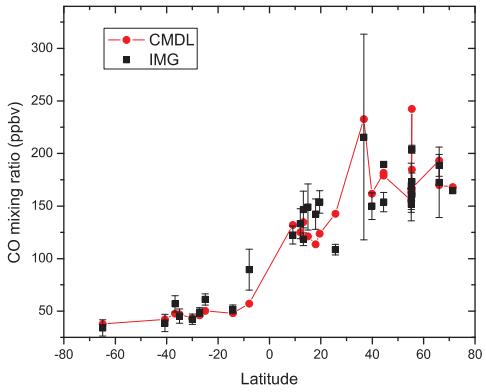

Figure 6: Comparison between the CO mixing ratios measured *in situ* at the surface by the CMDL, and coincident IMG lower tropospheric CO mixing ratios for April 1-10 1997. In the northern hemisphere, the IMG CO mixing ratio is calculated as the average over all observations lying within 6^o longitude and 3^o latitude from the location of the CMDL station and measured either the same day, the day before or the day after the *in situ* measurements. In the southern hemisphere, the spatial coincidence criteria has been relaxed to 9^o longitude and 4.5^o latitude and the temporal coincidence has been extended to one more day before and after the *in situ* observation. The altitude of the scene must be within 250 m from the altitude of the CMDL station. Only measurements for which the ratio of the retrieval error (sum of the smoothing and measurement errors) to the *a priori* variability does not exceed 0.5 are considered.

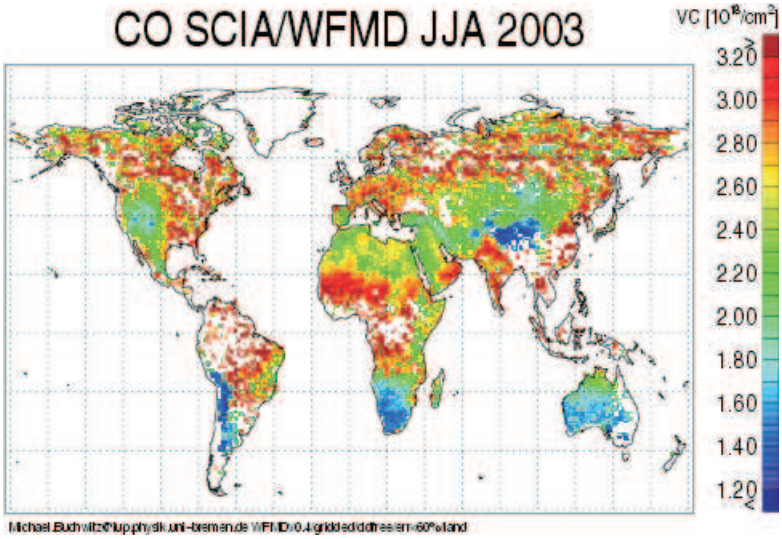

Figure 7: CO total columns retrieved from SCIAMACHY by WFM–DOAS, averaged over the period June-July-August 2003. Only measurements above land, with a retrieval error lower than 60 are shown. High CO levels due to anthropogenic emissions in the northern hemisphere and to biomass burning in the southern hemisphere can be seen. From http://www.iup.physik.uni-bremen.de/sciamachy/

infrared between 3.74 and 15.4 μm, using several non-adjacent bands. It operates in a cross-track-scanning mode. The instruments on AQUA constitute all togeteher an advanced operational sounding system, which is dedicated in priority to derive clear-column air-temperature profiles and surface temperatures with high vertical resolution (1 km) and accuracy (1 K).

AIRS include channels in the CO fundamentals bands. Work is presently ongoing to retrieve CO columns from AIRS.

IASI:

The Infrared Atmospheric Sounding Interferometer (IASI) consists of a Fourier Transform Spectrometer with an imaging system. Three IASI instruments with 5 years nominal lifetime have been built. They are to be carried for a period of 15 years on the Metop-1, 2, and 3 weather satellites deployed as part of the future EUMETSAT Polar System (EPS), starting from April 2006.

IASI is a Michelson Interferometer, designed to measure the infrared spectrum emitted by the Earth and the atmosphere, from 645 to 2760 cm^{-1} at 0.5 cm^{-1} — apodized — spectral resolution and high radiometric quality. The footprint on the ground will be characterized by a circular pixel of 12 km of diameter, assembled in 4 pixels matrix. CO total column distributions are expected to be provided by IASI, with an estimated accuracy of 5–10% [20].

3.2.2 Retrieval of CO from SWIR radiances

Since the MOPITT SWIR channels failed to give the expected results, the only instrument to date that successfully used this spectral region to sound CO, CH_4 and CO_2, is the SCanning Imaging Absorption spectroMeter for Atmospheric CHartographY (SCIAMACHY) [23, 24]. SCIAMACHY was launched on the ENVISAT satellite in March 2002. It is a grating spectrometer that measures the scattered, reflected and transmitted solar radiation in the UV and the visible, with three additional channels in the SWIR, covering the 1–1.75 μm (10000–5714 cm^{-1}),

1.94–2.04 μm (5155–4902 cm^{-1}) and 2.26–2.38 μm (4424–4201 cm^{-1}) ranges. The SCIAMACHY spectral resolution in the lowest energy SWIR channel, where CO absorbs, is about 0.2 nm (0.4 cm^{-1}). The footprint size on the ground is 30 km $\times$ 120 km at nadir.

Measurements of CO from SCIAMACHY are reported in the scientific literature [25, 26]. It is demonstrated that the SWIR measurements provide a higher sensitivity towards CO in the boundary layer compared to the thermal infrared measurements. Serious calibration issues and the unavoidable blending of CO lines by the dominant CH_4 and H_2O contributions make, however, the retrieval of concentrations from SCIAMACHY difficult. The first results show that the retrieved CO total column compare reasonably with independent data, including those of MOPITT. Anthropogenic emission sources and biomass burning events have been successfully identified [25, 26] (Figure 7).

4 Theory and methodology

This section surveys the assessment methods used in the present study for characterizing the sensitivity of the IRS and UVS measurements to the tropospheric CO content, in different atmospheric conditions, including aerosol or cloud-contaminated scenes. The forward models and the associated inputs are briefly described in section 4.1. The theoretical approaches and parameters used for retrieving and characterizing the CO profile from the IRS-7 and UVS-SWIR bands are then given in sections 4.2 and 4.3, respectively. A more detailed description for the UVS assessment methods is given by O'Brien [9].

4.1 Forward model

4.1.1 Model atmospheres

Aerosol free scenes:

Four different model atmospheres have been generated for the purpose of this study, using the Model for OZone and Related Tracers (MOZART) [27, 28], to represent four typical CO vertical distributions. These profiles, plotted in Figure 8, correspond to the following emission scenarios, locations and dates:

- Biomass burning: Togo, 15^{th} of March
- Clean: Off the coast of Chili, 15^{th} of March
- Urban: Seoul, 15^{th} of March
- Transport: Off the coast of South Africa, 15^{th} of October

The four situations are characterized by different total CO abundances (columns varying between 1.05 and 4.37×10^{18} molecules cm^{-2}), as well as distinctive features as a function of altitude: while the 'urban' and 'biomass burning' profiles display high but rapidly decreasing CO concentration in the troposphere, the 'transport' profile shows a maximum at about 12 km. The 'clean' profile is more uniform, with little variation with altitude.

Also given in Figure 8 is a global annual mean CO profile obtained using MOZART. The latter is used throughout the characterization section (sections 5.1.1– 5.1.3), in conjunction with temperature and humidity profiles typical of a tropical atmosphere (high temperature — about 295 K at the surface — and humidity) or a mid-latitude atmosphere (low temperature — about 280 K at the surface — and moderate humidity) (Figure 9).

Aerosol containing scenes:

Four types of aerosols (biomass burning, urban, maritime and stratospheric aerosols) and clouds have been considered in this study. For each type, different vertical profiles have been applied, including several with most likely overstated high loads, which are used in order to get an indication of the largest possible effect. When available, the radiative properties of the aerosols were obtained from the CADAPA aerosol database [29]. The aerosol types and profiles are briefly described below.

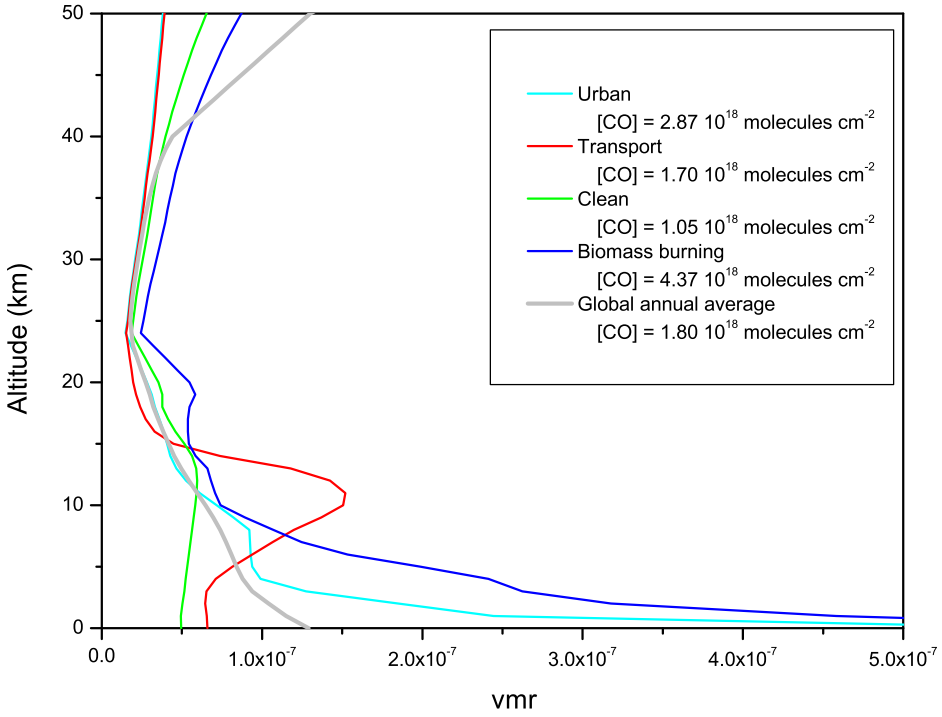

Figure 8: CO profiles for 4 selected model atmospheres and a global annual average.

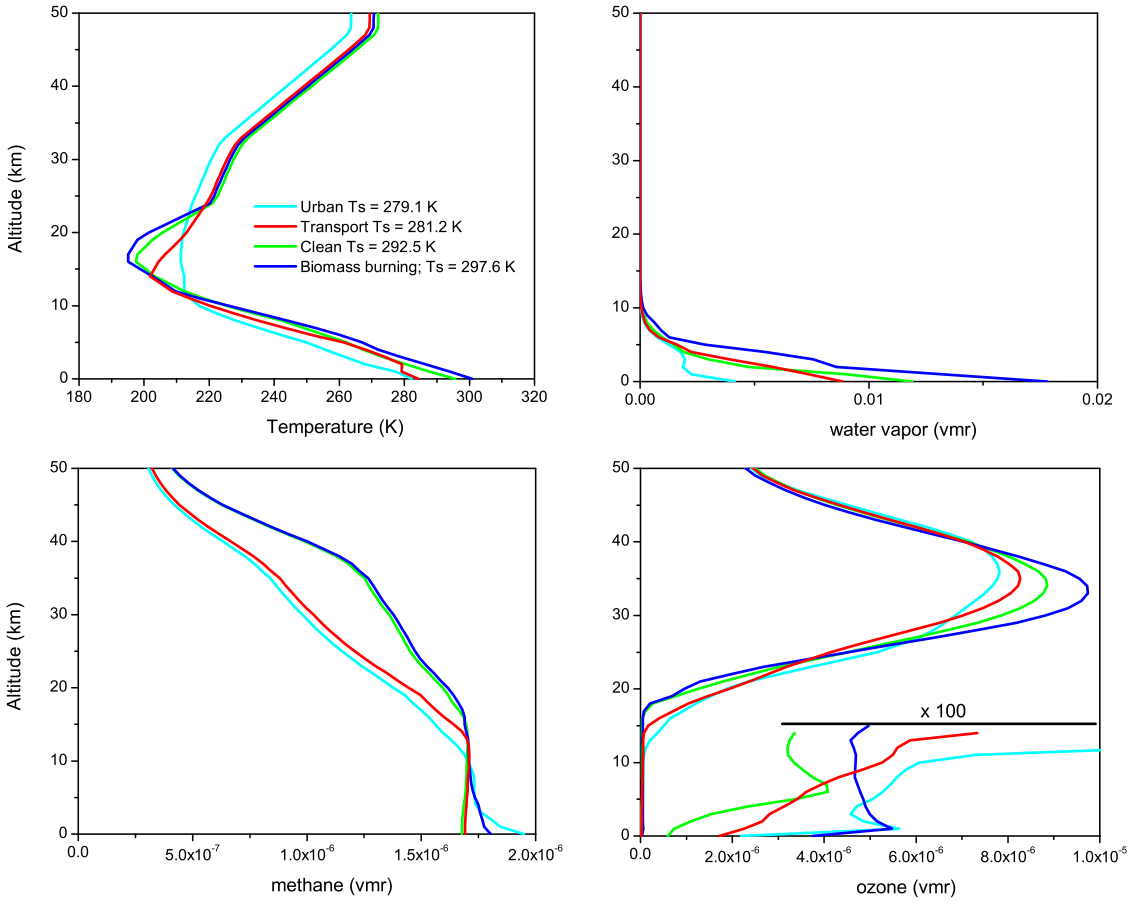

Figure 9: Temperature, humidity, methane and ozone profiles for the selected CO emission scenarios of Figure 8.

Urban aerosols

For the thermal infrared simulation, the urban aerosol radiative properties were those of the CADAPA aerosol type #12, which corresponds to the urban/industrial model of the WMO-112. Three scenarios were considered:
- a moderate scenario using the vertical profile of the LOWTRAN code for urban aerosol haze with a 5-km visibility and that includes aerosols up to an altitude of 3 km [30];
- a high scenario defined by doubling the concentration of the moderate one;
- a transported scenario for which the aerosol population is assumed to be transported from the boundary layer to higher altitude in the troposphere, between 4 and 7 km.

The first two scenarios are associated with the 'urban' CO emission scenario, while the last one is associated to the 'clean' CO emission scenario. In all cases, the aerosol properties are generated for a relative humidity of 70% below an altitude of 1 km, and 0% above.

For the SWIR simulations, the optical properties of urban aerosols were taken from [31]. In that case, urban aerosol was located in a narrow layer adjacent to the surface (0-1 km).

Maritime aerosols

The CADAPA aerosol types #10 or #17 have been considered and different scenarios defined:
- a LOWTRAN scenario based on the radiative properties and vertical profile of the LOWTRAN code for maritime aerosols [30] and which are defined in CADAPA as type #17;
- a moderate scenario with the same vertical profile but the CADAPA type #10 corresponding to the WMO-112 maritime aerosols;
- a high scenario defined by doubling the concentration of the moderate one.

The three scenarios are associated with the 'clean' CO emission scenario and their radiative properties are evaluated for a relative humidity of 70% below an altitude of 1 km, and 0% above.

Biomass burning aerosols

This aerosol population is modelled as a mixture of fine and coarse particles of both black and organic carbon. Based on compositions and size distributions of aerosols found in biomass burning plumes [32], the soot aerosols are assumed to include 8% of black carbon and to result in two log-normal size distributions with effective radius of 0.049 and 0.0981μm, respectively. The radiative properties are obtained using refractive indices extracted from the HITRAN database. Three scenarios are defined:
- moderate and high scenarios, the vertical profiles of which extend up to 5 km of altitude and are based on plume measurements taken during the SAFARI 2000 campaign [33, 34] ;
- a transported scenario based on simulations of fire emission transports [35].

The first two scenarios are associated with the 'biomass burning' CO emission scenario while the last one is associated to the 'clean' CO emission scenario.

Stratospheric aerosols

The CADAPA aerosol types #13 (WMO-112 background stratospheric aerosols) or #14 (WMO-112 volcanic aerosols) have been considered for the following scenarios:
- a moderate scenario combining the radiative properties of the CADAPA aerosol type #13 with the LOWTRAN profile for moderate background stratospheric aerosol load [30];
- a high scenario combining the same CADAPA type, but with the LOWTRAN profile for high background stratospheric aerosol load;
- a volcanic scenario combining the CADAPA aerosols type #14 with the LOWTRAN profile

for extreme background stratospheric aerosol load.

The three scenarios are associated with the 'clean' CO emission scenario.

Clouds

For the thermal IR simulations, only thin cirrus clouds have been considered. Their radiative properties are taken from the MODTRAN model of cirrus clouds [36] for the following scenarios:
- a low scenario, which uses the default profile of the MODTRAN model for cirrus cloud. The cirrus is located in a layer between 7 and 10 km;
- a moderate scenario, in which the cirrus cloud extends between 8 and 13 km;
- a high scenario, where the cirrus is modelled by two separated layers.

The 'clean' CO emission scenario is associated.

For the SWIR simulations, cloud water and cloud ice were taken from the ECMWF data base [37]. The profiles selected for this study are those indexed by 00295 (clear sky) and 01365 (thin layers of water cloud). The optical properties of water cloud, single scattering albedo, extinction coefficient and asymmetry parameter, were obtained using parameterizations developed by Hu and Stamnes [38] with an assumed effective radius r_e of 10μm. For ice clouds, parameterizations published by Key *et al.* [39] were used with r_e = 20μm. The scattering phase function of each cloud type was assumed to be that proposed by [40] with the calculated asymmetry parameter. For simulations with MOZART profiles, water clouds were located in the layers 1–2 km and 3–4 km, while an ice cloud was located in the layer 11–12 km. Urban aerosol was located in the layer adjacent to the surface (0–1 km), while a second water-soluble aerosol layer was located in the stratosphere (20–21 km). The properties of the aerosol layers were taken from [31].

4.1.2 General forward model equation

Given an a priori discretized atmosphere, the general forward radiative transfer equation, which relates the measured radiance to the true atmospheric state, is given by

$$\mathbf{y} = \mathbf{F}(\mathbf{x}; \mathbf{b}) + \boldsymbol{\epsilon}, \tag{2}$$

where $\mathbf{y}$ is the measurement vector containing measured radiances, $\mathbf{x}$ is the state vector containing the variables to be retrieved (*e.g.* atmospheric concentrations, surface temperature) and $\mathbf{b}$ represents all other model parameters having an impact on the measurement. $\boldsymbol{\epsilon}$ is the measurement noise and $\mathbf{F}$ is the forward radiative transfer function.

In the nadir mode, the radiance $\mathbf{y}$ that reaches the detector corresponds to the sum of the incident radiation, attenuated by the whole atmosphere, and the light emitted/scattered by each atmospheric layer, attenuated by the atmosphere remaining above it. In the thermal infrared the incident radiation is essentially that of the Earth surface's blackbody, whereas in the SWIR, it is dominated by the reflected/scattered sunlight.

A series of radiative transfer models have been used in this study to simulate MTG spectra in the IRS and the SWIR bands, depending also on whether the observed scene contains aerosols or not. They are summarized in Table 1, and briefly described below, separately for the two spectral regions of interest.

Table 1: Summary of the forward radiative transfer and retrieval software used for the study

Spectral domain	Scene	Forward model	Retrieval software and method
IRS	aerosol-free	Atmosphit	Atmosphit/OEM
	aerosol-free	LBLRTM	”
	aerosol containing	LBLRTM–CHARTS	”
SWIR	aerosol-free	LIDORT	DOAS
	aerosol containing	LIDORT	”

4.1.3 Model spectra in the IRS–7 band

In order to simulate spectra in the IRS–7 band, the forward model equation 2 is computed using high-resolution line-by-line radiative transfer models. The LBL Radiative Transfer Model [41, 42], eventually coupled to the multiple scattering model CHARTS [43] to include aerosols, is used to produce synthetic spectra, at the spectral resolutions and radiometric noises, described in section 2.2. These spectra are used as reference for the retrieval experiments, which use the Atmosphit sofware [17, 44, 45]. The latter, which relies on the Optimal Estimation Method (OEM) [4], is also used to characterize the retrievals, in terms of information content and error budget analyses. This choice is made to avoid possible biases due to model inconsistencies when doing the retrieval characterization.

For the forward calculations in IRS–7, the atmosphere is divided in 1km thick layers, from the ground to 100 km. The surface temperature was determined on the basis of the temperature of the first atmospheric layer, using a statistical relationship (random ΔT value added, with vanishing average and 4 K standard deviation). The emissivity was taken as one for all cases.

In both Atmosphit and LBLRTM, the synthetic spectra are computed from equation 2 using the line parameters (positions, intensities, broadening and shifting parameters, including their dependence on temperature) from the HITRAN 2000 database [46]. Both models also account for the absorption continua of water vapor, carbon dioxide, oxygen and nitrogen; for H_2O the MT-CKD formalism is used [42]. For the molecular lines, a Voigt line shape is used in each atmospheric layer.

In order to account for aerosols, LBLRTM was coupled to the high-resolution multiple scattering model CHARTS (version 4.0), which is a plane-parallel, monochromatic radiative transfer model with multiple scattering based on the adding-doubling method [43]. To be consistent with the reference model atmospheres, the CHARTS model has been slightly adapted in order to define the vertical profiles on a grid with 100 atmospheric layers, each of 1km width.

The high-resolution spectra computed using either LBLRTM or Atmosphit (aerosol-free scenes) and LBLRTM-CHARTS (aerosol-containing scenes) are ultimately processed to account for the instrument response, following the definition given by equation 1, and for the radiometric noise.

Figure 10 gives the LBLRTM spectra, for the four CO emission scenarios, at the different spectral resolutions. Figure11 shows examples of spectra simulated in the presence of aerosols,

at the highest spectral resolution. It is seen that the aerosols, which have radiative properties varying smoothly over the spectral range, affect the radiance uniformly.

4.1.4 Model spectra in the SWIR band

In this report, true spectra are taken to be those generated by LIDORT [47]. The true radiance at frequency ν_j is represented by L_j. Inputs to LIDORT are detailed profiles of chemical composition, temperature, cloud and aerosol. The profiles have either 60 or 100 layers, and are obtained from either the ECMWF data base described by [37] or from the MOZART scenarios described above. The ECMWF thermodynamic profiles are properly interpolated to the 1 km MOZART grid when appropriate.

The radiatively active gases included in the simulations are H_2O, CH_4, CO and N_2O, although the last is a very minor player in the spectral region considered. Optical properties of these gases were computed with the GENLN2 line-by-line program, using spectral line information from the HITRAN 2000 data base [46].

The line-by-line calculations were carried out with a resolution of 0.01 cm^{-1}. The solar and viewing zenith angles were fixed at 45° and 30°, respectively, while the relative azimuth was taken to be 0°, 90° and 180°. Only results for the case with relative azimuth 0° are presented in this report. The surface was assumed to a Lambertian reflector with albedo equal to 0.2, a relatively bright value, which not only helps to improve the SNR but also renders the scattering effects of thin cloud less important, so the results are likely to err towards optimistic.

The monochromatic radiances were filtered with a simulated instrument line-shape (ILS) function φ modelled by

$$\varphi(\nu) = (1-f)L_1(\nu) + fL_6(\nu), \tag{3}$$

where

$$L_1(\nu) = \frac{1}{\pi\alpha}\left(\frac{1}{1+(\nu/\alpha)^2}\right) \text{ and } L_6(\nu) = \left(\frac{6}{6+(\nu/\alpha)^2}\right)^{36}. \tag{4}$$

The parameter f controls the mixing of the two line shapes; a value of 0.99 was used. The Lorentz width α was chosen so that the resulting ILS has the prescribed FWHM. This model provides a good representation of the ILS of a grating spectrograph. Examples of monochromatic spectra and sampled spectra at various resolutions are shown in Figure 12, the purpose of which is to show that the structure of individual lines is washed out once the spectral resolution $\Delta\nu$ is greater than approximately 1 cm^{-1}. Figure 12 shows only a narrow subset of the CO band from 4220–4240 cm^{-1}, chosen because in this region there are CO lines that are relatively strong, yet not as contaminated by H_2O and CH_4 lines as elsewhere in the SWIR band of CO.

4.2 Characterization and retrieval methodology in IRS–7

4.2.1 General formulation of the inverse problem

The goal of the inverse problem is to determine the state vector from the measurement vector. Because some components of the state vector do not contribute to the measurement, this is an ill-conditioned problem, meaning that it has no unique solution. Therefore, in order to give a valid solution, the inversion has to be constrained or regularized with an additional source of information. The Optimal Estimation Method (OEM) [4] constrains the inversion with *a priori* information about the variables to be retrieved. This *a priori* information, composed of a mean *a priori* state, $\mathbf{x}_a$, and an *a priori* covariance matrix, $\mathbf{S}_a$, has to represent the best statistical knowledge of the state prior to the measurements. It should therefore be based on a 'real'

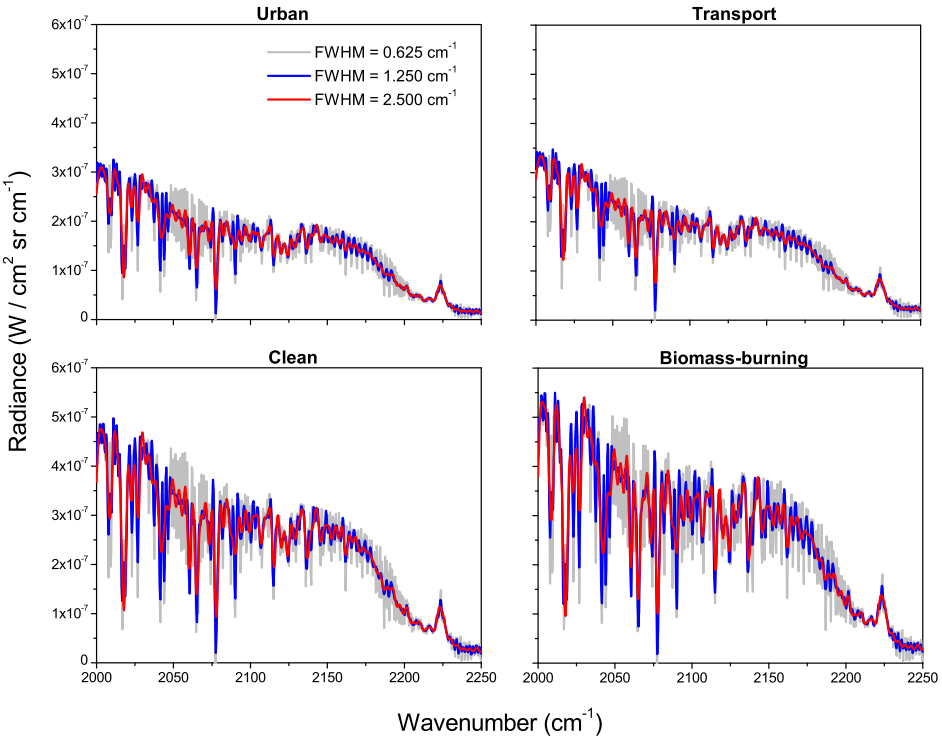

Figure 10: Synthetic spectra in the IRS–7 band, computed using LBLRTM for the four cloud- and aerosol-free model atmospheres, at the three specified spectral resolutions.

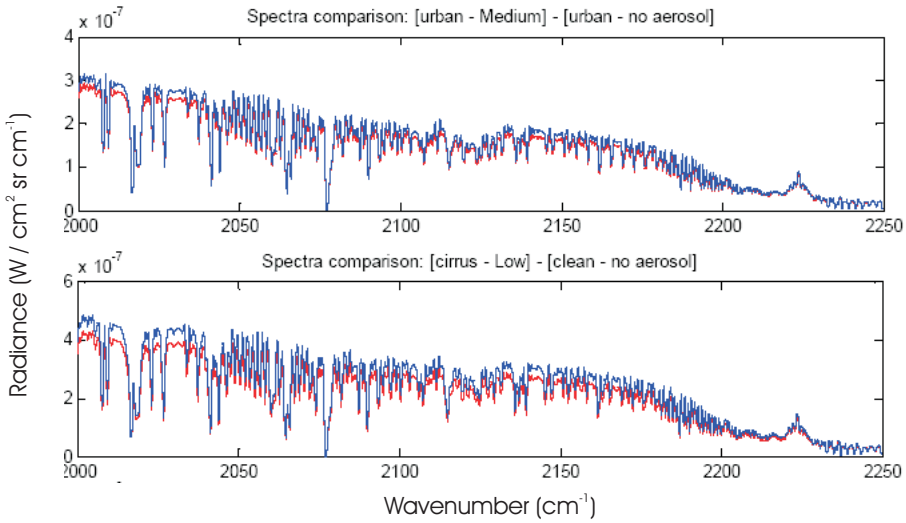

Figure 11: Impact of WMO-112 urban aerosols (CADAPA #12) in the boundary layer (top panel) and of thin cirrus cloud, located between 7 and 10 km (bottom panel), on the MTG-IRS–7 spectral radiance. The red and blue curves represent the spectra with and without aerosols, respectively.

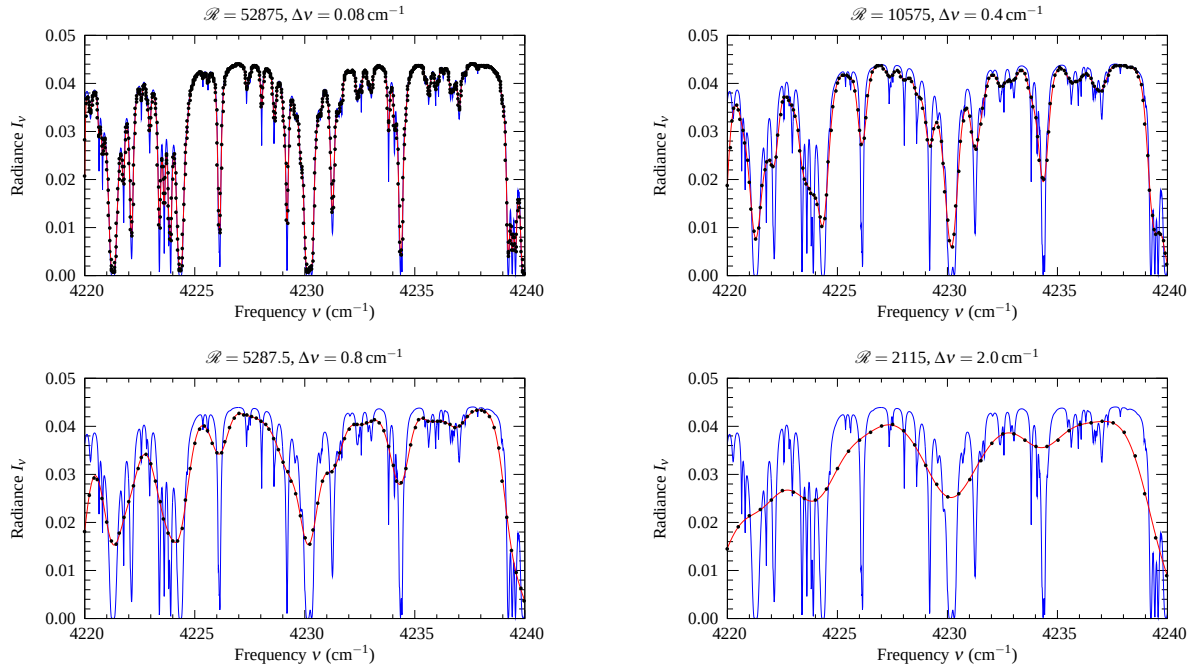

Figure 12: In each panel, the blue curve is a section of the monochromatic reflectance spectrum for a clear atmosphere with the urban CO profile, while the red curve is the result of convolution with the instrument line shape function. The dots represent samples, with four samples per full width at half height FWHM (over-sampling by four). The FWHM is denoted by $\Delta\nu$. The four panels have $\Delta\nu$ equal to 0.08, 0.4, 0.8 and 2.0 cm^{-1}.

ensemble of states coming from independent sources (*e.g.* climatology, other observations, atmospheric models).

For a linear problem, the retrieved state, solution of the OEM, is a combination of the measurement and the *a priori* state inversely weighted by their covariance matrices, and is given by [4]

$$\hat{\mathbf{x}} = (\mathbf{K}^T\mathbf{S}_\epsilon^{-1}\mathbf{K} + \mathbf{S}_a^{-1})^{-1}(\mathbf{K}^T\mathbf{S}_\epsilon^{-1}\mathbf{y} + \mathbf{S}_a^{-1}\mathbf{x}_a) \tag{5}$$

where $\mathbf{S}_\epsilon$ is the measurement covariance matrix, and $\mathbf{K} = \frac{\partial \mathbf{F}}{\partial \mathbf{x}}$ is the Jacobian of the forward model. The rows of $\mathbf{K}$ are the derivatives of the spectrum with respect to the retrieved variables.

In the case of a non-linear problem, as the retrieval of CO profiles, the Jacobian is a function of the retrieved state $\hat{\mathbf{x}}$ and the solution cannot be directly inferred from Equation 5. For the retrieval experiments presented in section 5.1.4, an iterative Gauss-Newton method is used instead. At the i+1 iteration, the state vector is then given by

$$\begin{aligned}\hat{\mathbf{x}}_{i+1} = \mathbf{x}_a \quad + \quad & (\mathbf{K}_i^T\mathbf{S}_\epsilon^{-1}\mathbf{K}_i + \mathbf{S}_a^{-1})^{-1}\mathbf{K}_i^T\mathbf{S}_\epsilon^{-1} \\ & [\mathbf{y} - \mathbf{F}(\hat{\mathbf{x}}_i) + \mathbf{K}_i(\hat{\mathbf{x}}_i - \mathbf{x}_a)]\end{aligned} \tag{6}$$

where $\mathbf{K}_i = \frac{\partial \mathbf{F}}{\partial \mathbf{x}}(\hat{\mathbf{x}}_i)$. The iteration procedure is stopped when the absolute difference between the radiances modelled at the two last iteration steps, $|\mathbf{F}(\hat{\mathbf{x}}_{i+1}) - \mathbf{F}(\hat{\mathbf{x}}_i)|$, is less than a fraction (20%) of the measurement noise. Convergence is generally achieved after less than five iterations, and tightening the convergence criterion does not produce significant changes in the retrieved profiles.

4.2.2 Information content analysis

Since the inverse problem is not strongly non-linear, we can use the linear approximation to characterize the retrievals [4]. For a linear retrieval, the retrieved state can be written as

$$\hat{\mathbf{x}} = \mathbf{x}_a + \mathbf{A}(\mathbf{x} - \mathbf{x}_a) + \mathbf{G}(\boldsymbol{\epsilon} + \mathbf{K}_b(\mathbf{b} - \hat{\mathbf{b}})), \tag{7}$$

where $\hat{\mathbf{b}}$ is the approximate vector of model parameters available to the user. The Jacobian, $\mathbf{K}_b = \frac{\partial \mathbf{F}}{\partial \mathbf{b}}$, characterizes the sensitivity of the forward model $\mathbf{F}$ to the model parameters. The gain matrix, $\mathbf{G}$, is the matrix whose rows are the derivatives of the retrieved state with respect to the spectral points. It is defined by

$$\mathbf{G} = \frac{\partial \hat{\mathbf{x}}}{\partial \mathbf{y}} = (\mathbf{K}^T \mathbf{S}_\epsilon^{-1} \mathbf{K} + \mathbf{S}_a^{-1})^{-1} \mathbf{K}^T \mathbf{S}_\epsilon^{-1}. \tag{8}$$

The averaging kernel matrix, $\mathbf{A}$, sensitivity of the retrieved state to the true state, is the product of the gain matrix by the Jacobian matrix,

$$\mathbf{A} = \frac{\partial \hat{\mathbf{x}}}{\partial \mathbf{x}} = \mathbf{G}\mathbf{K}. \tag{9}$$

The element $\mathbf{A}(i, j)$ is the relative contribution of the element $\mathbf{x}(j)$ of the true state to the element $\hat{\mathbf{x}}(i)$ of the retrieved state. The vertical resolution of the retrieved profile can be defined as the Full Width at Half Maximum (FWHM) of the rows of the averaging kernel matrix. The number of independent elements of information contained in the measurement can also be estimated as the Degrees Of Freedom for Signal (DOFS), defined as the trace of the averaging kernel matrix [4].

4.2.3 Error budget equations

In the linear approximation, the total error is computed from the linear retrieval equation (Equation 7) as the difference between the true state and the retrieved state:

$$\hat{\mathbf{x}} - \mathbf{x} = (\mathbf{A} - \mathbf{I})(\mathbf{x} - \mathbf{x}_a) + \mathbf{G}\boldsymbol{\epsilon} + \mathbf{G}\mathbf{K}_b(\mathbf{b} - \hat{\mathbf{b}}) + \mathbf{A}_{\mathbf{x}\tau}(\tau - \tau_a) \tag{10}$$

It can be decomposed in four terms:

(a) The smoothing error, $(\mathbf{A} - \mathbf{I})(\mathbf{x} - \mathbf{x}_a)$, accounts for the smoothing of the true state by the averaging kernels. The covariance matrix of the smoothing error is given by:

$$\mathbf{S}_s = (\mathbf{A} - \mathbf{I})\mathbf{S}_a(\mathbf{A} - \mathbf{I})^T \tag{11}$$

(b) The measurement error, $\mathbf{G}\boldsymbol{\epsilon}$, is due to the instrumental noise. Its covariance matrix is given by:

$$\mathbf{S}_m = \mathbf{G}\mathbf{S}_\epsilon\mathbf{G}^T \tag{12}$$

(c) The model parameters error, $\mathbf{G}\mathbf{K}_b(\mathbf{b} - \hat{\mathbf{b}})$, accounts for the imperfect knowledge of the model parameters. The covariance of this error term is given by:

$$\mathbf{S}_p = \mathbf{G}\mathbf{K}_b\mathbf{S}_b(\mathbf{G}\mathbf{K}_b)^T \tag{13}$$

Where $\mathbf{S}_b$ is the covariance matrix representing the uncertainty on the forward model parameters.

(d) The cross-state error, $\mathbf{A}_{\mathbf{x}\tau}(\tau - \tau_a)$ quantifies how the uncertainty on fitted model parameters reverbates on the error in the retrieved target quantity. The covariance of this error is:

$$\mathbf{S}_{cs} = \mathbf{A}_{\mathbf{x}\tau}\mathbf{S}_\tau {\mathbf{A}_{\mathbf{x}\tau}}^T \tag{14}$$

where $\mathbf{S}_\tau$ is the uncertainty on the fitted parameters. For the present retrievals, only the surface temperature is systematically fitted alongside CO and thus introduces a cross-state error. In some cases, water vapor is also considered as a fitted parameter, as discussed next.

The total error covariance matrix is then given by:

$$\mathbf{S}_T = \mathbf{S}_s + \mathbf{S}_m + \mathbf{S}_p + \mathbf{S}_{cs} \tag{15}$$

4.2.4 Retrieval parameters

Microwindow selection

In the IRS–7 band, the only significant molecular contributions to the atmospheric spectra presented in Figure 10 are due, in addition to CO, to H_2O, CO_2, O_3, N_2O, and OCS (Figure 13). The micro-window that has been selected here for the sensitivity studies and the CO retrievals extends from 2142 to 2185 cm^{-1}. It is chosen such as to minimize the interferences of other species, while keeping the relevant information from the spectra. This micro-window includes notably 26 out of the 30 channels taken into account for the operational retrieval of CO columns from IASI [20].

A priori profile and covariance matrix

The *a priori* profile and correlation matrix used for the characterization of the retrievals are depicted in Figure 14. They have been generated using the MOZART model [27, 28]: the *a priori* profile is a global annual mean profile and the covariance matrix represents the yearly spatial and temporal variability of CO.

For the retrieval experiments (section 5.1.4), the *a priori* profiles, used as initial guesses, have been set to represent more closely the targetted atmospheric state: they have been constructed from the MOZART profiles by considering monthly hemispheric means (Figure 15).

Measurement covariance matrix

The $\mathbf{S}_\epsilon$ covariance matrix is a diagonal matrix of σ^2 elements. In the following analyses, σ is strictly taken as the value of the measurement noise. It will be shown in the results section that a pseudo-noise, introduced by uncertainties on the model parameters, makes in some situations the total noise to be larger than considered in the calculations. As unstable effects on the characterization and retrievals can be caused by such an underestimation of the σ^2 elements, some care has to be taken in analysing the results falling in the regime where pseudo–noise becomes important.

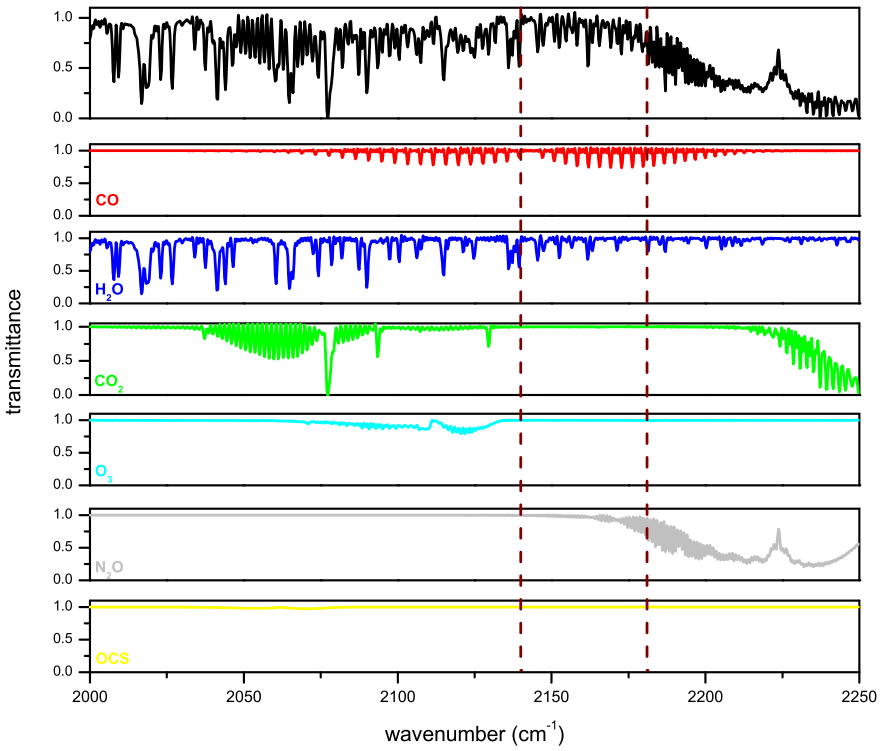

Figure 13: IRS–7 spectrum for the clean scenario (top panel) and associated individual molecular contributions. The dotted vertical lines show the limits of the selected micro-window for the CO retrieval in IRS–7.

4.3 Characterization and retrieval methodology in SWIR

4.3.1 General formulation of the assessment methods

The principal difficulty facing the proposed CO measurements is that the SWIR band of CO lies beneath stronger bands of H_2O and CH_4 (see Figure 1). While the difficulty is intuitively clear, it may be made quantitative with the following simple calculations. In the SWIR, where Rayleigh scattering is weak and the optical thickness of aerosol generally is small, the radiance I reflected from a cloud-free atmosphere is given approximately by

$$I = \frac{F}{\pi} \cos\theta_i \; R \, e^{-m\tau},$$

where F is the solar flux density at the top of the atmosphere, R is the surface reflectance, θ_i and θ_r are the solar and satellite zenith angles, m is the air-mass factor

$$m = \sec\theta_i + \sec\theta_r,$$

and τ is the absorption optical thickness of the atmosphere. As a first approximation,

$$\tau = \sum_g \tau_g \qquad \text{with} \qquad \tau_g = u_g k_g,$$

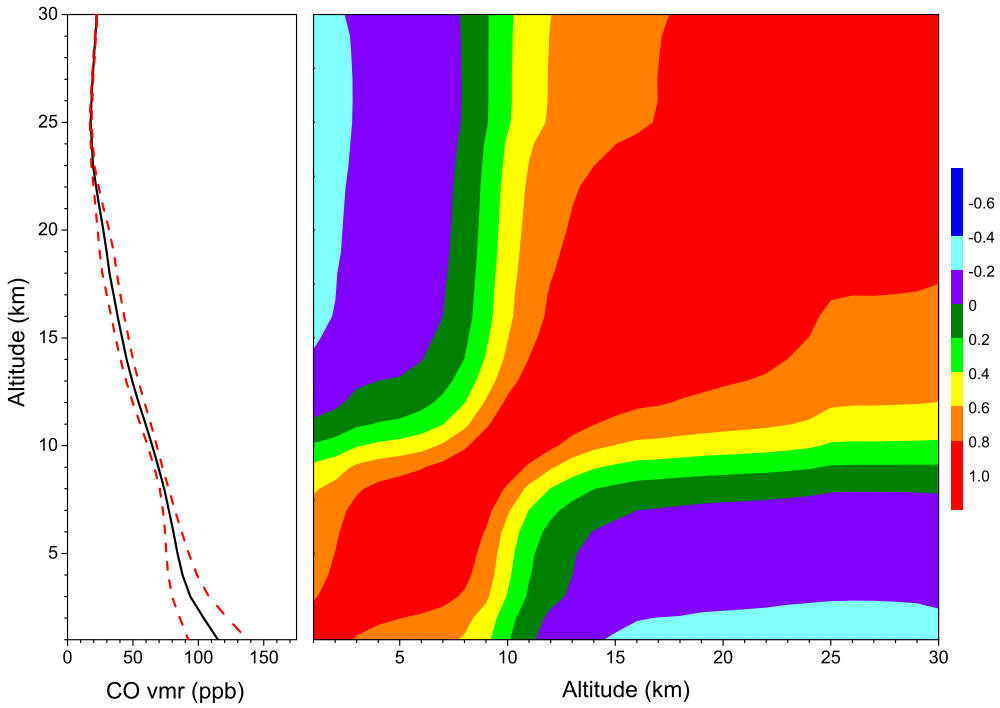

Figure 14: *A priori* CO profile (left panel) and associated correlation matrix, in relative units, (right panel) used for the characterization of retrievals (section 5.1.1– 5.1.3). The red dotted lines in the left panel represent the variability extracted from the MOZART covariance matrix.

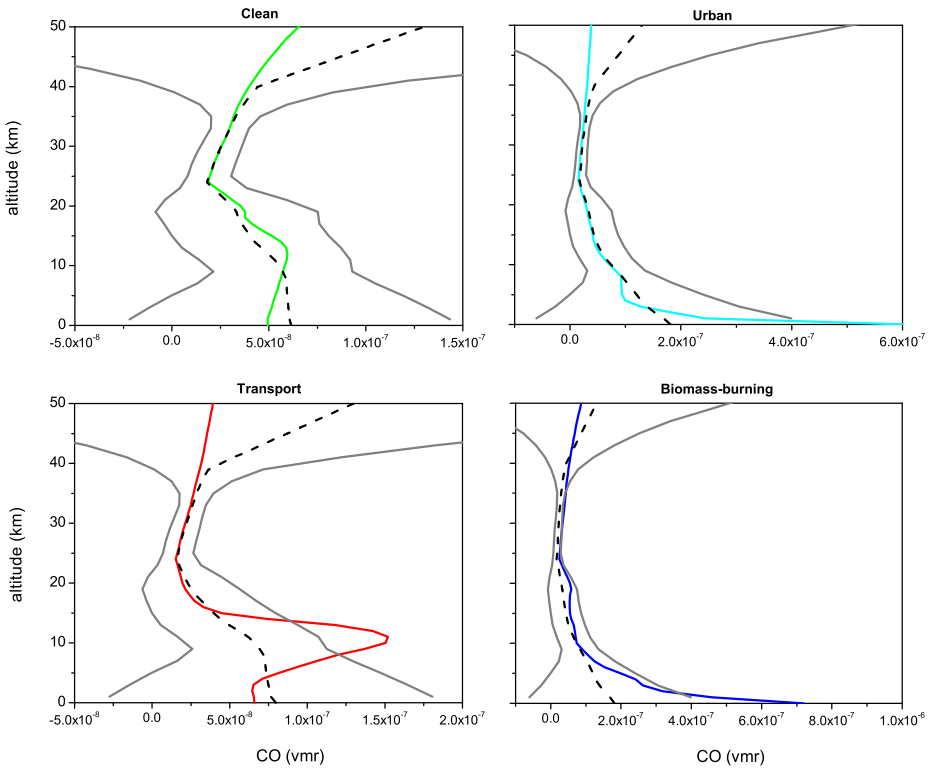

Figure 15: MOZART *a priori* CO profiles used for the retrieval experiments on the four model atmospheres (section 5.1.4). The gray lines represent the 3σ variability extracted from the MOZART covariance matrix

where τ_g is the optical thickness of the absorbing gas indexed by g, k_g is the corresponding absorption coefficient and u_g is the column mass density (in mol m^{-2}). Thus, the sensitivity of the radiance to gas g is

$$\frac{\partial I}{\partial u_g} = -mk_g I,$$

from which it follows immediately that

$$u_g \frac{\partial I}{\partial u_g} = -mu_g k_g I = -m\tau_g I. \tag{16}$$

Thus, we should expect that the sensitivities of the spectra to the trace gases will be in proportion to their optical thicknesses. As shown in Figure 1, the monochromatic optical thickness of CO is orders of magnitude smaller than those of H_2O and CH_4. The change in radiance ΔI produced by changes Δu_{H_2O} and Δu_{CO} in the column mass densities of H_2O and CO will be given to first order by

$$\Delta I = \left(\frac{\partial I}{\partial u_{H_2O}}\right) \Delta u_{H_2O} + \left(\frac{\partial I}{\partial u_{CO}}\right) \Delta u_{CO},$$

which may be recast trivially into the form

$$\Delta I = \left(u_{H_2O} \frac{\partial I}{\partial u_{H_2O}}\right) \left(\frac{\Delta u_{H_2O}}{u_{H_2O}}\right) + \left(u_{CO} \frac{\partial I}{\partial u_{CO}}\right) \left(\frac{\Delta u_{CO}}{u_{CO}}\right).$$

Using the sensitivity from equation (16), we see that the fractional change in the radiance is

$$I^{-1}\Delta I = -m\tau_{H_2O} \left(\frac{\Delta u_{H_2O}}{u_{H_2O}}\right) - m\tau_{CO} \left(\frac{\Delta u_{CO}}{u_{CO}}\right). \tag{17}$$

Equation (17) shows that two scenarios with different profiles of H_2O and CO will produce the same radiance if

$$\left(\frac{\Delta u_{CO}}{u_{CO}}\right) = -\frac{\tau_{H_2O}}{\tau_{CO}} \left(\frac{\Delta u_{H_2O}}{u_{H_2O}}\right). \tag{18}$$

Alternatively, equation (18) gives the error in CO required to mask the error in the radiance caused by an error in H_2O. We see that the relative error in H_2O is magnified by the ratio τ_{H_2O}/τ_{CO}, which is very large. Consequently, tiny errors in u_{H_2O}, the column mass density of H_2O, or the absorption coefficient k_{H2O} of H_2O will cause large relative errors in u_{CO}, the column mass density of CO. Similar observations apply to CH_4.

The practical consequence of this observation is that the column mass densities of H_2O, CH_4 and CO must be estimated simultaneously, which adds considerably to the complexity of the error analysis. In this report, quantitative assessment of the feasibility of measuring CO is provided in three ways.

(a) The first involves a series of case studies with increasing complexity to illustrate the biases and errors that can arise. Each case involves inverting simulated data to estimate scale factors for the column mass densities of H_2O, CO and CH_4, along with four other parameters that account for the components of the spectrum that vary slowly with frequency, such as surface albedo, Rayleigh scattering, cloud and aerosol. Figure 16 is typical of the results; large errors in CO are likely unless the spectral resolution is chosen in a very narrow range.

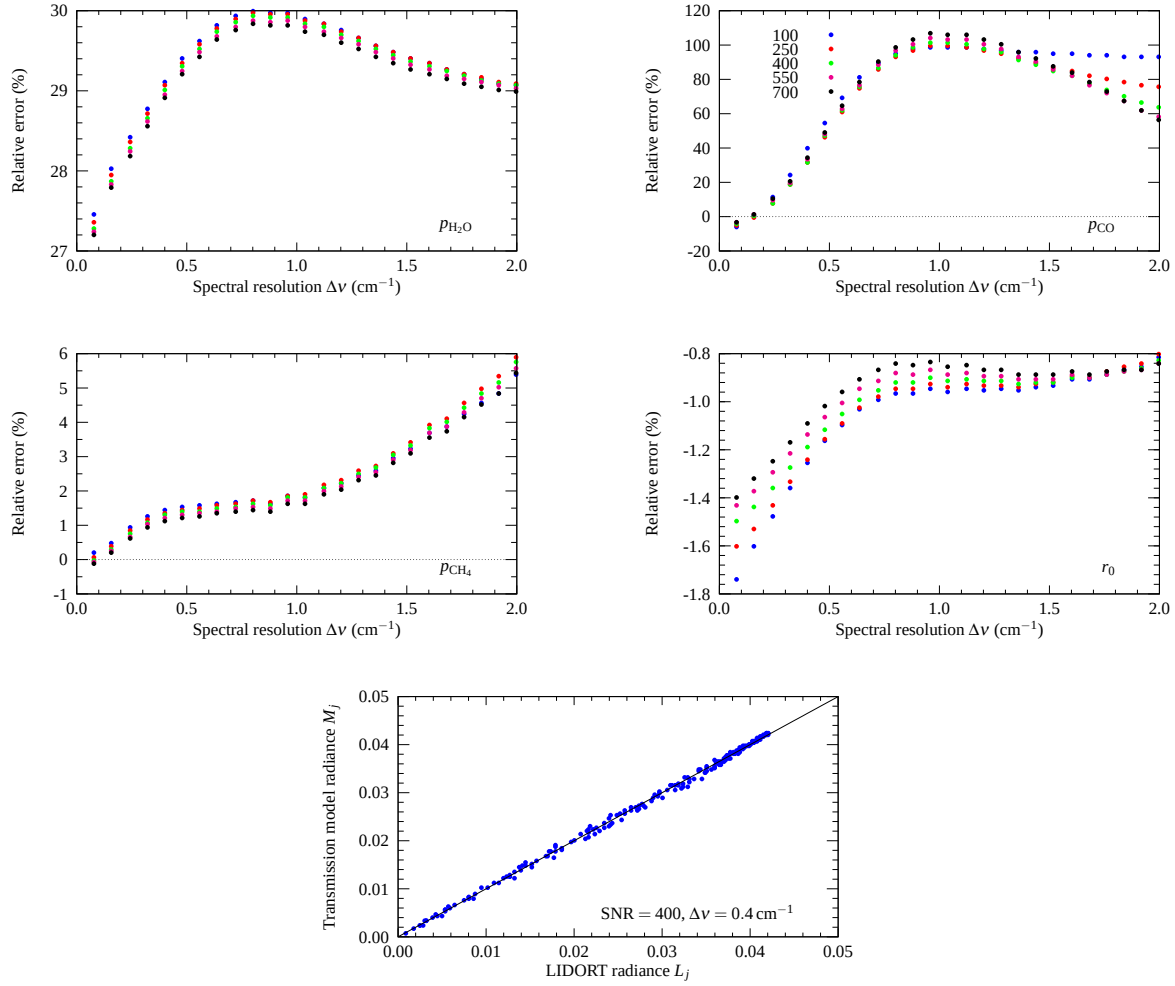

Figure 16: The top four panels show the errors in the scaling factors ($p_{\mathrm{H_2O}}$, p_{CO} and $p_{\mathrm{CH_4}}$) for the mass densities of the trace gases and the apparent albedo (r_0). The atmosphere assumed in the inversion is clear with the clean CO scenario, whereas the simulated spectrum was generated using an atmosphere with thin cloud (optical thickness $\tau_C \approx 0.15$), a different thermodynamic profile and the clean CO scenario. The prior estimate of the scaling factor for CO differs from the true value by a factor of two. Each panel has results for five values of SNR; the common legend is contained in the panel for CO. The bottom panel is a scatter plot of 'true' radiances from LIDORT and the fitted radiances from the inversion algorithm for the case where the SNR is equal to 400 at the reference albedo of 5% and the spectral resolution is $0.4\,\mathrm{cm}^{-1}$.

(b) The second assessment examines the random errors and biases using the methods of Bayesian estimation, as advocated by [4]. This analysis requires statistics of the errors in the measurements and the model parameters, as well as prior information about the atmospheric state, the latter consisting of estimates of the mean and covariance of the ensemble of states in the real world.

(c) The third approach uses Monte Carlo simulation; noisy spectra are submitted to an inversion algorithm, similar in principle to the DOAS algorithm. This approach allows the bias and random errors in the estimated parameters to be assessed without the ambiguity introduced by the assumption that the prior mean is the true mean of the ensemble.

4.3.2 Retrieval parameters

Microwindow selection

In the SWIR band of CO, the absorbing species are H_2O, CO and CH_4, with the optical thickness of CO generally much smaller than those of H_2O and CH_4.[1] A narrow window of the SWIR band was selected, spanning 4220–4240 cm^{-1}, where absorption by CO is stronger and the structure of H_2O and CH_4 lines is less complicated, as shown in Figure 17. Even in this window, the CO lines are weaker than those of H_2O and CH_4, but the distinctive regularity of the spacing is likely to assist in distinguishing the CO component of the spectrum. There are similar windows elsewhere within the SWIR band, but the results for such windows are unlikely to differ from those obtained here.

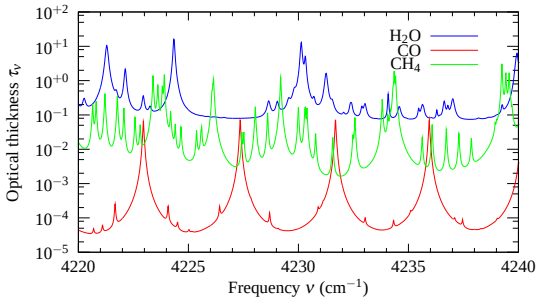

Figure 17: Monochromatic spectra of optical thickness for H_2O, CO and CH_4 in a clean atmosphere.

In addition to the error analysis using the selected spectral window, simulations with the full band 4180–4320 cm^{-1} were conducted, leading to very similar conclusions. A selection of the full band results is presented in an appendix of the attached report by [9], where full details of the SWIR calculations and results may be found.

[1] N_2O also is a minor absorber in the SWIR band of CO. However, its contribution in the nominated window is negligible.

5 Results

5.1 Retrieval of CO from IRS–7

5.1.1 Sensitivity to the atmospheric state variables

Surface properties

In the nadir mode, the surface temperature controls the amount of thermal infrared radiation at the top of the atmosphere. It is a crucial parameter to take into account in the measurements, as it impacts directly on the signal-to-noise ratio of the spectra and hence on the quantities that can be retrieved, in terms of information content and errors. This effect has been highlighted from the analysis of both MOPITT [13] and IMG measurements [17].

Figure 18 illustrates the effect for the MTG–IRS measurements at 0.625 cm^{-1}, by plotting the $\mathbf{K}/\epsilon$ values calculated in the 2142–2185 cm^{-1} micro-window, for surface temperatures of 295 and 280 K. It is observed that the higher the surface temperature, the higher the sensitivity to CO, at all altitudes, including the lower troposphere.

The surface emissivity affects the radiance at the top at the atmosphere in a similar way but, as it varies only little on the globe, its impact from scene to scene will be relatively limited.

Temperature and humidity profiles

The net effect of the upper air temperature and water vapor profiles onto the radiances measured at the top of the atmosphere is shown in Figure 19, which gives the radiance error for the two parameters, for the best spectral resolution (FWHM = 0.625 cm^{-1}). The radiance error is calculated according to:

$$\mathbf{y}_{error} = \mathbf{K_b}\epsilon_\mathbf{b} \tag{19}$$

where $\epsilon_\mathbf{b}$ are the uncertainties on the temperature and humidity profiles. 1.5 K and 10% have respectively been considered for the uncertainties on the two parameters. The 1.5 K value exceeds somewhat the expectations of next-generation meteorological sounder (1 K accuracy with 1 km vertical resolution) and should therefore be considered as a worst case scenario. On the contrary, the 10% accuracy on the humidity profile matches the expectations from the operation of next-generation meteorological sounders.

From Figure 19, it is seen that the radiance error exceeds 1 10^{-9} W / (cm^2 sr cm^{-1}) at almost all wavenumbers. At the best spectral resolution, the impact on well-isolated CO lines (e.g. at 2158.3 or 2169.2 cm^{-1}) of the uncertainty on the temperature profile is larger than that of the humidity profile. When H_2O lines are closely located to the CO lines (e.g. at 2150.4 or 2172.6 cm^{-1}), both errors contribute significantly. The radiance error can reach up to about 3 10^{-9} W / (cm^2 sr cm^{-1}) in the worst situation, where CO and H_2O lines overlap. At the coarser spectral resolutions (FWHM = 1.250 and 2.500 cm^{-1}), the CO and H_2O lines become blurred together at all wavenumbers, and the radiance errors due to the temperature and humidity profile uncertainties contribute over the entire spectral region.

The important conclusion that can be drawn at this point is that temperature and water vapor profile uncertainties generate a pseudo-noise on the IRS spectra, which is of the same order of magnitude as the measurement noise. The accuracy at which these parameters will

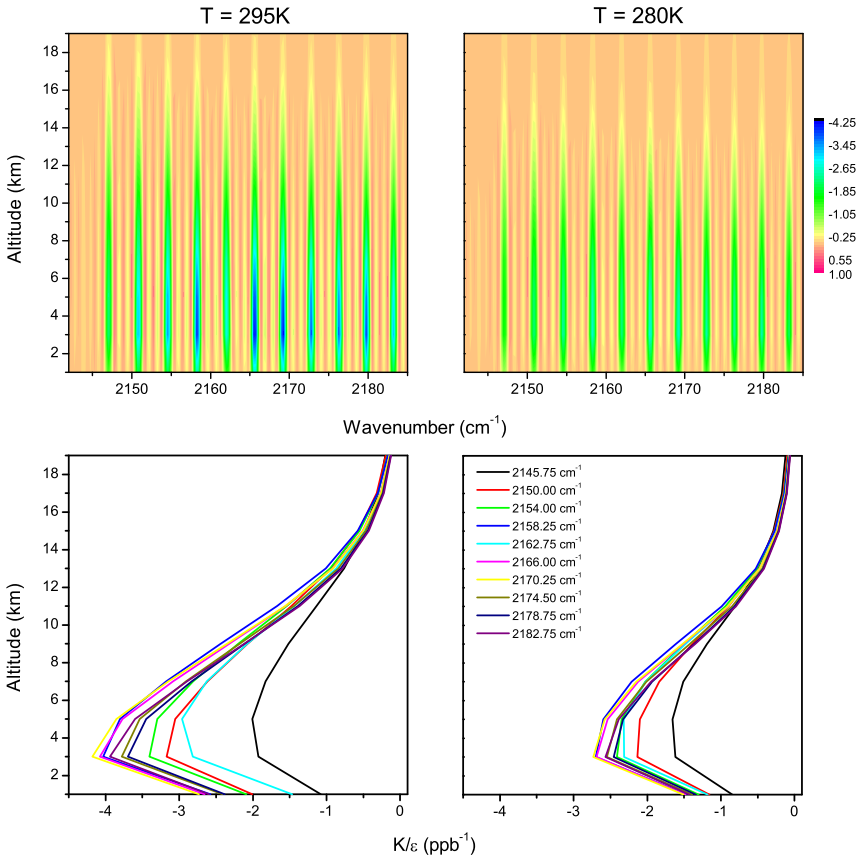

Figure 18: Whitened jacobians ($\mathbf{K}/\epsilon$) for CO (units of vmr), calculated for the entire micro-window selected in IRS–7 (2142-2185 cm^{-1}). The calculations were made with the global annual mean MOZART profile, at the highest spectral resolution (FWHM = 0.625 cm^{-1}) and radiometric noise of 2.5 $\times 10^{-9}$ W / (cm^2 sr cm^{-1}). The surface temperature is 295 K (tropical atmosphere, left panel) and 280 K (Northern mid-latitude atmosphere, right panel).

be measured by MTG is therefore important in assessing the radiometric performances of IRS. For instance, considering 1.5 K and 10% for the uncertainties on the temperature and humidity profiles, respectively, suggests that it is not worth achieving radiometric performances better than 1 10^{-9} W / (cm^2 sr cm^{-1}) at the best spectral resolution (FWHM = 0.625 cm^{-1}). The value increases by a factor 2–3 as the resolution degrades.

5.1.2 Sensitivity to the instrumental performances

Spectral resolution

Degrading the spectral resolution of the IRS worsens the sensitivity to the CO measurement, at all altitudes. This can be seen by comparing the Jacobians calculated in the 2142–2185 cm^{-1} micro-window, for the three reference spectral resolutions (FWHM = 0.625 cm^{-1}, 1.250 cm^{-1}, 2.500 cm^{-1}) (Figure 20). Obviously, the information becomes especially poor at the coarser spectral resolution, where the CO lines are blurred together and to the adjacent H_2O lines.

Further analysis of the averaging kernels (Figure 21), calculated at the two extreme spectral resolutions, for CO partial columns corresponding to the lower troposphere (0-6 km), upper troposphere (6-12 km) and UTLS (12-18 km), as well as the total troposphere (0-12 km) and total columns, shows that:

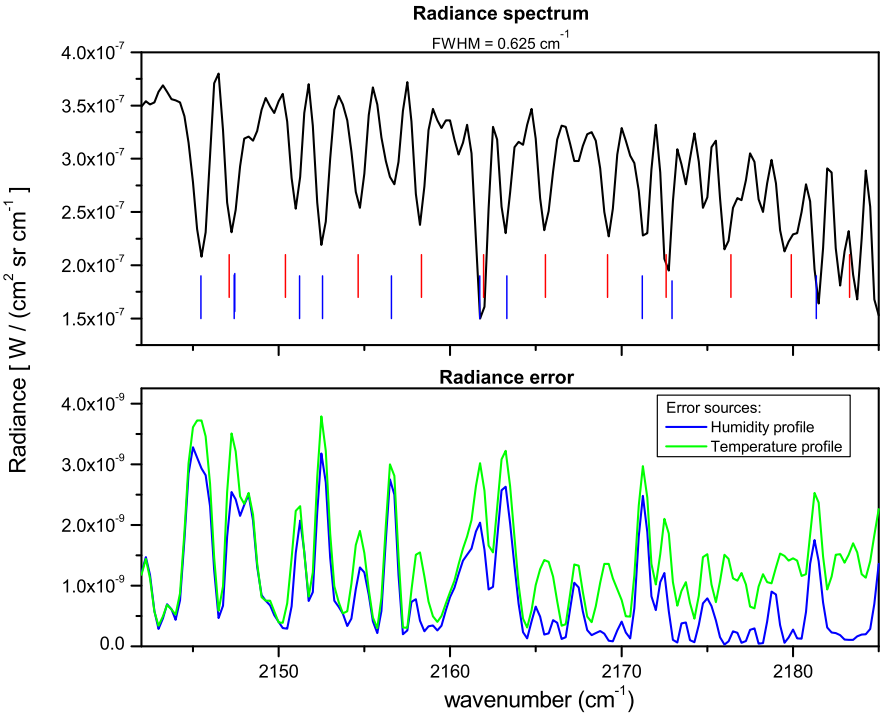

Figure 19: Radiance spectrum (top) in the 2142-2185 cm^{-1} micro-window, at a resolution of 0.625 cm^{-1}, and radiance error (bottom) due to uncertainties on the temperature (1.5 K) and the humidity profile (10%). The spectrum was calculated with the global annual mean MOZART CO profile and the temperature and water vapor profiles of the biomass burning scenario. The position of the main CO and H_2O lines are marked on the top panel by red and blue lines respectively.

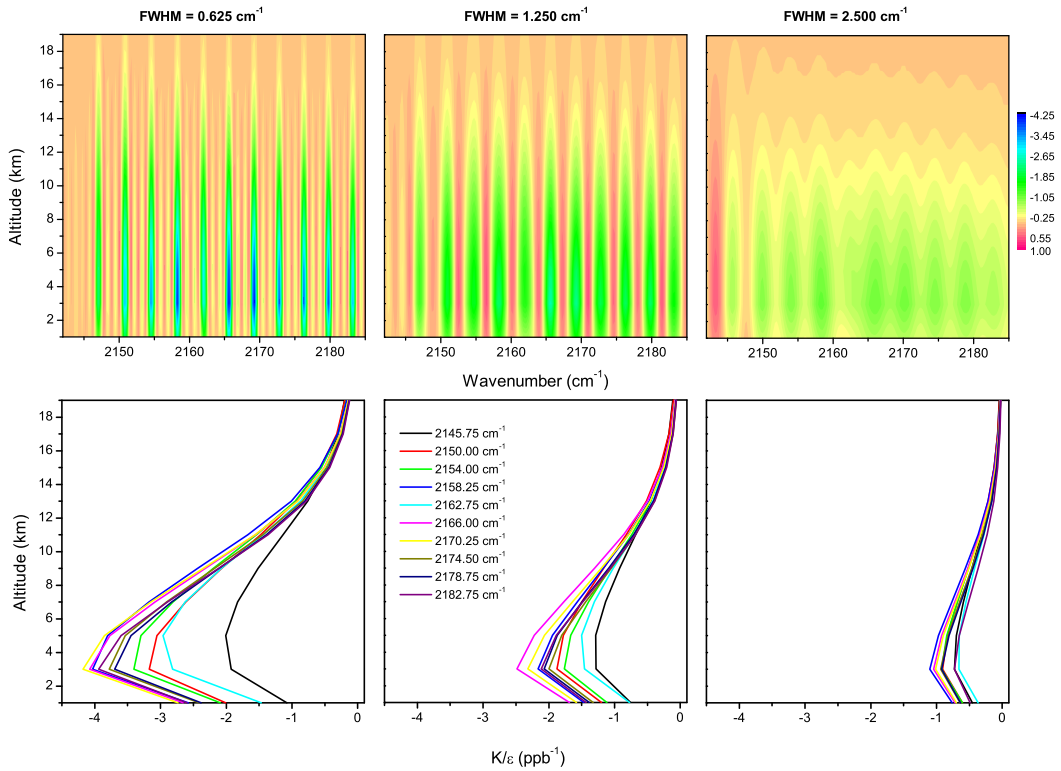

Figure 20: Same as Figure 18, for surface temperature of 295 K, and at different spectral resolutions.

- At the best spectral resolution (FWHM = 0.625 cm^{-1}), the information can be separated between contributions from the lower and upper troposphere. The measurements also provide some information on the UTLS.

- At the coarser spectral resolution (FWHM = 2.500 cm^{-1}), the measurements do not contain information on the vertical distribution of CO.

- In all cases, the information is maximum in the free troposphere.

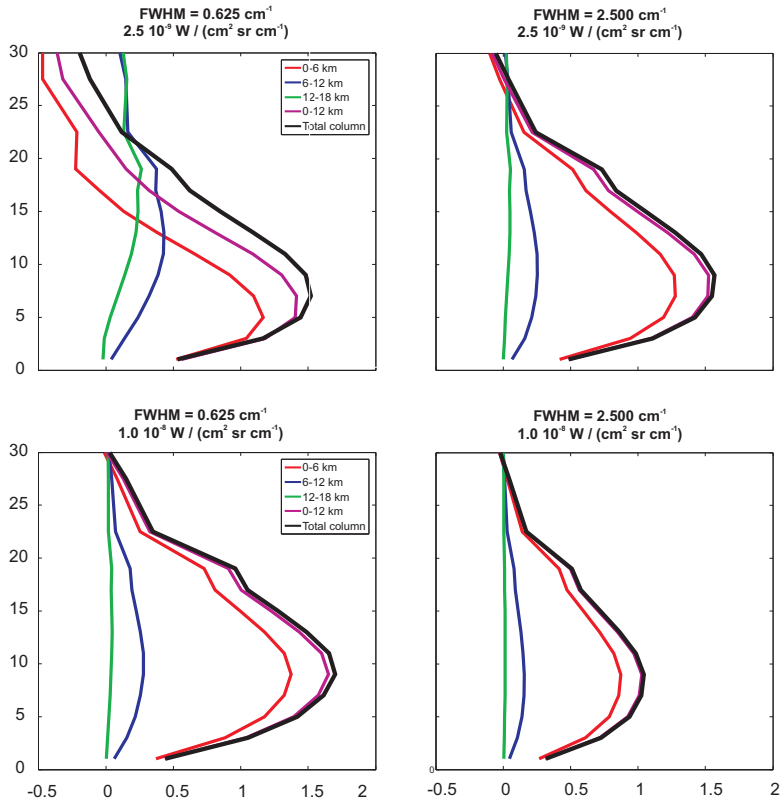

Figure 21: Averaging kernels for CO partial columns for a radiance spectrum with FWHM = 0.625 cm^{-1} (left panel) and FWHM = 2.500 cm^{-1} (right panel), for radiometric noise of 2.5 10^{-9} W / (cm^2 sr cm^{-1}) and 1.0 10^{-8} W / (cm^2 sr cm^{-1}). The CO profile is the global annual mean. Water vapor and temperature profiles are from the 'clean' scenario.

Measurement noise

The impact of the radiometric noise can also partly be established by examining the averaging kernels. They are plotted for illustration at the best spectral resolution in Figure 21, for low (2.5 10^{-9} W / (cm^2 sr cm^{-1})) and high (1.0 10^{-8} W / (cm^2 sr cm^{-1})) noise. As for the spectral resolution, it is seen that high noise values induce a loss of vertical information.

The results show thus that lower and upper tropospheric CO columns can be separated to a certain extent only with an infrared sounder combining sufficiently high spectral resolution and good radiometric performances. This has obviously to be mitigated as a function of the measured absolute radiance and thus the surface temperature, as discussed above. Figure 22 offers a summary of the impact of the instrumental performances to the vertical sensitivity of the CO

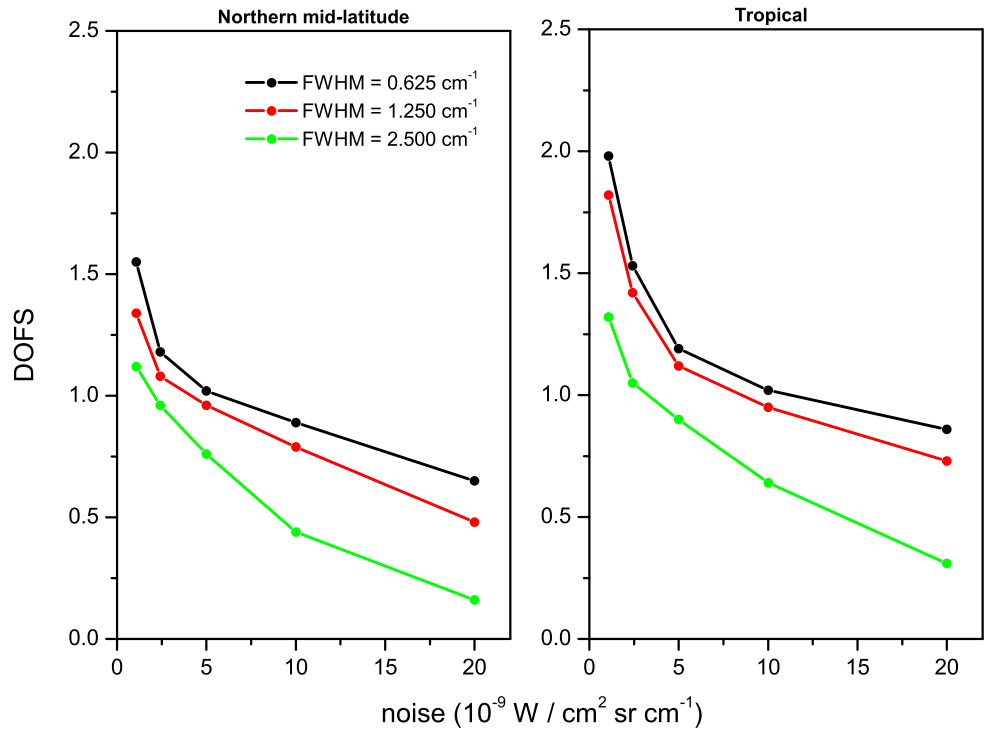

Figure 22: Degrees of freedom for signal, as function of radiometric noise and spectral resolution. The values refer to the global annual mean MOZART profile, for two reference atmospheres, corresponding to the northern mid-latitudes (T_s=280 K, moderate humidity) and tropical (T_s=295 K, large humidity) scenes.

retrievals, by reporting the DOFS for different noise values and spectral resolution, for tropical (high temperature and humidity) and northern mid-latitude atmospheres (moderate temperature and humidity). It is calculated that:

- For relatively high surface temperatures (295 K), the DOFS reaches 2 in the best cases but drops rapidly below 1.5 when the noise exceeds about 3 10^{-9} W / (cm^2 sr cm^{-1}).
- In case of a lower surface temperature (280 K), the measurements contain more than a single piece of information only if the spectral resolution is high and the measurement noise low.
- At the coarser spectral resolution, one can hardly extract more than one independent piece of information.

5.1.3 Global error budget

The total error (equation 15) can be expressed as the sum of the retrieval error (smoothing and measurements error) and of the errors introduced by uncertainties in the model parameters. In the 2142–2185 cm^{-1} micro-window, which we have selected in order to minimize interferences due to O_3 and to a lesser extent N_2O, the main uncertainties to be considered in the error budget

are those on the surface properties (surface temperature and emissivity) and on the temperature and humidity profiles[2].

In order to quantify the different sources of errors, and how they relate to the radiometric noise and the spectral resolution, the following uncertainties on the model parameters have been considered: 10% on the water vapor profile and 1.5 K on the upper-air temperature profile, 2 K on the surface temperature and 5% on the Earth's emissivity. The surface temperature is fitted along with the CO profile.

The following series of figures provides a detailed view of the error budget. Figures 23–26 show the total error for the northern mid-latitude (280 K surface temperature) and tropical scenes (295 K surface temperature) as a function of the spectral resolution and the radiometric noise; the results are given for the CO total column and tropospheric (0–12 km) column, and separately for the lower tropospheric (0–6 km) and upper tropospheric (6–12 km) columns. Figures 27–29 separates the individual error contributions from the total error, for the two typical atmospheres, at the highest spectral resolution. Here the results are given for the CO total column, tropospheric (0–12 km) and lower tropospheric (0–6 km) columns. Figures 30–32 provides similar plots, but for the northern mid-latitude case only, as a function of the spectral resolution[3]. Figure 33 gives finally an illustration of the error profile, for selected instrumental performances.

The analysis of the different figures reveals the following:

- At low noises, the errors on the total and partial columns (Figures 23–26) are larger for the tropical reference atmosphere than for the Northern mid-latitude reference atmosphere, although the former is characterized by higher surface temperature and hence contains more information. The explanation for this result can be found in Figures 30–32, which shows that the error generated by uncertainties on the water vapor profile dominate the budget at low noises for the very humid tropical atmosphere as compared to the moderately humid northern mid-latitude atmosphere. As expected, the impact of the humidity is especially marked at the coarser spectral resolution, with errors that even exceed the *a priori* variability.

- For all partial columns and most instrumental performances (exception being the coarse spectral resolution / low noise of the tropical atmosphere) the total error is significantly smaller than the CO natural variability. This gives evidence that the retrieval allows to reduce the *a priori* uncertainty on the CO profile.

  Despite this, it is seen from Figures 23–26 that the chemistry requirements are met only in some situations. In particular the threshold (10%) accuracy on the measurement of the CO tropospheric (0-12 km) column is reached or close to be reached for noise levels smaller than 5 10^{-9} W / (cm^2 sr cm^{-1}) and spectral resolution not exceeding 1.25 cm^{-1}

[2]Aerosols, which attenuate radiation uniformly in the IRS–7 band are also likely to contribute. Because the Atmosphit software used in the characterization does not account for aerosols in the computation of the radiative transfer, their impact on the retrievals of the CO vertical profiles is assessed by means of 'retrieval experiments'. The results are presented in section 5.1.4.

[3]In the figures 23–32, the results for radiometric noise values lower than 4 10^{-9} W / (cm^2 sr cm^{-1}) fall in the regime where pseudo-noise, due to the uncertainties on the temperature and humidity profiles (see Figure 19), are likely to contribute significantly. As it cannot be excluded that unstable results are obtained in this regime, the corresponding region of low noises has been highlighted by a gray dashed area.

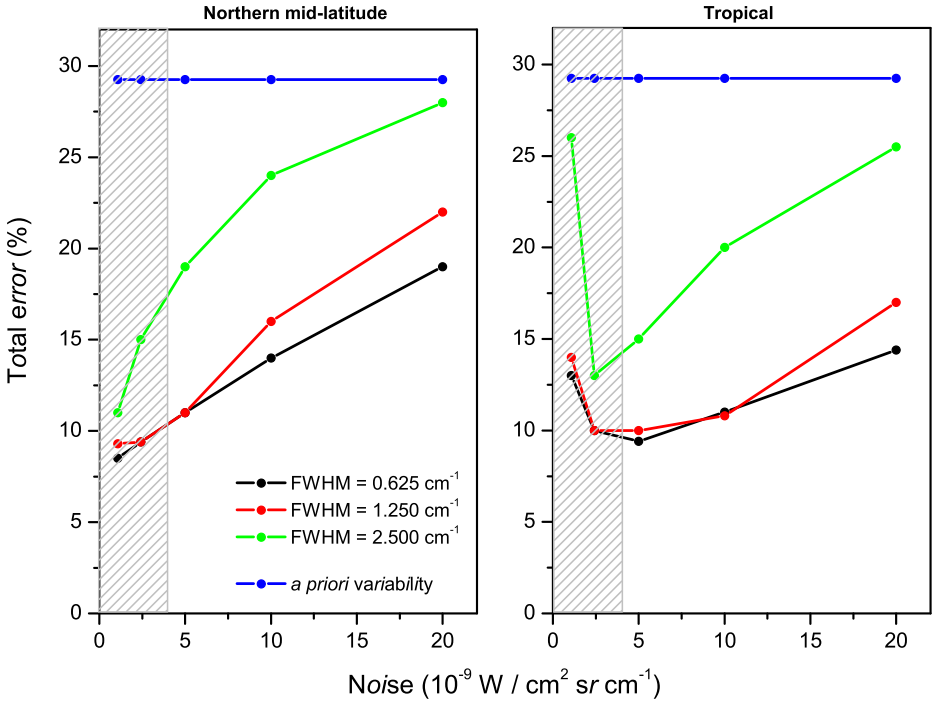

Figure 23: Total errors on the CO total column, as function of radiometric noise and spectral resolution. The values refer to the global annual mean MOZART profile, for two reference atmospheres, corresponding to the northern mid-latitudes (T_s=280 K, moderate humidity) and tropical (T_s=295 K, large humidity) scenes. The blue curve gives the *a priori* MOZART variability.

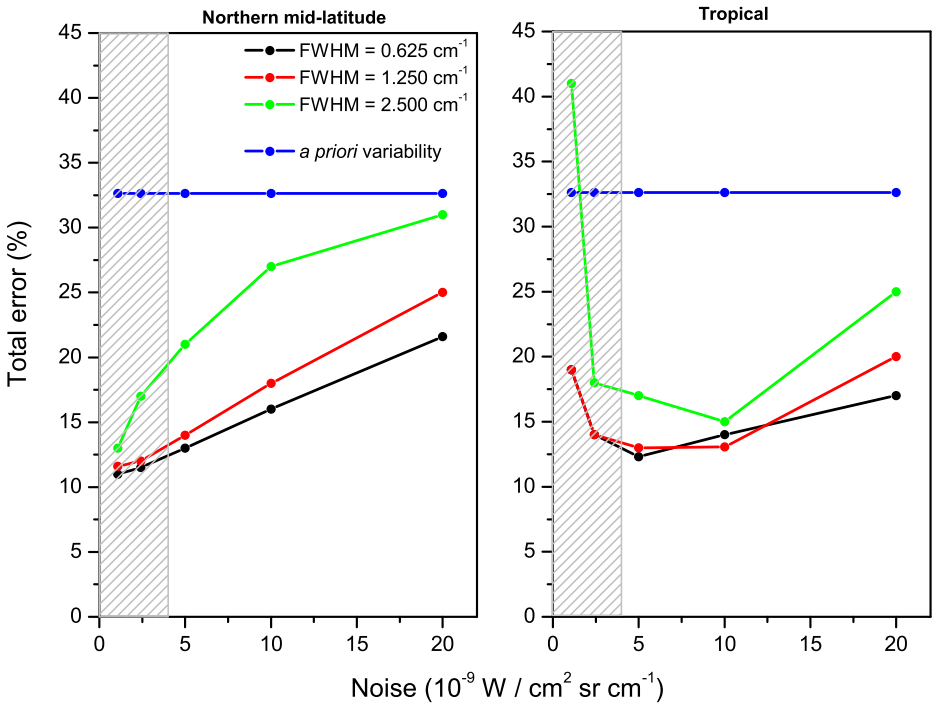

Figure 24: Same as Figure 23 for the tropospheric (0-12 km) column.

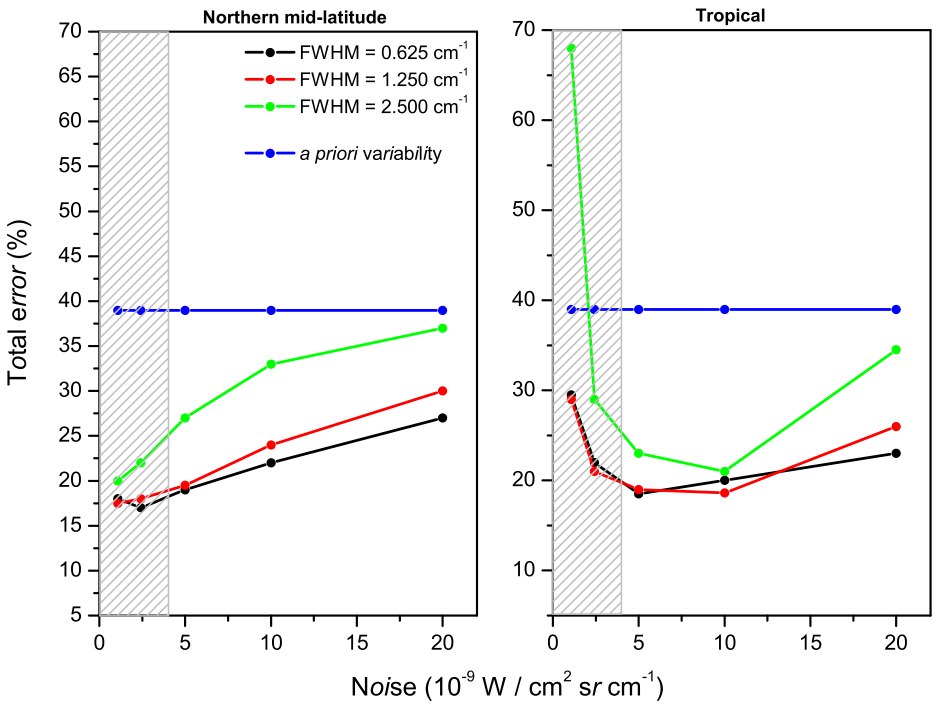

Figure 25: Same as Figure 23 for the lower tropospheric (0-6 km) column.

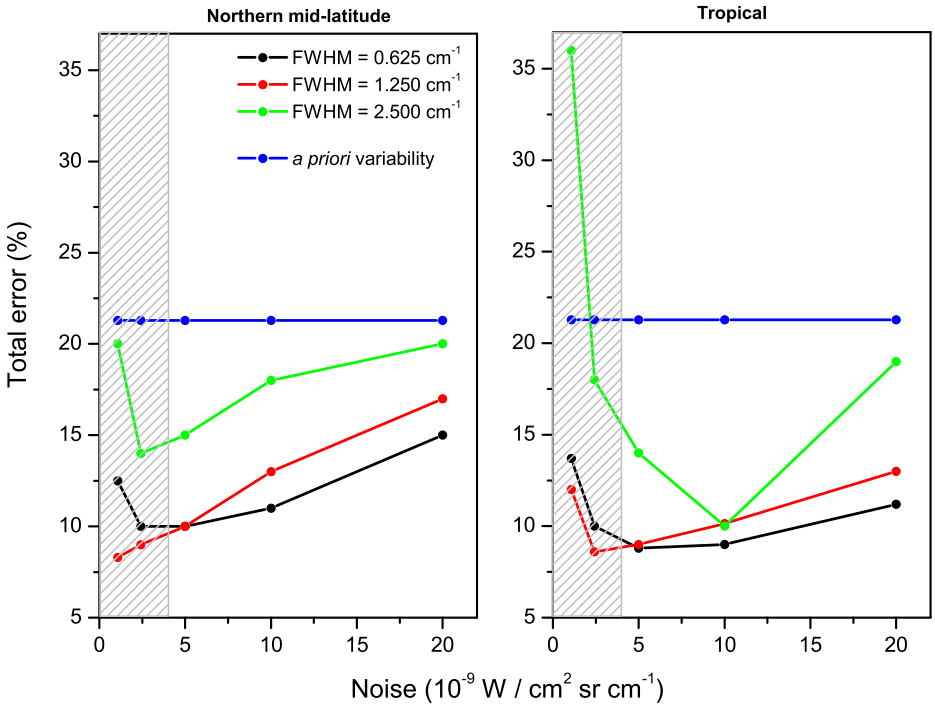

Figure 26: Same as Figure 23 for the upper tropospheric (6-12 km) column.

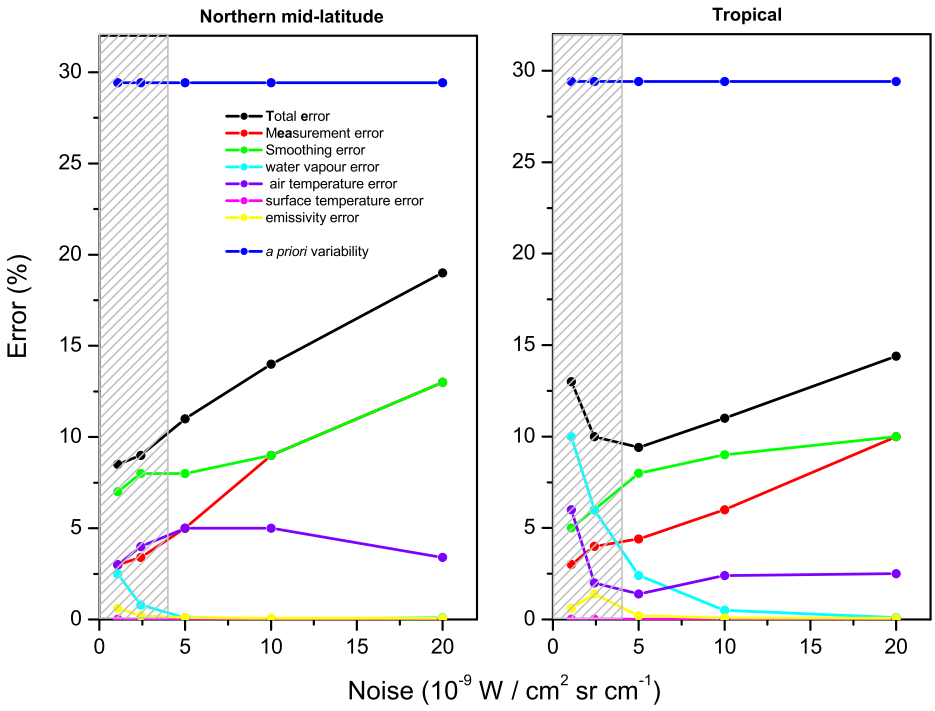

Figure 27: Error budget for CO total column retrieval. The values refer to the global annual mean MOZART profile, for two reference atmospheres, corresponding to the northern mid-latitudes (T_s=280 K, moderate humidity) and tropical (T_s=295 K, large humidity) scenes. The spectral resolution is 0.625 cm^{-1}.

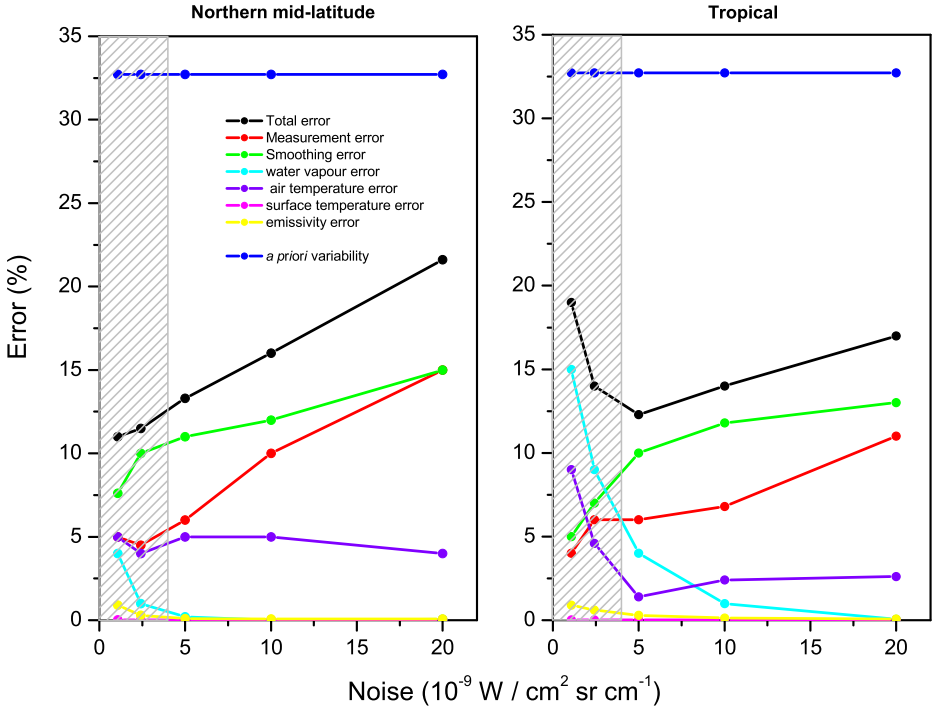

Figure 28: Same as Figure 27 for the tropospheric (0-12 km) column.

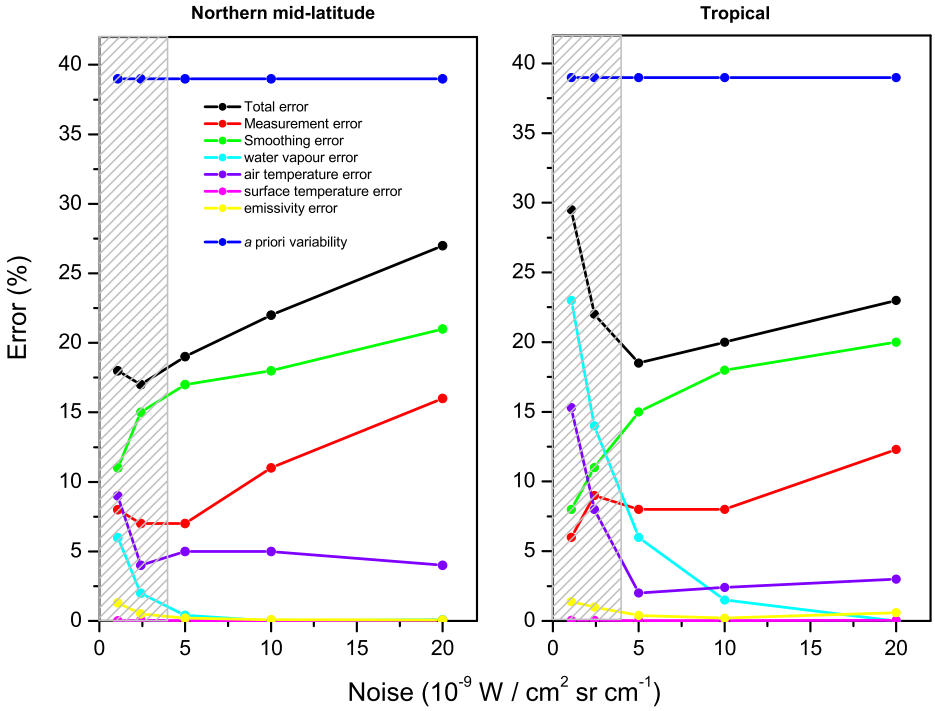

Figure 29: Same as Figure 27 for the lower tropospheric (0-6 km) column.

(Figure 24). Furthermore, the goal (5%) accuracy for the tropospheric measurements can not be achieved with the assumptions made. It is not excluded that this goal be reached, at very low noises, and provided that the temperature profile is known to better than 1.5 K.

With noise levels smaller than 5 10^{-9} W / (cm^2 sr cm^{-1}), the measurement of the lower tropospheric column (0-6 km) can also be made with about 15–20% accuracy (Figure 25).

- For noise levels lower than 5 10^{-9} W / (cm^2 sr cm^{-1}), the difference between the best (FWHM = 0.625 cm^{-1}) and medium (FWHM = 1.250 cm^{-1}) spectral resolution is relatively limited.

- Figures 27–29 show that at the highest spectral resolution and for radiometric noise larger than 5 10^{-9} W / (cm^2 sr cm^{-1}), smoothing is the dominant source of error. Logically the measurement error plays an increasing role as the noise increases. The relative contributions of smoothing and measurement error is largest for the 0–6 km partial column, due to a weaker sensitivity of the measurements towards the surface and a larger *a priori* variability.

  At lower noise values, the errors introduced by uncertainties on the temperature and humidity profile contribute significantly. As stated above, this is especially the case for the humid tropical atmosphere. On the contrary, the errors due to the surface properties (surface temperature and emissivity) are negligible.

  Degrading the spectral resolution (Figures 30–32) increases most sources of errors. The errors related to the uncertainties on the model parameters (temperature and humidity profiles) become especially large at the coarser spectral resolution.

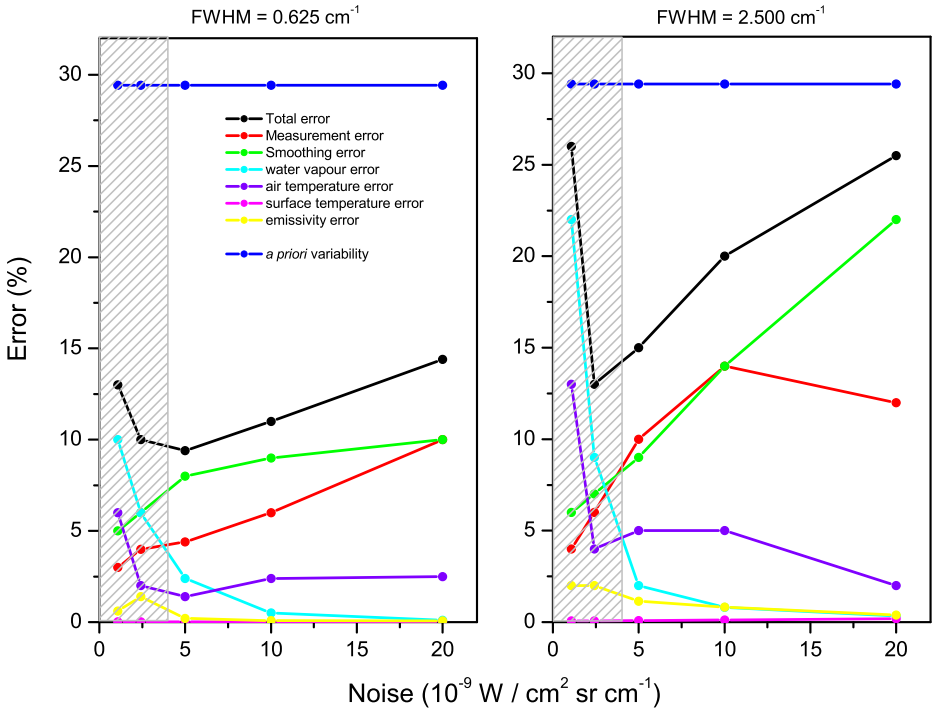

Figure 30: Error budget for CO total column retrieval. The analysis is performed for the MOZART reference mean profile, and the tropical reference atmosphere. Results for the two extreme spectral resolutions (FWHM = 0.625 cm^{-1} and 2.500 cm^{-1}) are given.

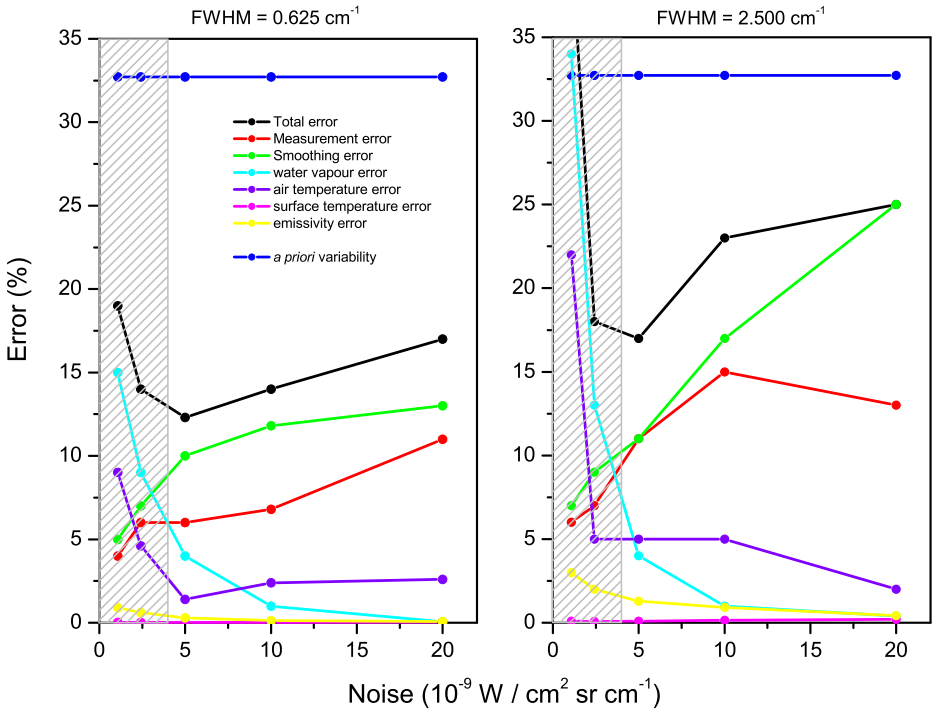

Figure 31: Same as Figure 30 for the tropospheric (0-12 km) column.

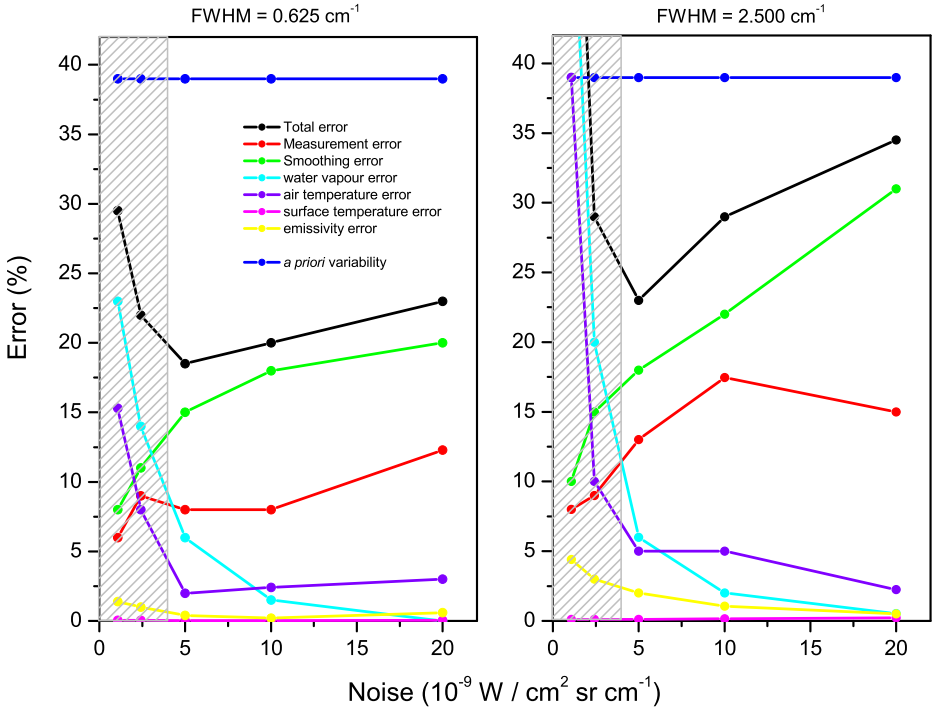

Figure 32: Same as Figure 30 for the lower tropospheric (0-6 km) column.

- The analysis of the error profile shows that in the best case (FWHM = 0.625 cm^{-1} and low noise), the thermal infrared measurements provide information from the ground to 12 km, with the highest sensitivity between 3 and 8 km (Figure 33). The measurements rapidly loose information, at all altitudes, as the resolution or the radiometric noise performances are degraded.

5.1.4 Retrieval experiments

The aim of the retrieval experiments is to illustrate the capabilities of MTG-IRS to monitor CO by approaching situations that will be encountered during operation. This section describes the result of retrieval experiments made on the model spectra described in section 4.1.3.

The retrieval experiments are performed on the set of model spectra obtained using LBLRTM, for the aerosol-free atmosphere, or LBLRTM-CHARTS, for the aerosol-containing atmosphere. The synthetic spectra were randomly modified to account for the radiometric noise, as well as for uncertainties on the temperature and water vapor profiles. In order to allow for a statistical representation of the results, the perturbations in the radiometric noise, the temperature and water vapor profiles were repeated five times, for each atmospheric scenario and each spectral resolution.

In the retrieval experiments, the CO profile is retrieved along with the surface temperature. Aerosols are not taken into account and are thus compensated for by the other fitted parameters.

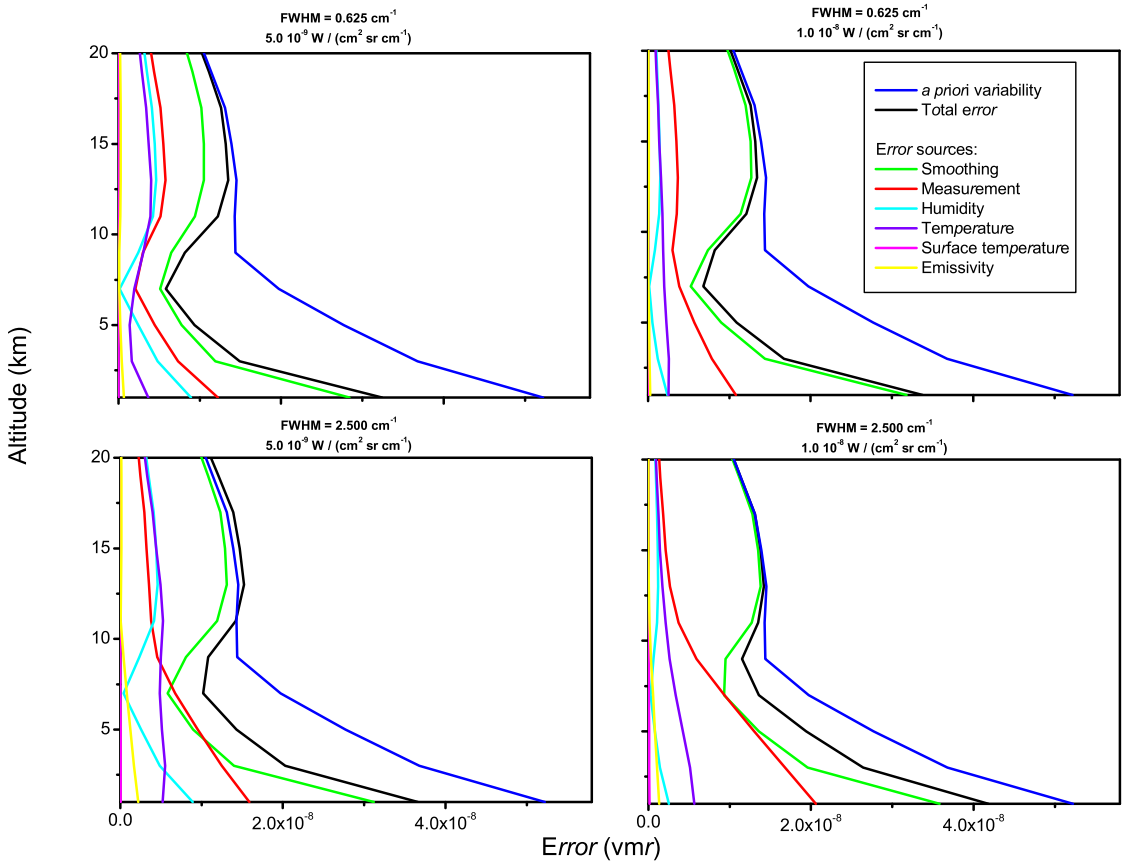

Figure 33: Error profiles for CO retrievals from a radiance spectrum with FWHM = 0.625 cm^{-1} (top panels) or FWHM = 2.500 cm^{-1} (bottom panels) and radiometric noises of 5 10^{-9} (left panels) or 1 10^{-8} (right panels) W / (cm^2 sr cm^{-1}). The CO profile is the global annual mean. Water vapor and temperature profiles are from the clean scenario.

Aerosol-free atmosphere

Retrieval results from noise-free spectra measured at the best spectral resolution are plotted in Figure 34. The corresponding retrieved columns are given in Table 2, for the three different spectral resolutions. Similar retrieval results were obtained on the set of spectra perturbed by noise, water vapor and temperature.

From Figure 34 and Table 2, it is first seen that the retrievals lead to good results for the 'clean' scenario, with relative differences that do not exceed 20% from the ground up to 40 km, and a bias on the total column of 3 to 4% depending on the spectral resolution. On the contrary, the results obtained for the three other cases are poor, with biases on the total columns in the range 20 to 30%. In particular, the high CO abundances characterizing the boundary layer of the 'urban' and the 'biomass burning' cases cannot be reproduced well. The situation is even worse for the 'transport' scenario, with relative differences reaching 100%, due to the difficulty of modelling the CO maximum found in the upper troposphere. The reasons for the poor retrievals can partly be explained by inappropriate *a priori* information, as can be seen from the deviations to the 3σ values extracted from the MOZART covariance matrix in Figure 15. Improvements are therefore possible using *a priori* information closer to the targeted atmospheric situations. It should also be pointed out that with the exception of the 'clean'

Table 2: Results of the retrieval experiments in IRS–7, for aerosol-free scenes. The retrieved CO total column is in 10^{18} molecules cm^{-2}. The results are for noise-free spectra. The bias on the CO column is calculated with respect to the *a priori* and is given in %.

			FWHM 0.625 cm^{-1}		FWHM 1.250 cm^{-1}		FWHM 2.500 cm^{-1}	
	a priori	True values	Retrieved values					
	[CO]	[CO]	[CO]	Bias (%)	[CO]	Bias (%)	[CO]	Bias (%)
Clean	1.12	1.05	1.08	$\mathbf{-2.9}$	1.08	$\mathbf{-3.3}$	1.09	$\mathbf{-3.6}$
Urban	2.29	2.87	2.09	$\mathbf{+27.1}$	2.10	$\mathbf{+26.9}$	2.10	$\mathbf{+26.9}$
B.-burning	2.16	4.37	3.55	$\mathbf{+18.9}$	3.52	$\mathbf{+19.5}$	3.47	$\mathbf{+20.5}$
Transport	1.37	1.70	2.18	$\mathbf{-28.2}$	2.18	$\mathbf{-27.9}$	2.03	$\mathbf{-19.4}$

case, the three other cases discussed here correspond to CO profiles that represent a small fraction of the situations encountered in the atmosphere. However, from the results presented in section 5.1.1– 5.1.3, it is also important to note that part of the explanation for the poor retrieval results is to be found in the limitations of the observing method and the instrument, which provide small sensitivity in the boundary layer and less than 2 independent pieces of information on the vertical.

The limitations described above for modelling the extreme CO scenarios apply obviously for all the perturbed spectra analysed, with additional random errors originating from the radiometric noise and the imperfect knowledge of upper-air temperature and water vapor profiles, as discussed in section 5.1.1. The random deviations found from the statistical analysis of the retrievals for all cases match indeed the values estimated from the error analysis.

Aerosol-containing atmosphere

The retrieval results are plotted in Figure 35, and summarized in Table 3. Because aerosols are not accounted for in the retrieval algorithm, much of the deviation in the baseline radiance caused by their presence in the line of sight is compensated for by a lowering of the surface temperature. The effect is weak for most of the tropospheric aerosols but reaches almost 2–8 K for stratospheric aerosols and cirrus clouds (Table 3).

As it could be anticipated from the net effect on the radiances, the higher altitude aerosols have a larger impact on the CO retrievals: 10 to 30% bias is calculated on the CO total column with respect to an aerosol-free reference case, depending on the aerosol concentration. In contrast, tropospheric (maritime, biomass burning and urban) aerosols have a small impact on the CO retrievals (maximum 3% bias on the CO total column). The results suggest that the retrieved CO columns tend to be overestimated in the presence of aerosols. Figure 35 shows further that the impact is stronger in the troposphere, reaching 25–50% for the high altitude aerosols, while rarely exceeding 5–7% for the tropospheric aerosols.

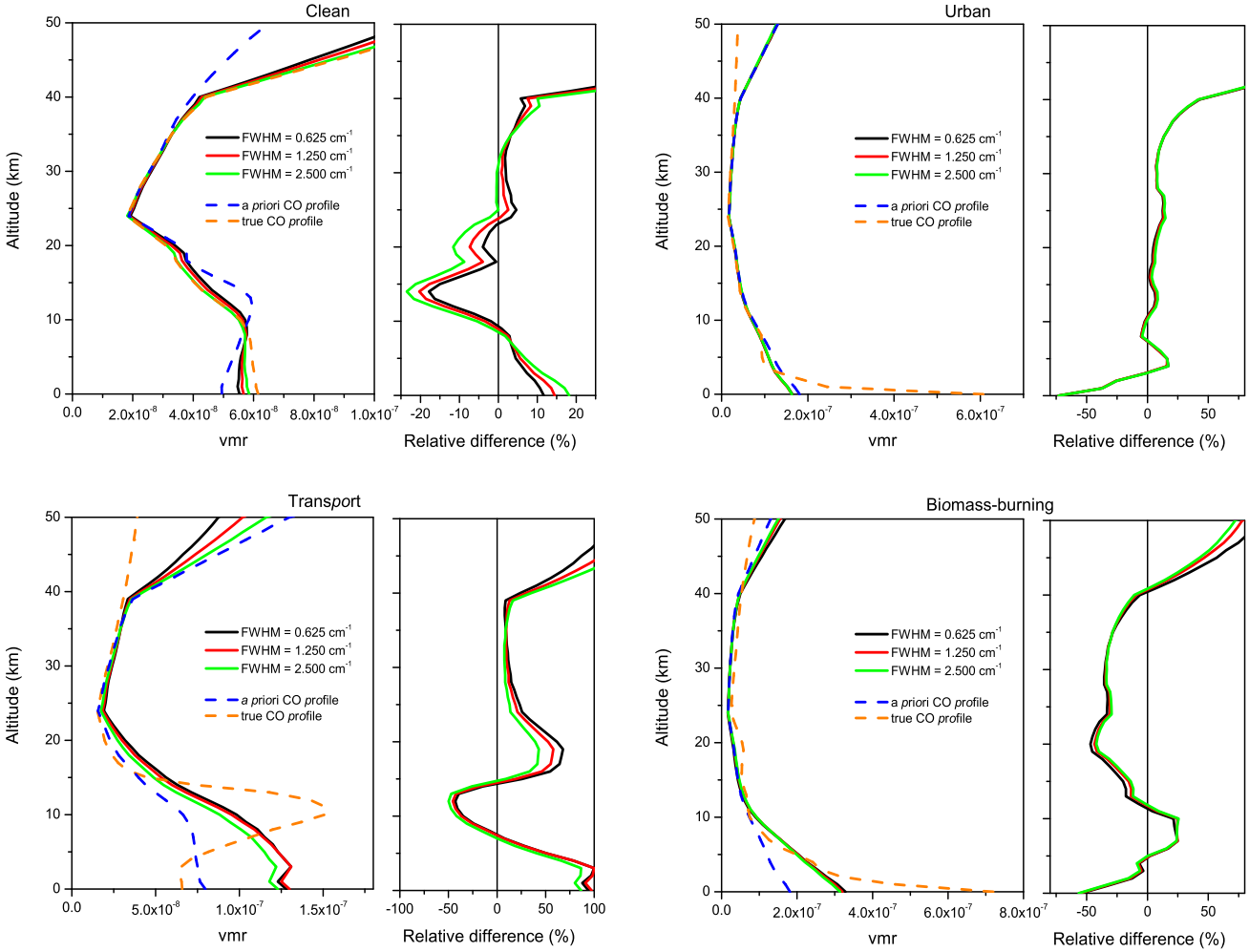

Figure 34: Retrieval experiments for the four CO model atmospheres, in aerosol–free and cloud–free conditions, starting from the monthly hemispheric MOZART *apriori* profiles and the MOZART annual covariance matrix. The model spectra are noise free.

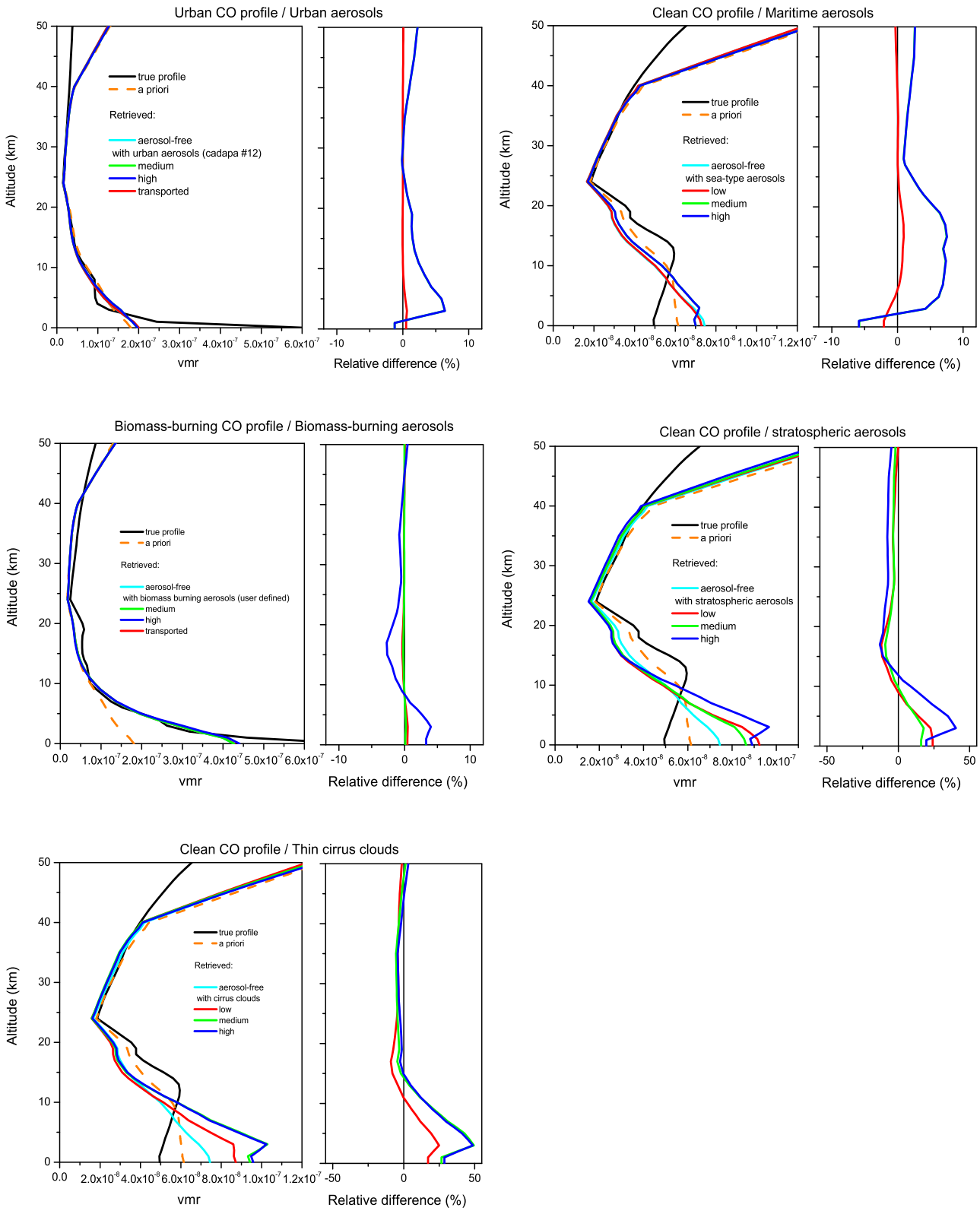

Figure 35: Same as Figure 34 for the aerosol-containing model atmospheres. The relative differences are calculated with respect to the retrievals made for the aerosol-free scenes.

Table 3: Results of the retrieval experiments in IRS–7 for aerosol-containing scenes. The retrieved quantities are surface temperature (K) and CO total columns ([CO] in 10^{18} molecules cm^{-2}). The results are for noise-free spectra, with FWHM = 0.625 cm^{-1}. ΔT_s is in K, while the bias on the CO column is given in %.

CO profile	**Aerosol type**	**Aerosol loading**	**True values**		**Retrieved values**		**Bias**	
			T_s	[CO]	T_s	[CO]	ΔT_s	[CO]
Clean	Aerosol-free		292.5	1.05	292.1	1.18		
	Stratospheric	Moderate			290.0	1.29	-2.1	9.9
		High			286.2	1.43	-5.9	21.9
		Volcanic			290.8	1.33	-1.3	12.9
	Maritime	Low			291.8	1.17	-0.2	-0.7
		Moderate			287.0	1.21	-5.1	2.7
		High			287.0	1.21	-5.1	2.6
	Cirrus	Low			288.4	1.34	-3.7	13.8
		Moderate			283.5	1.52	-8.5	29.6
		High			283.3	1.53	-8.8	29.8
Urban	Aerosol-free		279.1	2.87	278.7	2.29		
	Urban	Moderate			276.8	2.35	-1.9	2.7
		High			276.8	2.35	-1.9	2.7
		Transported			278.7	2.30	-0.1	0.4
B.-burning	Aerosol-free		297.6	4.37	297.2	3.97		
	B.-burning	Moderate			297.1	3.98	0.0	0.1
		High			296.1	4.08	-0.4	2.7
		Transported			297.1	3.99	-0.1	0.3

5.2 Retrieval of CO from UVS SWIR band

This subsection contains only a selection of the principal results. Full details may be found in the attached report by O'Brien [9].

The results of all three approaches described in section 4.3 are qualitatively consistent. It is calculated that in addition to the random errors, large biases can be introduced by cloud, aerosol and errors in the prior estimates of the trace gas mass densities. However, if the spectral resolution $\Delta\nu$ is forced to lie in a narrow range, then the bias and many of the random errors are minimized. This effect is illustrated by Figure 36, which shows biases (expressed in percent) in the scaling factor for the tropospheric mass density of CO caused by errors in the prior, high cloud and stratospheric aerosol. The biases potentially are very large, except in the narrow region indicated.

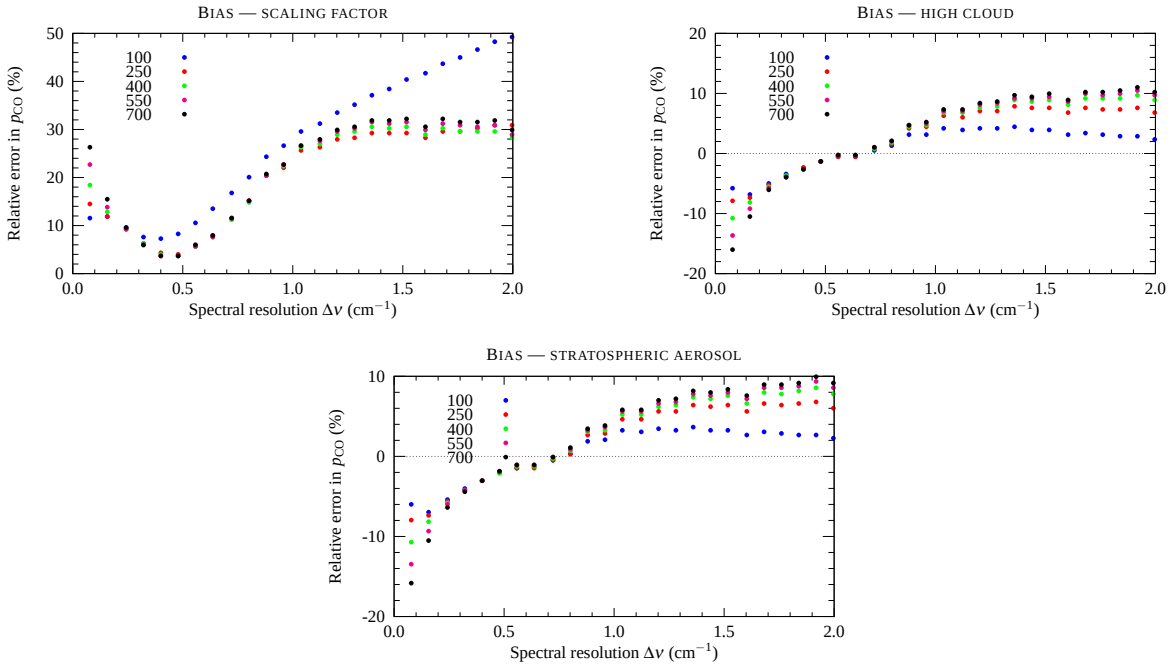

Figure 36: Bias in the CO tropospheric scaling factor produced by errors in the prior scaling factors for the trace gases, high cloud and stratospheric aerosol. In this figure and those that follow, results are shown for five values of signal-to-noise ratio (100, 250, 400, 550, 700), spanning the range specified in the Statement of Work.

Similar results hold for the random components of the errors; Figure 37 illustrates the smoothing and retrieval errors, while Figure 38 shows the model parameter errors for high cloud, stratospheric aerosol and temperature.

The principal difficulty, however, is that the resolution required to minimize the errors depends upon both the scenario and the method of assessment. For example, the errors shown in Figure 16 for the clean scenario with thin cloud ($\tau_C \approx 0.15$), derived by inverting synthetic data, suggest that the optimal spectral resolution is approximately 0.15 cm^{-1}, corresponding to resolving power $\mathcal{R} = 28000$. However, figures 36–38, based upon statistical analysis with assumed distributions rather than inversions of synthetic data, suggest that the optimal $\Delta\nu$ is in the range 0.4–0.6 cm^{-1}. At the centre of this range, the error determined by inverting simulated data is approximately 50% (Figure 16), which is unacceptably high. Conversely, at $\Delta\nu = 0.15$ cm^{-1},

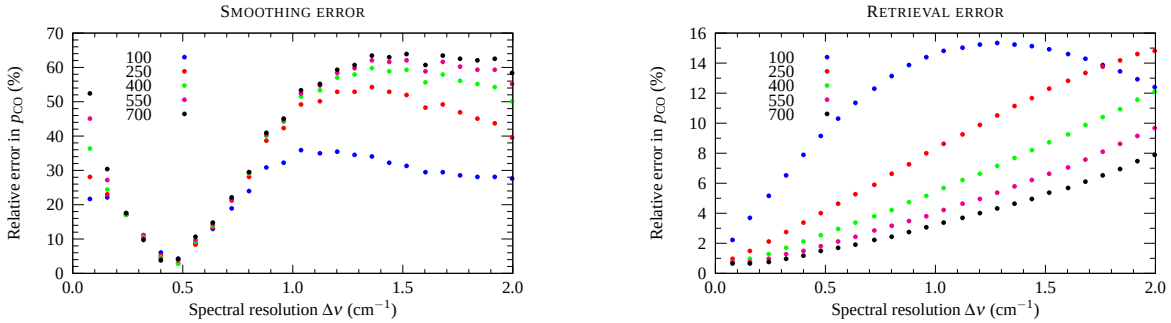

Figure 37: Smoothing and retrieval errors in the tropospheric CO scaling factor.

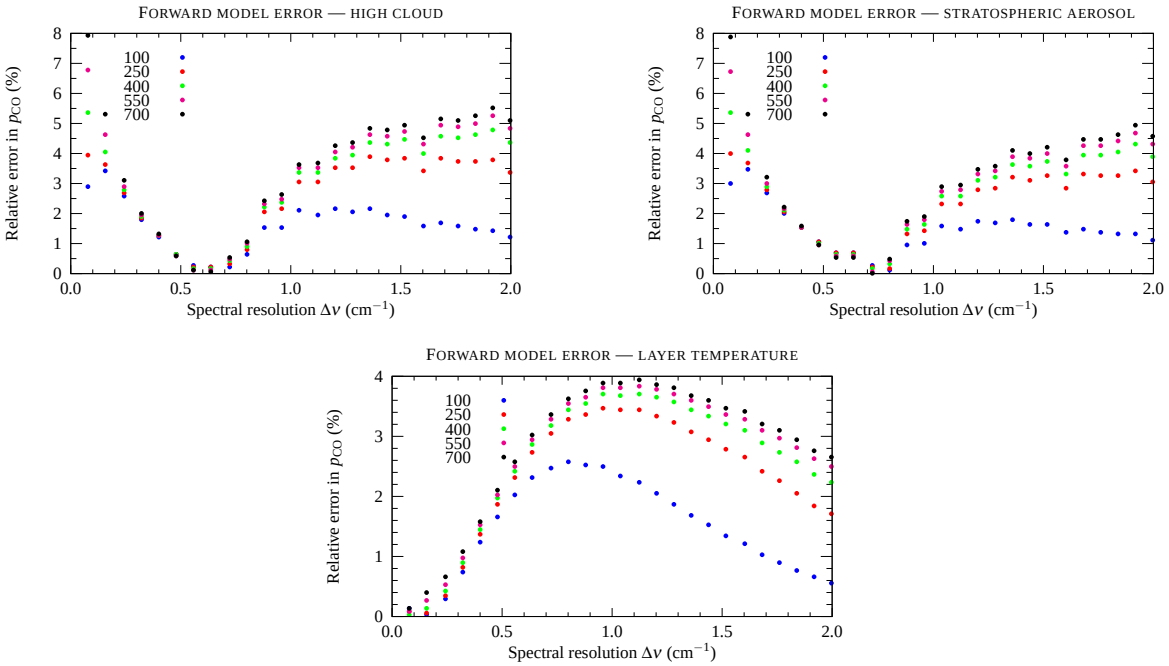

Figure 38: Forward model parameter error in the tropospheric CO scaling factor produced by errors in high cloud, stratospheric aerosol and layer temperature.

suggested by Figure 16, the statistical analysis indicates that the smoothing error alone will be approximately 25%, also unacceptably high.

In addition to its sensitivity to the method of assessment, the optimal spectral resolution also depends upon the scenario. Figure 39 is similar in format to Figure 16, except that the simulated spectra are for the urban scenario, rather than the clean. At $\mathrm{SNR} = 700$, the optimal $\Delta\nu$ is approximately 0.3 cm^{-1}, whereas at the spectral resolution optimal for the clean scenario (0.15 cm^{-1}) the error is approximately 10%. The CO tropospheric mass density (in mol m^{-2}) for the urban scenario is 2.5 times that for the clean, so the dynamic range is small, and therefore it is reasonable to expect the measurements to be feasible in both scenarios.

These sensitivities highlight the difficulty of the proposed measurements. In general, when a measurement process is well-posed, the role of the prior information is secondary to the measurements; the prior is necessary, but the answers do not depend strongly upon it. Such is not the case for the proposed measurements of tropospheric CO. Not only are the results sensitive to the prior, but the errors pass steeply through zero at a critical value of the spectral resolution that depends upon both the scenario considered and the degree of contamination of the field of view by cloud or aerosol.

In summary, the statistical analysis in isolation suggests that the target accuracy of 10% may be reachable for some scenarios if the spectral resolution $\Delta\nu$ lies in the range 0.4–0.5 cm^{-1} and the signal-to-noise ratio is approximately 400. Alternatively, Monte Carlo inversions of noisy simulated data suggest that $\Delta\nu$ in the range 0.2–0.3 cm^{-1} would be more appropriate. Both analyses agree that the target accuracy cannot be reached if $\Delta\nu \geq 0.6\,\mathrm{cm}^{-1}$ using spectra within the selected window (4220–4240 cm^{-1}).

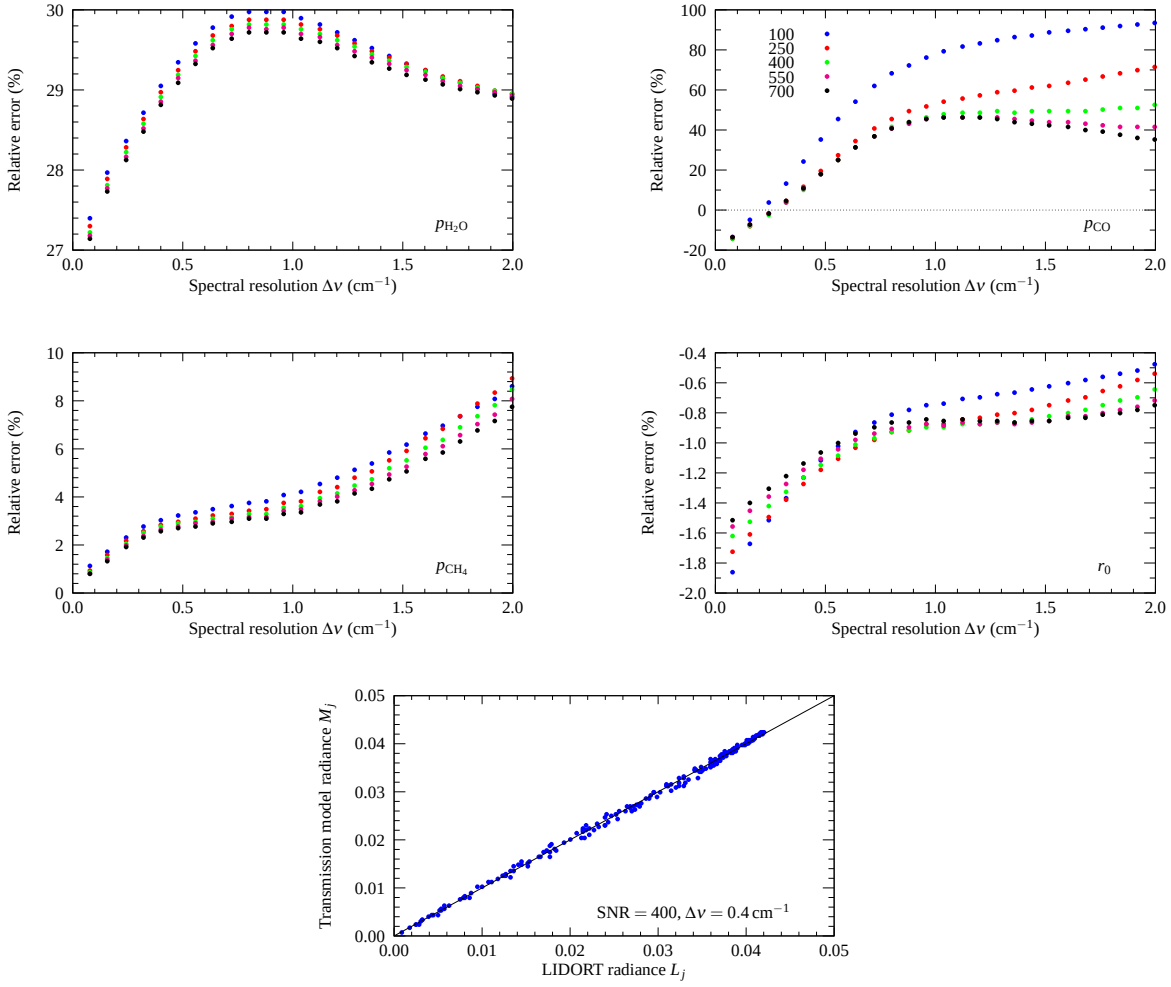

Figure 39: As for Figure 16, except that the spectra were synthesized for the urban scenario.

5.3 Retrieval of CO from a synergetic use of IRS band 7 and UVS SWIR band

The results presented in sections 5.1 and 5.2 and in the annexed report by O'Brien [9] have assessed the capabilities of both the IRS and the UVS to measure CO at the required accuracy, using respectively the intense CO 1–0 fundamental and the weaker 2–0 overtone absorption band. This section examines the possible improvements, in terms of accuracy and vertical sensitivity on the CO vertical profile, that would be gained by a synergetic use of both IRS–7 and SWIR channels. The instrumental combination that has been considered has the following characteristics:

- SWIR band:
  – Spectral resolution: 0.4 cm^{-1}
  – SNR: 500 at 5% albedo
- IRS–7 band:
  – Spectral resolution: 0.625 cm^{-1}
  – Radiometric noise: 5 10^{-9} W/(cm^2 sr cm^{-1})

The formalism for the coupled analysis is similar to the one used to characterize the retrievals from the thermal IR spectra, the only difference being that the measurement vector, $\mathbf{y}$, the measurement noise covariance matrix, $\mathbf{S}_\epsilon$, and the weighting function, $\mathbf{K}$, are extended from the IRS–7 micro-window to include the SWIR micro-window. Equations 9 to 15 are then respectively used to compute the averaging kernels and the errors.

Figure 40, which depicts the jacobians of the forward models, highlights the very different altitude sensitivity of both instruments, with the thermal IR observations that are mostly sensitive to the middle troposphere (2-8 km) and the SWIR observations that have their maximum sensitivity in the boundary layer. The information content analysis demonstrates that the coupling of the IRS–7 and SWIR channels to retrieve CO profiles takes obvious advantage of the specific sensitivities of both instruments. The DOFS, close to 1 when the instruments operate separately (Table 4), increases to almost 2 when the instruments are combined. This means indeed that the information provided by the two instruments is complementary and that the coupling is optimal. The averaging kernels, displayed in Figure 41 confirm the analysis, showing that the combined averaging kernels have high sensitivity both in the lower troposphere, thanks to the use of the short-wave IR channel, and in the middle troposphere, thanks to the use of the thermal IR channel.

The error profiles are displayed on Figure 42 for the retrieval errors (sum of smoothing and measurement errors). As could be anticipated from the information content analysis, it is seen that the retrieval error decreases at all levels and especially in the lower troposphere when both instruments are combined (Figure 42 and Table 4). The retrieval error on the tropospheric (0–12 km) column is 3.3% and matches thus both the threshold (10%) and goal accuracies (5%). The threshold accuracy is also reached for the lower (0–6 km) and upper tropspheric column (6–12 km) taken separately (Table 4).

This view of the error budget from the IRS–7–SWIR combination is, however, simplified, as it does not account for possible uncertainties on the model parameters. Figure 42 shows error profiles for the most significant error sources. These include the retrieval error, which dominates in the thermal infrared at the selected spectral resolution and noise, and the errors due to uncertainties on the temperature (1.5 K), humidity (10%), and methane (5%) vertical

Table 4: Retrieval errors for CO partial columns and DOFS values associated to retrievals using IRS–7 and SWIR bands alone and in synergy. The spectral resolution and instrumental noise are respectively 0.625 cm^{-1} and 5 10^{-9} W/(cm^2 sr cm^{-1}) in IRS–7 and 0.4 cm^{-1} and 500 (SNR) in the SWIR. Only the smoothing and the measurement errors are taken into account.

Spectral band	**Retrieval error (%)**				**DOFS**
	0-6 km	6-12 km	0-12 km	Total	
IRS–7	17.3	8.8	11.3	8.7	1.16
SWIR	8.2	12.0	3.8	1.6	1.22
IRS–7 + SWIR	5.7	7.2	3.3	1.6	1.93

profiles, which have a dramatic impact in the SWIR, if not fitted alongside CO, as considered in the present analysis. Figure 43 suggests that the large errors in the SWIR channels would preclude an optimal retrieval of CO, even by combining IR and SWIR channels. The way to decrease the errors in the SWIR is to perform a simultaneous retrieval of CO, H_2O and CH_4, as for instance done for the UVS-SWIR analyses presented here and detailed by O'Brien [9], or also in the treatment of the SCHIAMACHY data [25, 26] using the DOAS approach. Due to model inconsistencies, it has not been possible to judge the extent of improvement that would be obtained by such approach.

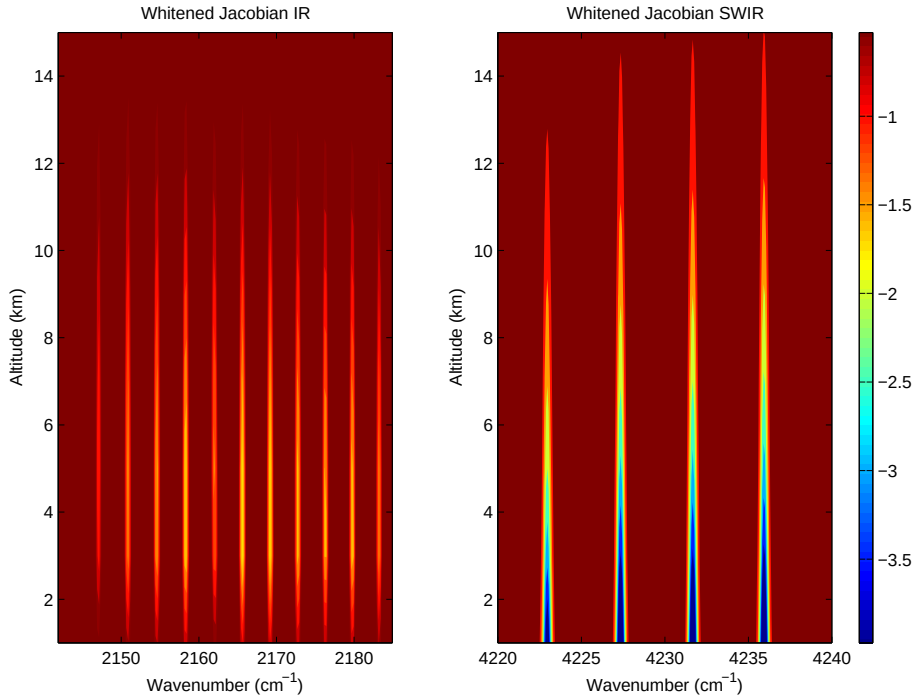

Figure 40: Jacobian for CO in the selected micro-windows of the IRS–7 and SWIR bands. The spectral resolution and instrumental noise are respectively 0.625 cm^{-1} and 5 10^{-9} W/(cm^2 sr cm^{-1}) in IRS–7 and 0.4 cm^{-1} and 500 (SNR) in the SWIR.

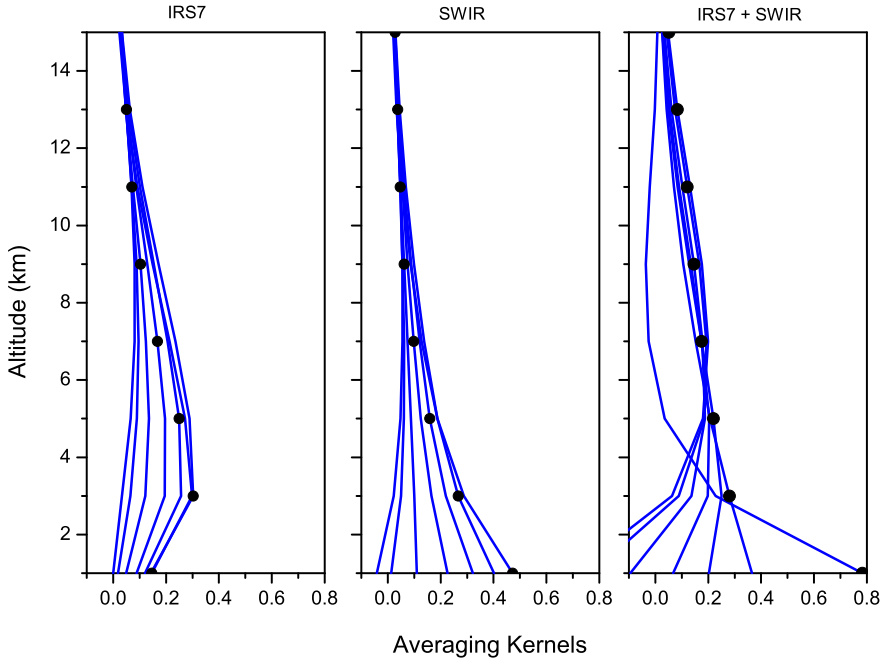

Figure 41: Averaging kernels for CO from IRS–7 and SWIR bands alone and in synergy. The spectral resolution and instrumental noise are respectively 0.625 cm^{-1} and 5 10^{-9} W/(cm^2 sr cm^{-1}) in IRS–7 and 0.4 cm^{-1} and 500 (SNR) in the SWIR.

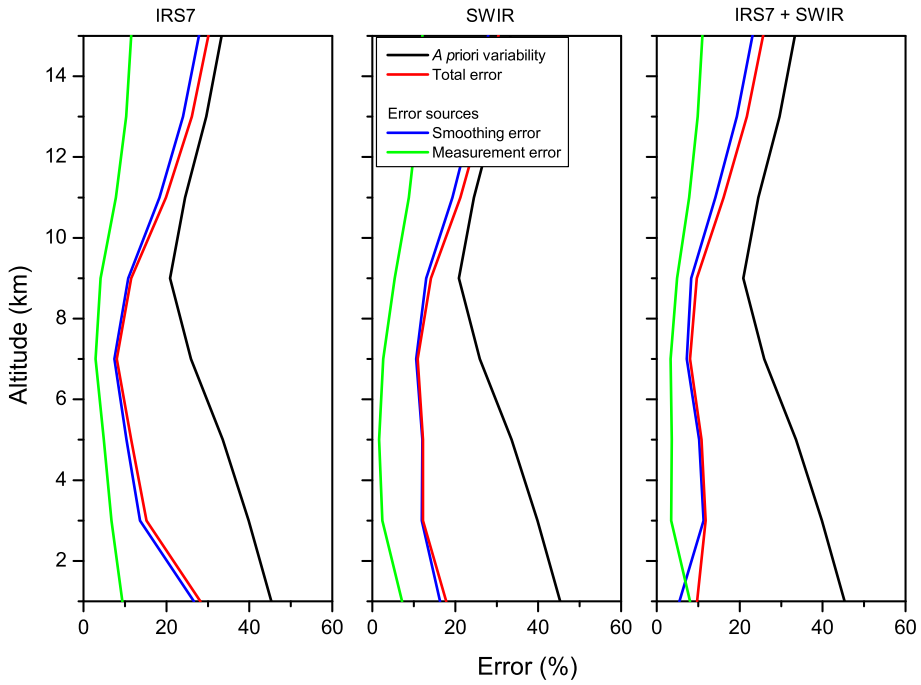

Figure 42: Error profiles for CO retrieval from IRS–7 and SWIR bands alone and in synergy. The spectral resolution and instrumental noise are respectively 0.625 cm^{-1} and 5 10^{-9} W/(cm^2 sr cm^{-1}) in IRS–7 and 0.4 cm^{-1} and 500 (SNR) in the SWIR. Only the retrieval errors (measurement and smoothing) are shown.

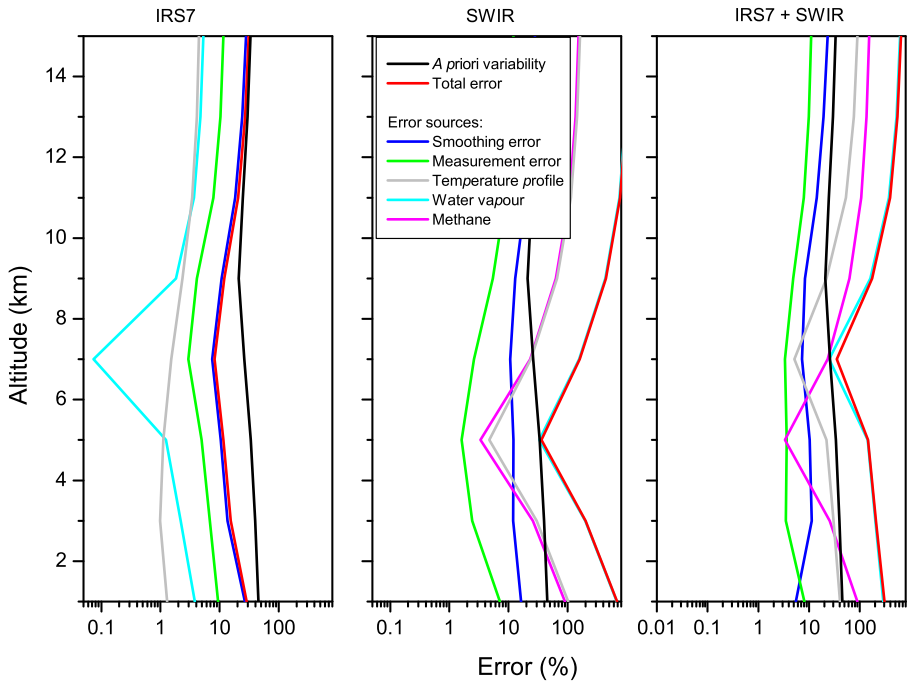

Figure 43: Same as Figure 42, where additional errors, due to uncertainties on the temperature, humidity and methane profiles, have been added. See text for details.

6 Conclusions

The feasibility of measuring CO tropospheric columns from MTG-IRS and MTG-UVS missions, using the spectroscopic information from the IRS–7 (2000-2200 cm^{-1}) and SWIR bands (4180-4320 cm^{-1}) alone or in synergy, was investigated, as a function of

- Instrumental performances: Spectral resolution and radiometric noise
- Surface properties: Surface temperature and emissivity
- Atmospheric state variables: Temperature, humidity and other trace gases vertical profiles, aerosols and clouds.

The analyses relied on chemistry requirements for measuring CO (5–10% accuracy on the tropospheric column, with 0.5–2 hours sampling and 2–10 km horizontal resolution), and on preliminary instrument specifications for the IRS and UVS. They make use of a set of radiative transfer models, retrieval algorithms, statistical analysis and characterization tools. The principal conclusions from this study are as follows.

Retrieval of CO vertical profiles from IRS

The chemistry requirements in terms of accuracy on the retrieved tropospheric CO column can only be met with some IRS instrumental specifications:

(a) A 10% accuracy is reached on CO total column measurements for radiometric noise values smaller than 5 10^{-9} W / (cm^2 sr cm^{-1}) and a spectral resolution of either 0.625 cm^{-1} or 1.250 cm^{-1}. The total error increases smoothly with noise level at all spectral resolutions investigated. At the coarser spectral resolution (2.5 cm^{-1}) the error on the CO column is unacceptably large. The results apply for different atmospheric conditions, characterized by either low or high surface temperatures and either low or high humidity profiles.

(b) The chemistry requirements, which are defined as a 10% accuracy on the tropospheric (0-12 km) column, can only be reached with the best IRS characteristics, corresponding to low noises (2–5 10^{-9} W / (cm^2 sr cm^{-1})) and high spectral resolution (0.625 cm^{-1} and to a lesser extent 1.250 cm^{-1}). Even in these very favorable situations, the uncertainties on the temperature profile and on the humidity profile can have large impacts in some atmospheric conditions (e.g. a humid tropical atmosphere) if not known to a high accuracy. The goal accuracy (5%) is not achieved in general.

(c) The separation between the lower (0-6 km) and upper (6-12 km) tropospheric columns can only be achieved at the higher spectral resolution (0.625 cm^{-1}) and a noise level as low as 2.5 10^{-9} W / (cm^2 sr cm^{-1}). This combination brings also some additional information at higher altitudes.

The errors in the retrieval of CO from the IRS–7 channel are due to the smoothing and the measurement, which are both tightly related to the instrument specifications, but also to the possible uncertainties on the surface properties and the atmospheric state variables:

(d) The uncertainties on the surface properties (emissivity and temperature) contribute little to the total error. These quantities are, however, important in that they determine the amount of radiation at the top of the atmosphere, and hence the net measured radiances.

With the best instrumental performances, the measurements contain between 1.5 and 2 independent pieces of information on the CO vertical distribution, depending on the surface temperature.

(e) The uncertainties on the temperature and humidity profiles have an important impact on the CO tropospheric column retrieval, the extent of which depends strongly on the atmospheric conditions and instrumental performances. For instance, the uncertainty on the temperature profile (a 1.5 K uncertainty was considered), generates a radiance error of about 1 10^{-9} W / (cm^2 sr cm^{-1}), which is of the same order of magnitude as the radiometric noise at the center of the CO lines. The error introduced on the CO retrieval varies from a few percent at the highest spectral resolution to about 5% at the coarser spectral resolution. The uncertainty on the humidity profile (10% was considered) generates also considerable errors, which could partly be avoided at the best spectral resolution by selecting narrow micro-windows where H_2O lines are absent. At the coarser spectral resolution, however, the impact of water vapor can hardly be avoided, and errors from 5–10% are likely to result, especially in the case of a very humid atmosphere.

(f) For the IRS, the impact of interfering trace gases is negligible, provided that an optimal micro-window is selected. Tropospheric aerosols, including urban, biomass-burning and maritime aerosols, are shown not to produce a large impact on either the radiances or the CO tropospheric column (less than 3%). High-altitude aerosols, such as stratospheric aerosols and thin cirrus clouds, have a larger impact, reaching 20%, if not properly considered in the radiative tranfer, as assumed here.

The conclusions for the IRS were globally confirmed by performing retrieval experiments corresponding to selected scenes, associated to 'clean', 'urban', 'biomass-burning' and 'transport' CO emission scenarios. The results have pointed out to the limits of the IRS instrument, even in the best configuration of spectral resolution and noise, to catch extreme CO vertical distributions, such as those characterizing high pollution and biomass-burning (high level of CO in the boundary layer) or pollution transport events.

Retrieval of CO vertical profiles from UVS

The attached report by O'Brien [9] used a combination of illustrative examples, statistical analysis and Monte Carlo simulations to investigate whether the mass density of tropospheric CO might be deduced with an accuracy of 10% from spectra in the SWIR band of CO from 4180–4320 cm^{-1} (2315–2392 nm). The principal conclusions from this study are as follows.

(a) Spectra at the top of the atmosphere in the SWIR band of CO show very little sensitivity to the vertical distribution of CO. At best one can hope to resolve the stratospheric and tropospheric components of the CO mass density.

(b) Spectra in the narrow window 4220–4240 cm^{-1} are less contaminated by the absorption features of H_2O and CH_4 than elsewhere in the band. If this window is used, then the errors in the retrieved CO are unacceptably large unless the spectral resolution lies in a narrow range, within which the random errors (smoothing, cloud, aerosol and temperature) are minimized, while the biases introduced by cloud and aerosol pass through zero. There is only qualitative agreement on the location of this range between the different methods of assessment; the statistical analysis suggests 0.4–0.6 cm^{-1}, whereas the Monte Carlo simulations indicate 0.2–0.3 cm^{-1}. The sensitivity of the error to the spectral resolution is so great that this difference is significant.

(c) Even with the spectral resolution so chosen, achievement of the required accuracy for tropospheric CO is marginal for SNR within the range specified in the Statement of Work. In the best case studied, the random error is about 4%, while the biases due to high cloud and aerosol are 2.5% and 3%, respectively. Temperature errors contribute an additional bias, estimated at 2.9%. However, other cases (such as the bio-mass scenario with clean prior) have biases and random errors outside the acceptable range.

(d) Monte Carlo simulations broadly support the conclusions of the statistical analysis, though there is some disagreement over the optimal spectral resolution. Furthermore, the magnitude of the biases appears to be sensitive to the scenario assumed for CO. This instability reinforces the conclusion that the proposed measurement strategy is marginal.

Retrieval of CO vertical profiles from IRS and UVS

The retrieval of CO vertical profile from IRS and UVS was investigated for a particular combination of instrument performances (0.4 cm^{-1} spectral resolution and SNR = 500 in the SWIR, and 0.625 cm^{-1} with noise 5 10^{-9} W/(cm^2 sr cm^{-1}) in IRS–7). The following was concluded:

(a) The combination of both instruments takes full advantage of the different sensitivity of the thermal infrared and short-wave channels to the CO vertical distribution. While the measurements taken individually do not contain much more than a single piece of information on the vertical CO profile, their combined use increases the DOFS to about 2. The sensitivity becomes important in both the boundary layer, where the SWIR measurements are mostly sensitive, and in the middle troposphere, where the thermal IR measurements show high sensitivity.

(b) The combination allows significant reduction of the retrieval error (smoothing and measurement errors), which is of the order of 3% on the tropospheric column.

(c) The errors due to model parameter uncertainties and trace gases interferences are difficult to establish due to the different models used for the IRS and SWIR calculations. The results suggest that the errors remain important for CO tropospheric column retrieval, unless water vapor and methane contents are known very accurately. As these two species have very large optical thicknesses compared to CO in the SWIR, it is essentially the latter measurement that drives the error when both instruments are combined.

General conclusions

Finally it is useful to examine the results obtained in this study in light of the achievements and expectations from instruments on LEO satellites, detailed in section 3. The comparison is provided in Table 5. An obvious result is that the threshold accuracy required for measuring CO (10% on a tropospheric column) is reached with most of the instruments on LEO, but that the target accuracy (5%) is not. Among the existing measurements, the retrieval of CO from the short-wave infrared radiances (*e.g.* SCIAMACHY) appears to be the most challenging. It is also worth stressing here that, at present, space-borne instruments have not been able to derive information on the CO vertical distribution with more than two independent pieces of information, and thus with a vertical resolution better than about 6 km. The best vertically resolved profiles have been derived from the high-resolution (about 0.1 cm^{-1}) and low-noise (about 0.2 K) IMG FTS measurements.

The results presented in this report have shown that spectroscopic instruments onboard MTG should enable measuring CO with an accuracy similar to that of the demonstrated instruments on LEO. The combination of the thermal infrared radiances from the IRS with the shortwave infrared radiances from the UVS would in principle be the most suitable for measuring CO, as it would allow retrieving vertically resolved profiles (2 independent pieces of information), with good sensitivity in the boundary layer and in the middle troposphere. The IRS measurements alone is expected to deliver CO products with an accuracy matching the requirements, provided, however, that the spectral resolution and radiometric performances are not relaxed significantly beyond the target values, as defined in the MRD issue 1.1. The high resolution of the IRS is a further requisite for measuring a vertically resolved CO profile, if not combined to the UVS. Finally, while the UVS measurements theoretically should provide CO columns with the required accuracy, achieving the accuracy in practice appears to be challenging.

Table 5: Comparison between the accomplishments of spectroscopic instruments on LEO satellites for measuring CO and the expectations from the MTG IRS and UVS, in terms of accuracy, horizontal and vertical resolution, and spatio-temporal coverage. TC refers to the total column.

Mission	**Instrument concept**	**accuracy in CO tropospheric column (%)**	**vertical information**	**horizontal resolution**	**spatio-temporal coverage**	**Reference**
IMG	FTS (TIR)	10%	1.5–2.2	8 km $\times$ 8 km	—	[17]
MOPITT	Correlation rad. (TIR)	5–10%	≤ 1.5	22 km $\times$ 22 km	Global / 3 days	[12, 13]
SCIAMACHY	Grating spect. (SWIR)	20–25%	TC	30 km $\times$ 60 km	Global / 3–6 days	[6]
TES	FTS (TIR)	10%	TC	5.3 km $\times$ 8.4 km	—	[22]
IASI	FTS (TIR)	10%	≤ 1.5	2 $\times$ 2 circular pixels of 12 km	Global / 1 day	[20]
MTG						
IRS		$\approx 10\%$	≈ 1.5	≤ 10 km	Full disk / 1 hour	
UVS		$\approx 10\%$	TC		Full disk / 1 hour	
IRS–UVS		$< 10\%$	2		Full disk / 1 hour	

7 Limitations

Impact of aerosols on the retrieval of CO from the IRS

In the retrieval experiments (section 5.1.4), the aerosols are not retrieved nor considered in the forward calculation module of the inversion algorithm. The calculated errors are therefore to be considered as a 'worst estimate'. Furthermore, in the operational phase, strong cloud-containing or aerosol-containing scenes are likely to be filtered out, thereby reducing the possible biases.

Impact of atmospheric state variables on the retrieval of CO

In the computation of the error budget using the OEM (section 5.1 for the IRS alone and section 5.3 for the IRS-SWIR combination), we have considered temperature, humidity and methane profiles with uncertainties of 1.5 K, 10% and 5% respectively. None of these parameters has been retrieved along with the CO profile, and their associated errors have accordingly been calculated from equation 13. As advocated by [4], the resulting large forward model parameters errors can be reduced by considering the parameters as elements of the state vector and by retrieving them from the measurement. In that case, equation 14 is used. The effect on the results is illustrated in Figure 44, where error budgets for a standard retrieval of CO from the IRS are computed without and with water vapor as part of the state vector. If the impact is relatively limited in the IRS, the simultaneous retrieval of CO, H_2O and CH_4 from the SWIR radiance would strongly reduce the error estimate shown in Figure 43.

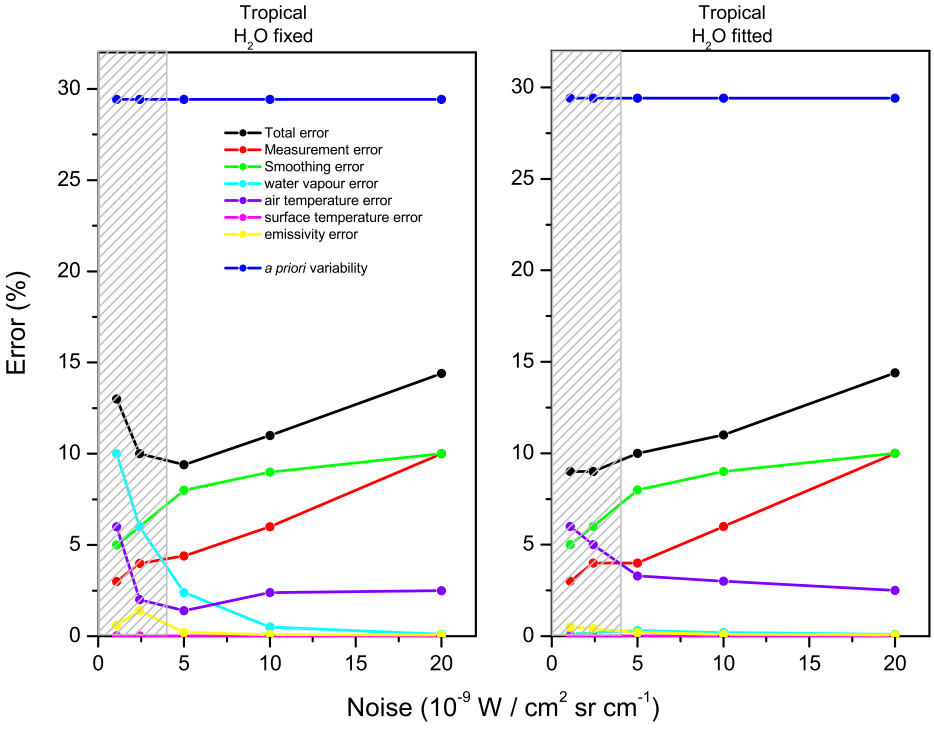

Figure 44: Error budget for CO total column retrieval, with water vapor considered as a fixed model parameter (left panel) or retrieved along with the CO profile (right panel). The values refer to the global annual mean MOZART profile, for the reference tropical atmosphere (T_s=295 K, large humidity). The spectral resolution is 0.625 cm^{-1}

It should also be remarked that the 1.5 K uncertainty on the temperature profile, assumed for computing the error budgets throughout this study, is somewhat larger than the expectations of advanced meteorological platforms (1 K with 1 km vertical resolution). Also, the temperature error covariance matrix was assumed to be diagonal, thus neglecting the correlations between the different altitudes. In future studies, a more realistic covariance matrix should be used. On the overall, the estimated error on the CO profile retrieval introduced by an inaccurate knowledge of the temperature, as calculated in this study, is therefore to be considered as an upper limit.

Acknowledgments

The authors are grateful to the IMGDIS (Japan) for providing the Level 1 IMG data and to Tony Clough (AER, US) for LBLRTM. Daniel Hurtmans is strongly acknowledged for his development of the Atmosphit sofware and for his help throughout the duration of the project.

References

[1] B.W. Golding, S. Senesi, K. Browning, B. Bizzari, W. Benesh, D. Rosenfeld, V. Levizzani, H.P. Roesli, U. Platt, T.E. Nordeng, J.T. Carmona, P. Ambrosetti, P. Pagano, and M. Kurz. Observation requirements for nowcasting and very short range forecasting in 2015-2025. Position paper for EUMETSAT, 2001.

[2] J. Lelieveld. Geostationary satellite observations for monitoring atmospheric composition and chemistry applications. Technical report for EUMETSAT, 2003.

[3] R. Stuhlmann, S. Banfi, J. Gonzalez, V. Casanovas, S. Tjemkes, and A. Rodriguez. MTG Mission Requirements Document, issue 1.1. EUMETSAT document, 2004.

[4] C.D. Rodgers. *Inverse methods for atmospheric sounding: Theory and Practice*, volume 2 of *Amosph. Oceanic Planet. Phys;*. World Sci., River Edge, N.J., 2000.

[5] D.M. O'Brien and C.A. Pickett-Heaps. Feasibility of trace gas measurements from geostationary orbit using VIS/UV radiances. Technical report for EUMETSAT, contract EUM/CO/03/1150/SAT, 2003.

[6] H. Bovensmann, K. U. Eichmann, S. Noel, V. Rozanov, M. Vountas, and J. P. Burrows. Capabilities of a UV-VIS instrument in geostationary orbit to meet user requirements for atmospheric composition and operational chemistry applications. Technical report for EUMETSAT, contract EUM/CO/03/1166/SAT, 2004.

[7] R. Siddans and B.J. Kerridge. Review of MTG UVS mission requirements. Technical report for EUMETSAT, contract EUM/CO/04/1317/SAT, 2004.

[8] C. Clerbaux, P.F. Coheur, S. Turquety, and J. Hadji-Lazaro. Capabilities of infrared sounder observations for monitoring atmospheric composition and chemistry applications. Technical report for EUMETSAT, contract EUM/CO/03/1127/SAT, 2003.

[9] D.M. O'Brien. Feasibility of measuring tropospheric CO from geostationary orbit using high resolution SWIR radiances. Technical report for EUMETSAT, contract EUM/CO/04/1296/SAT, 2005.

[10] H. G. Reichle, B. E. Anderson, V. S. Connors, T. C. Denkins, D. A. Forbes, B. B. Gormsen, R. L. Langenfelds, D. O. Neil, S. R. Nolf, P. C. Novelli, N. S. Pougatchev, M. M. Roell, and L. P. Steele. Space shuttle based global CO measurements during April and October 1994, MAPS instrument, data reduction, and data validation. *J. Geophys. Res.*, 104(D17):21443–21454, 1999.

[11] L. Pan, J. C. Gille, D. P. Edwards, and P.L. Bailey. Retrieval of tropospheric carbon monoxide from the MOPITT experiment. *J. Geophys. Res.*, 103(D24):32,277–32,290, 1998.

[12] M. N. Deeter, L. K. Emmons, G. L. Francis, D. P. Edwards, J. C. Gille, J. X. Warner, B. Khattatov, D. Ziskin, J. F. Lamarque, S. P. Ho, V. Yudin, J. L. Attie, D. Packman, J. Chen, D. Mao, and J. R. Drummond. Operational carbon monoxide retrieval algorithm and selected results for the MOPITT instrument. *J. Geophys. Res.*, 108(D14):doi:10.1029/2002JD003186, 2003.

[13] M. N. Deeter, L. K. Emmons, D. P. Edwards, J. C. Gille, and J. R. Drummond. Vertical resolution and information content of CO profiles retrieved by MOPITT. *Geophys. Res. Lett.*, 31(15):doi:10.1029/2004GL020235, 2004.

[14] C. Clerbaux, J. Gille, and D. Edwards. New directions: Infrared measurements of atmospheric pollution from space. *Atmospheric Environment*, 38(27):4599–4601, 2004.

[15] H. Kobayashi, A. Shimota, K. Kondo, E. Okumura, Y. Kameda, H. Shimoda, and T. Ogawa. Development and evaluation of the interferometric monitor for greenhouse gases: a high-throughput Fourier-transform infrared radiometer for nadir Earth observation. *Appl. Opt.*, 38(33):6801–6807, 1999.

[16] C. Clerbaux, J. Hadji-Lazaro, S. Payan, C. Camy-Peyret, and G. Mégie. Retrieval of CO columns from IMG ADEOS spectra. *IEEE. Trans. Geosci. Remote Sens.*, 37(3):1657–1661, 1999.

[17] B. Barret, S. Turquety, D. Hurtmans, C. Clerbaux, J. Hadji-Lazaro, I. Bey, M. Auvray, and P. F. Coheur. Global carbon monoxide vertical distributions from spaceborne high-resolution FTIR nadir measurements. *Atm. Chem. Phys.*, submitted, 2005.

[18] J. Hadji-Lazaro, C. Clerbaux, and S. Thiria. An inversion algorithm using neural networks to retrieve atmospheric CO total columns from high-resolution nadir radiances. *J. Geophys. Res.*, 104(D19):23841–23854, 1999.

[19] C. Clerbaux, J. Hadji-Lazaro, D. Hauglustaine, G. Mégie, B. Khattatov, and J. F. Lamarque. Assimilation of carbon monoxide measured from satellite in a three-dimensional chemistry-transport model. *J. Geophys. Res.*, 106(D14):15385–15394, 2001.

[20] S. Turquety, J. Hadji-Lazaro, C. Clerbaux, D. A. Hauglustaine, S. A. Clough, V. Cassé, P. Schlüssel, and G. Mégie. Operational trace gas retrieval algorithm for the Infrared Atmospheric Sounding Interferometer. *J. Geophys. Res.*, 109(D21):doi:10.1029/2004JD004821, 2004.

[21] R. Beer, T. A. Glavich, and D. M. Rider. Tropospheric emission spectrometer for the Earth Observing System's Aura Satellite. *Appl. Opt.*, 40(15):2356–2367, 2001.

[22] J. Worden, S. S. Kulawik, M. W. Shephard, S. A. Clough, H. Worden, K. Bowman, and A. Goldman. Predicted errors of tropospheric emission spectrometer nadir retrievals from spectral window selection. *J. Geophys. Res.*, 109(D9):doi:10.1029/2004JD004522, 2004.

[23] J. P. Burrows, E. Holzle, A. P. H. Goede, H. Visser, and W. Fricke. Sciamachy - Scanning Imaging Absorption Spectrometer for Atmospheric Chartography. *Acta Astronautica*, 35(7):445–451, 1995.

[24] H. Bovensmann, J. P. Burrows, M. Buchwitz, J. Frerick, S. Noel, V. V. Rozanov, K. V. Chance, and A. P. H. Goede. SCIAMACHY: Mission objectives and measurement modes. *J. Atm. Sci.*, 56(2):127–150, 1999.

[25] M. Buchwitz, R. de Beek, K. Bramstedt, S. Noel, H. Bovensmann, and J. P. Burrows. Global carbon monoxide as retrieved from SCIAMACHY by WFM-DOAS. *Atm. Chem. Phys.*, 4:1945–1960, 2004.

[26] C. Frankenberg, U. Platt, and T. Wagner. Retrieval of CO from SCIAMACHY onboard ENVISAT: detection of strongly polluted areas and seasonal patterns in global CO abundances. *Atm. Chem. Phys.*, 4:8425–8438, 2004.

[27] G. P. Brasseur, D. A. Hauglustaine, S. Walters, P. J. Rasch, J. F. Müller, C. Granier, and X. X. Tie. MOZART, a global chemical transport model for ozone and related chemical tracers 1. Model description. *J. Geophys. Res.*, 103(D21):28265–28289, 1998.

[28] D. A. Hauglustaine, G. P. Brasseur, S. Walters, P. J. Rasch, J. F. Müller, L. K. Emmons, and C. A. Carroll. MOZART, a global chemical transport model for ozone and related chemical tracers 2. Model results and evaluation. *J. Geophys. Res.*, 103(D21):28291–28335, 1998.

[29] C. Levoni, M. Cervino, R. Guzzi, and F. Torricella. Atmospheric aerosol optical properties: a database of radiative characteristics for different component and classes. *Appl. Opt.*, 36:8031–8041, 1997.

[30] F.X. Kneysis, E. P. Shettle, L.W. Abreu, J.H. Chetwynd, G.P. Anderson, W.O. Gallery, J.E.A. Selby, and S.A. Clough. Users Guide to LOWTRAN 7. Technical Report AFGL-TR-88-0177, 1988.

[31] E. P. Shettle and R. W. Fenn. Models for the aerosols of the lower atmosphere and the effects of humidity variations on their optical properties. Technical report environmental research papers, no. 676, afgl-tr-79-0214, Hanscom Air Force Base, Massachusetts 01731., 1979.

[32] J. Trentmann, M.O. Andreae, H.-F. Graf, P.V. Hobbs, R.D. Ottmar, and T. Trutmann. Simulation of a biomass-burning plume: comparison of model results with observations. *J. Geophys. Res.*, 107(D2), 2002.

[33] A. Keil and J.M. Haywood. Solar radiative forcing by biomass burning aerosol particles during SAFARI 2000: A case study based on measured aerosol and cloud properties. *J. Geophys. Res.*, 108(D13):doi:10.1029/2002JD002315, 2003.

[34] T. Elias, S.J. Piketh, R. Burger, and A.M. Silva. Exploring the potential of combining columns-integrated atmospheric polarization with airborne in situ size distribution measurements for the retrieval of an aerosol model: A case study of a biomass burning plume during SAFARI 2000. *J. Geophys. Res.*, 108(D13):doi:10.1029/2002JD002426, 2003.

[35] C. Forster, U. Wandinger, G. Wotawa, P. James, I. Mattis, D. Althausen, P. Simmonds, S. O'Doherty, S. G. Jennings, C. Kleefeld, J. Schneider, T. Trickl, S. Kreipl, H. Jäger, and A. Stohl. Transport of boreal fire emissions from Canada to Europe. *J. Geophys. Res.*, 106(D19):22887–22906, 2001.

[36] A. Berk, L.S. Bernstein, and D.C. Robertson. MODTRAN: A Moderate Resolution Model for LOWTRAN 7. Technical Report GL-TR-89-0122, 1989.

[37] F. Chevallier. Sampled database of 60-level atmospheric profiles from the ECMWF database, SAF Research program, 4. Technical report, EUMETSAT/ECMWF, 2001.

[38] Y.X. Hu and K. Stamnes. An accurate parameterization of the radiative properties of water clouds suitable for use in climate models. *J. Clim.*, 6:728–742, 1993.

[39] J. R. Key, P. Yang, B. A. Baum, and S. L. Nasiri. Parameterization of shortwave ice cloud optical properties for various particle habits. *J. Geophys. Res.*, 107(D13):doi:107(D13):10.1029/2001JD00742., 2002.

[40] L.G. Henyey and J.L. HGreenstein. Diffuse radiation in the galaxy. *Astrophys. J.*, 93:70–83, 1941.

[41] S. A. Clough and M. Iacono. Line-by-line calculation of atmospheric fluxes and cooling rates: 2. Application to carbon dioxide, ozone, methane, nitrous oxide and halocarbons. *J. Geophys. Res.*, 100:16519–16535, 1995.

[42] S. A. Clough, M. W. Shephard, E. Mlawer, J. S. Delamere, M. Iacono, K. Cady-Pereira, S. Boukabara, and P. D. Brown. Atmospheric radiative transfer modeling: a summary of the AER codes. *J. Quant. Spectros. Rad. Transfer*, 91(2):233–244, 2005.

[43] J.L. Moncet and S.A. Clough. Accelerated monochromatic radiative transfer for scattering atmospheres: Application of a new model to spectral radiance observations. *J. Geophys. Res.*, 102(21):21,853–21,866, 1997.

[44] B. Barret, D. Hurtmans, M. R. Carleer, M. De Mazière, E. Mahieu, and P.F. Coheur. Line narrowing effect on the retrieval of HF and HCl vertical profiles from FTIR ground-based measurements. *J. Quant. Spectros. Rad. Transfer*, in press, 2005.

[45] P. F. Coheur, B. Barret, S. Turquety, D. Hurtmans, J. Hadji-Lazaro, and C. Clerbaux. Retrieval and characterization of ozone vertical profiles from a thermal infrared nadir sounder. *J. Geophys. Res.*, submitted, 2005.

[46] L. S. Rothman, A. Barbe, D. C. Benner, L. R. Brown, C. Camy-Peyret, M. R. Carleer, K. Chance, C. Clerbaux, V. Dana, V. M. Devi, A. Fayt, J. M. Flaud, R. R. Gamache, A. Goldman, D. Jacquemart, K. W. Jucks, W. J. Lafferty, J. Y. Mandin, S. T. Massie, V. Nemtchinov, D. A. Newnham, A. Perrin, C. P. Rinsland, J. Schroeder, K. M. Smith, M. A. H. Smith, K. Tang, R. A. Toth, J. Vander Auwera, P. Varanasi, and K. Yoshino. The HITRAN molecular spectroscopic database: edition of 2000 including updates through 2001. *J. Quant. Spectros. Rad. Transfer*, 82(1-4):5–44, 2003.

[47] R. J. D. Spurr, T. P. Kurosu, and K. V. Chance. A linearized discrete ordinate radiative transfer model for atmospheric remote-sensing retrieval. *J. Quant. Spectros. Rad. Transfer*, 68(6):689–735, 2001.

[3]References [3] to [8] are available from http://www.eumetsat.de; in the Preparation of future programmes; Meteosat Third Generation section

Acronyms

AIRS: Atmospheric Infrared Sounder
CMDL: Climate Monitoring and Diagnostics Laboratory
CTM: Chemistry Transport Model
DOFS: Degrees Of Freedom for Signal
DOAS: Differentiel Optical Absorption Spectroscopy
FTS: Fourier Transform Spectrometer
FWHM: Full Width at Half Maximum
GEO: Geostationnary Orbit
IRS: InfraRed Sounder
IASI: Infrared Atmospheric Sounding Interferometer
IMG: Interferometric Monitor for Greenhouse gases
ISRF: Instrumental Response Function
LEO: Low-Earth Orbit
MSG: Meteosat Second Generation
MOPITT: Measurement Of Pollution In The Throposphere
MAPS: Measuring Atmosphric Pollution with Satellite
MTG: Meteosat Third Generation
MRD: Mission Requirement Document
NWP: Numerical Weather Prediction
OEM: Optimal Estimation Method
SA-NN: Service d'Aéronomie Neural Network
SCIAMACHY: SCanning Imaging Absorption spectroMeter for Atmospheric CHartographY
SNR: Signal-to-Noise Ratio
SWIR: Short–Wave Infrared
TES: Tropospheric Emission Spectrometer
UTLS: Upper Troposphere – Lower Stratosphere
UVS: UV–visible Sounder
WMO: World Meteorological Organization